博士論文

令和五年度

Establishment of a ribosome purification system in zebrafish embryos and analysis of ribosome ubiquitination during zebrafish development

京都産業大学大学院
生命科学研究科
博士後期課程 3 年
187068
宇賀神　希

Contents

論　文　要　旨

氏　名	宇賀神　希

The ribosome is a large ribonucleoprotein complex that translates mRNAs into proteins. The ribosome was traditionally viewed as a homogenous molecular machine with little regulatory functions. However, emerging evidence shows that the ribosome is a heterogeneous molecular machine in components and that variations of individual components of the ribosome endow the ribosome with functional diversity. It is now clear that such heterogeneity of the ribosome and its specialized functions are very important in various physiological aspects. Post-translational modifications on ribosomal proteins are particularly important as they mediate dynamic responses to multiple stimuli and stress. Ubiquitination is highly conserved post-translational modifications on ribosomal proteins. Current research elucidates multiple roles of ribosome ubiquitination, including ribosome degradation, quality control pathway to maintain proteostasis, and modulation of translation in response to stress conditions. However, it is currently unclear to what extent ribosome ubiquitination is essential for animal development. This is mainly due to the limited number of research conducted with embryos of various developmental time-points. Difficulties in purifying ribosomes quickly, easily, and efficiently from multiple samples have hampered the progress in this field. Here, I took advantage of zebrafish (*Danio rerio*) and sought to overcome the above technical limitation and extend our understanding of post-translational modifications on ribosomal proteins in animal development. In Chapter 1, toward the establishment of a ribosome purification system, I sought to generate a zebrafish strain that expresses an epitope-tagged ribosomal protein endogenously by using the CRISPR-Cas9-mediated genome editing system. As a result, I succeeded in developing the *rpl36*-FLAG strain with no noticeable effect of a FLAG-tag for viability and ribosome assembly. I and Dr. Koshi Imami demonstrated that this strain allowed the purification of fully assembled and translation-engaging 80S ribosomes from zebrafish embryos by a simple FLAG-immunoprecipitation strategy. In Chapter 2, by combining the ribosome purification system with immunoblotting analysis, I detected the dynamics of ribosome ubiquitination during zebrafish development. Furthermore, I and Dr. Koshi Imami revealed that Rps10/eS10 is one of the ribosomal proteins dynamically ubiquitinated during development. Since the Rps10/eS10 ubiquitination-sites mutation reduced the overall ubiquitination pattern of ribosomes, I concluded that ribosomes are ubiquitinated in a hierarchical manner during development and Rps10/eS10 ubiquitination lies at the core of the cascade. Although the biological relevance and the underlying molecular mechanism of this ubiquitination pattern remain elusive, the present study provides unique insights into the dynamics of ribosome ubiquitination during animal development and paves the way for future studies.

Abbreviation

- hpf: hours post fertilization
- dpf: days post fertilization
- sgRNA: single guide RNA
- ssODN: single-strand oligodeoxynucleotide
- nanoLC/MS/MS: nano-scale reversed-phase liquid chromatography coupled with tandem mass spectrometry
- PIC: preinitiation complex
- CPE: cytoplasmic polyadenylation elements
- CPEB: CPE-binding protein
- PABP: poly(A)-binding protein
- UTR: untranslated region
- mESCs: mouse embryonic stem cells
- RQC: ribosome-associated quality control
- ER: endoplasmic reticulum
- DUB: deubiquitinating enzyme
- HTN: harringtonine
- CHX: cycloheximide
- HDR: homology-directed repair
- cryo-EM: cryogenic-electron microscopy

General Introduction

Gene expression is strictly controlled in a spatiotemporal manner during the developmental process, in which an entire organism is built from a single totipotent cell, and stem cells sustain tissue integrity by generating newly differentiated cells. Various steps of gene expression, from the transcription of a gene to the translation of an mRNA, have been well characterized (Dever et al. 2018; Hellen 2018; Liu et al. 2013; Sonenberg and Hinnebusch 2009). Historically, transcriptional regulation, such as chromatin modifications, has been the focal point for the study of gene expression during development (Lee et al. 2014; Tadros and Lipshitz 2009). With the development of high-throughput methods, such as ribosome footprint profiling (Ingolia 2014) and mass spectrometry (Aebersold and Mann 2016; Selbach et al. 2008), we are now able to comprehensively analyze the changes in translation during development (Kronja et al. 2014; Winata et al. 2018; Lee et al. 2013). Importantly, these emerging techniques reveal that mRNA levels are poorly correlated with protein levels, especially during the rapid transition of cell fate, such as embryogenesis and stem cell differentiation (Liu et al. 2016; Lu et al. 2009; Peshkin et al. 2015). Therefore, a comprehensive understanding of complex changes in gene expression during development requires an analysis of not only transcriptional mechanisms but also translational mechanisms.

Translation is a very complicated process mediated by various factors. Of those, the ribosome plays a central role in translation. The eukaryotic ribosome is generally composed of four ribosomal RNA (rRNA) molecules and 79 distinct ribosomal proteins. These components are organized into small and large ribosomal subunits, which together form an 80S ribosome (Bashan and Yonath 2008; De La Cruz et al. 2015). Using mRNA as a template, one ribosome reads each codon of the mRNA and pairs the codon with the appropriate amino acid provided by an aminoacyl-tRNA to form a nascent polypeptide chain with the aid of initiation factors, elongation factors, and termination factors (Dever et al. 2018; Hellen 2018; Sonenberg and Hinnebusch 2009). It is now clear that specific sequences of mRNAs can also modulate every step of translation via interacting with trans-acting factors, such as RNA-binding proteins and microRNAs (Carpenter et al. 2014; Truitt and Ruggero 2016; Vejnar et al. 2019). Therefore, these factors orchestrally act in the translation process.

Because in many animal species, late-stage oocyte maturation and early embryogenesis proceed with little or no transcription of the zygotic genome, translational control of maternally provided mRNAs exclusively plays a critical role in this process (Lee et al. 2014; Tadros and Lipshitz 2009). Thus far, the mechanisms of translational control during oocyte maturation, egg activation, and cell differentiation at early embryonic stages, have been intensively studied with clams, flies, frogs, and mice (Kronja et al. 2014; Kang and Han 2011; Richter and Lasko 2011; Teixeira and Lehmann 2019; Radford et al. 2008; Seydoux 1996; Avilés-Pagán and Orr-Weaver 2018; Sheets et al. 2018; Gabut et al. 2020). For example, during *Xenopus* oocyte maturation, translational activation of cyclin

B1 mRNA is regulated by poly(A)-tail lengthening, or polyadenylation (Kim and Richter 2006; Nakahata et al. 2003; Radford et al. 2008) (Figure 1). Maternally provided cyclin B1 mRNA contains cytoplasmic polyadenylation elements (CPE) in the 3′ untranslated region (UTR). CPE-binding protein (CPEB) binds to CPE and interacts with poly(A) polymerase Gld2, poly(A) ribonuclease PARN, and RNA-binding protein Pumilio. In the absence of hormonal stimulation, both PARN and Gld2 are in an active state, but PARN is more active, and thus poly(A)-tail is shortened. In addition, at this immature phase, Pumilio also prevents poly(A)-tail elongation by interacting with an uncharacterized deadenylase. In response to progesterone, CPEB is phosphorylated by Aurora A kinase or an uncharacterized kinase. Phosphorylation of CPEB triggers the dissociation of PARN and Pumilio from the CPEB-cyclin B1 mRNA complex, allowing elongation of poly(A)-tail. The elongated poly(A)-tail then recruits poly(A)-binding protein (PABP), which activates translation initiation via interacting with eukaryotic initiation factor eIF4G. Through these processes, cyclin B1 mRNA is translationally activated during oocyte maturation (Figure 1).

The ribosome was traditionally viewed as a homogenous molecular machine with little regulatory functions, thus the study of translational control during development mainly focused on other factors such as mRNA-binding factors as mentioned above. However, two concepts “the ribosome filter hypothesis” and “a ribosome code” propose that the ribosome acts as a regulatory element that modulates the translational efficiency of distinct subsets of mRNAs by interacting with particular mRNAs (Komili et al. 2007; Mauro and Edelman 2002). Indeed, accumulating evidence has highlighted variations in the composition of the ribosome and its biological relevance (Emmott et al. 2019; Gilbert 2011; Genuth and Barna 2018a; Norris et al. 2021; Genuth and Barna 2018b; Li and Wang 2020; Xue and Barna 2012). Therefore, these observations show that the ribosome is a heterogeneous molecular machine in components and that variations of individual components of the ribosome endow the ribosome with functional diversity. It is now clear that such heterogeneity of the ribosome and its specialized functions are very important in various physiological phenomena including development. The functional diversity of the ribosome can allow cells to quickly and flexibly respond to stimuli by directly changing protein abundance. Recent examples of ribosome heterogeneity are at the level of core ribosomal proteins, ribosome-associated proteins, posttranslational modifications, and rRNAs (Figure 2).

The original report revealing heterogeneity at the level of core ribosomal proteins came from Rpl38/eL38-deficient mice (Kondrashov et al. 2011). The ribosome containing Rpl38/eL38 is known to selectively translate a subset of Homeobox mRNAs by recognizing the particular RNA structure in 5′ UTR of the Homeobox mRNAs, and thus the Rpl38/eL38-deficient mouse exhibits tissue-specific patterning defects (Kondrashov et al. 2011; Xue et al. 2015). Subsequently, ribosomes containing Rpl10a/uL1, Rps25/eS25, Rps26/eS26, or Rpl3L, a paralogue of core ribosomal protein Rpl3/uL3 were also found to preferentially translate specific subsets of mRNAs in mammalian cells or yeast

(Ferretti et al. 2017; Genuth et al. 2022; Shi et al. 2017; Shiraishi et al. 2023). In addition, ribosomes containing Rpl39L, a paralogue of core ribosomal protein Rpl39/eL39 are known to regulate cotranslational protein folding of a subset of male germ-cell-specific proteins (Li et al. 2022a).

Ribosome-associated proteins are another layer of ribosome heterogeneity and its function. In mouse embryonic stem cells (mESCs), ~430 proteins were identified as ribosome-associated proteins and they include not only components of canonical translation machinery but also proteins controlling metabolism, cell redox homeostasis, and cell cycle (Simsek et al. 2017). PKM2 is well characterized as a glycolysis enzyme and one of the identified ribosome-associated proteins. Uncoupled from its role in metabolism, PKM2 preferentially binds to ribosomes bound to the endoplasmic reticulum (ER) and upregulates the translational efficiency of mRNAs encoding membrane and ER-localized proteins. Most recently, a contribution of ribosome-associated proteins in translational control during early embryogenesis was reported (Leesch et al. 2023). This study demonstrated in zebrafish and *Xenopus* eggs that in addition to canonical translation factors eEF2 and eIF5a, Hapb4 and Dap1b/Dap also bind to ~40% of ribosomes simultaneously and keep the dormant state of those ribosomes. This mechanism could account for changes in translational rate during embryogenesis from the perspective of ribosome-associated proteins. The mRNA decay rate is also regulated cotranslationally by ribosome-associated proteins. Codon optimality has been established as a major parameter for regulating mRNA half-life in eukaryotes (Bazzini et al. 2016; Buschauer et al. 2020; Hanson and Coller 2018; Mishima and Tomari 2016; Radhakrishnan et al. 2016). In yeast, when the ribosome translates mRNAs enriched with nonoptimal codons, ribosome A-site and E-site lack tRNAs due to slow decoding kinetics. Not5, a component of the Ccr4-Not complex serving as a cytoplasmic deadenylase, specifically binds to the unaccommodated ribosome E-site, which explains the shorter half-lives of mRNAs enriched in nonoptimal codons (Buschauer et al. 2020). The same mechanism may contribute to maternal mRNA degradation during zebrafish embryogenesis (Mishima and Tomari 2016).

Another part of ribosome heterogeneity is post-translational modifications on ribosomal proteins. Ribosomal proteins have been reported to be subject to a range of post-translational modifications including phosphorylation (Imami et al. 2018; Martin et al. 2014), ubiquitination (Back et al. 2019; Higgins et al. 2015; Matsuki et al. 2020; Silva et al. 2015; Spence et al. 2000), methylation (Małecki et al. 2021; Matsuura-Suzuki et al. 2022), acetylation (Zhang et al. 2022), and UFMylation, a ubiquitin-like modifier UFM1 is attached to substrates (Walczak et al. 2019; Wang et al. 2020). Some of these modifications are introduced to the ribosome in response to various stimuli and affect protein synthesis both in quality and in quantity by regulating translational efficiency (Matsuura-Suzuki et al. 2022; Takehara et al. 2021), translational preference (Imami et al. 2018; Matsuki et al. 2020; Zhang et al. 2022), and cotranslational protein degradation (Inada 2020; Joazeiro 2017, 2019; Walczak et al. 2019; Wang et al. 2020). For example, phosphorylation of Rpl12/uL11 is more

prevalent in monosomes than in polysomes, which affects cell cycle progression by regulating the translation of a specific subset of mitosis-related mRNAs (Imami et al. 2018). Ubiquitination of Rps10/eS10 and Rps20/uS10 and UFMylation of Rpl26/uL24 are implicated in protein quality control in the cytoplasm and ER, respectively (Walczak et al. 2019; Wang et al. 2020; Joazeiro 2017, 2019; Inada 2020).

rRNA also represents an important source of heterogeneity. Heterogeneity of rRNA levels arises from both rRNA sequences and rRNA modifications. Eukaryotic rRNA consists of four elements: 5S, 5.8S, and 28S in the large ribosomal subunit, and 18S in the small ribosomal subunit (Yusupova and Yusupov 2014). Whereas 5S rRNA is transcribed independently, 5.8S, 28S, and 18S rRNAs are transcribed as a single 47S precursor rRNA and then generated by the processing of the precursor rRNA (Xue and Barna 2012). Both 5S rRNA and 47S rRNA reside in tandem repetitive clusters in the vertebrate genome, in some cases totaling hundreds of copies (Kobayashi 2011). It is known that there are sequence variations among 5S rRNA gene copies and among 47S rRNA gene copies (Kuo 1996; Parks et al. 2018). Recent studies indicate that during zebrafish embryogenesis, ribosomes initially contain oocyte-specific sequences for all four rRNAs and then later switch to somatic rRNA variants although the significance of these variations in rRNAs is yet unclear (Locati et al. 2017a, 2017b). Similarly, multiple variations in rRNA sequence were also identified in other animals (Rothschild et al. 2023; Wormington and Brown 1983). Furthermore, rRNA is a target of various chemical modifications. Over 200 residues of human rRNA are targeted by chemical modifications such as methylation, pseudouridylation, ribosylation, or acetylation (Roundtree et al. 2017; Sharma and Lafontaine 2015). A recent study indicates that the loss of the 2′-O-metylation at 28S:U3904 upregulates the translational efficiency of mRNAs related to the WNT signaling pathway, thus affecting tri-lineage differentiation (Häfner et al. 2023).

An alternative, but not mutually exclusive, regulatory mechanism of translation is quantity itself, i.e. the abundance of ribosomes. While it is estimated that up to 100 million ribosomes exist in a mammalian cell, ribosome abundance is strictly regulated through the balance between biosynthesis and degradation mechanisms under various physiological conditions (An and Harper 2020; Dalla Venezia et al. 2019). For example, under various conditions of nutrient and proteotoxic stresses, ribosomes can be subject to selective degradation via autophagy (An and Harper 2020). In contrast, the mammalian target of the rapamycin complex (mTORC) directly stimulates RNA polymerase I and RNA polymerase III by interacting with their promoters, and thus positively controls the production of the four rRNAs in response to several stimuli such as nutrients, hormones, and oncogenic signaling pathways (Dalla Venezia et al. 2019). In addition, ribosomes are removed from specific cell lineages such as during the formation of red blood cells via the ubiquitin-proteasome pathway (Glowacki and Millette 1965). Accumulating studies also indicate that damaged or non-functional ribosomes are degraded (Li et al. 2022b; Sugiyama et al. 2019). Importantly, a recent study connects the ribosome

abundance and its impact on translational preference during hematopoiesis (Khajuria et al. 2018).

Taken together, the ribosome could be an essential and attractive target when we study the mechanism of translational control during development. Compared to the heterogeneity at rRNA levels, which is generated during the biosynthesis of ribosomes in the nucleus, the heterogeneity in ribosomal proteins or ribosome-associated proteins can be generated more quickly and flexibly, leading to functional diversity. In particular, post-translational modifications on ribosomal proteins are even more dynamic events in response to multiple stimuli and stress. However, post-translational modifications on ribosomal proteins have been mainly studied using cultured cells and yeast, and thus the knowledge of their dynamic changes in animal development is limited. This is partly caused by technical reasons. Generally, ribosomes are purified using sucrose gradient centrifugation, which requires long-experimental durations and substantial quantities of biological materials (Johannes et al. 1999; Reschke et al. 2013). Since the analysis of the dynamic change during development requires multiple samples from different time-points, the traditional purification method was hardly applied. An alternate promising method could be the affinity purification of ribosomes with an epitope-tagged ribosomal protein expressed in animals. Affinity purification would be quicker and less labor intensive so that multiple samples can be processed at the same time.

In my doctoral thesis, I sought to overcome the above technical limitation and extend our understanding of post-translational modifications on ribosomal proteins in animal development. Here, I use zebrafish *Danio rerio* because zebrafish lays hundreds of eggs that develop in a synchronous manner at a relatively rapid speed (Kimmel et al. 1995). In addition, the large size of zebrafish eggs allows for the microinjection of molecules. In Chapter 1, to purify ribosomes efficiently and easily from embryos of several developmental time-points, I established an affinity purification system in zebrafish. In Chapter 2, using ribosomes purified by this newly established system, I analyzed the levels of ubiquitination, one of the post-translational modifications on ribosomal proteins, during zebrafish development. I and Dr. Koshi Imami found a unique and complex ubiquitination pattern on ribosomal proteins during development. Although the biological relevance and the underlying molecular mechanism of this ubiquitination pattern remain elusive, the present study provides unique insights into the dynamics of ribosome ubiquitination during animal development and a good starting point for future studies.

Chapter 1: Establishment of a ribosome affinity purification system in zebrafish embryos

Introduction

The eukaryotic ribosome consists of about 80 ribosomal proteins and four rRNAs, and they are hierarchically assembled into two ribosomal subunits: the large 60S ribosomal subunit and the small 40S ribosomal subunit (Bashan and Yonath 2008; Yusupova and Yusupov 2014). These two ribosomal subunits cyclically associate and dissociate in the translation process. In the translation initiation phase, the 40S ribosomal subunit interacts with various initiation factors (eIF1, eIF1A, eIF2, eIF3, and eIF5) and methionine-tRNA, forming the 43S preinitiation complex (PIC). Then the 43S PIC attaches to the 5′ cap structure of an mRNA via eIF4F and scans the 5′ UTR in the 5′ to 3′ direction to the initiation codon, forming 48S PIC. After initiation codon recognition, the 60S ribosomal subunit joins to the 48S PIC with the eIF5B function, forming the 80S ribosome competent for protein synthesis (Sonenberg and Hinnebusch 2009). In the translation elongation phase, with the aid of translation elongation factors (eEF1a, eIF5a, and eEF2), multiple 80S ribosomes simultaneously translate a single mRNA molecule, thus forming polysomes (Dever et al. 2018). In the translation termination phase, the release factors (eRF1 and eRF3) recognize the stop codon and mediate the release of the nascent polypeptide chain (Hellen 2018). The post-termination 80S ribosome is dissociated into the 40S ribosomal subunit and the 60S ribosomal subunit by a recycling factor ABCE1 (Hellen 2018). Finally, the dissociated ribosomal subunits participate in the next rounds of the translation cycle. Thus, ribosomes are present as different subcomplex states in the cell. Historically, conventional sucrose gradient centrifugation was utilized to purify and discriminate these subcomplexes. The components of each subcomplex were characterized by one- or two-dimensional gel electrophoresis and sequence analysis of the individual polypeptides (Martini and Gould 1975). Now that mass spectrometry and cryogenic-electron microscopy (cryo-EM) are powerful tools, these approaches are combined with the ribosome purification technique, allowing the analysis of the structure and composition of ribosome subcomplexes in greater detail (Yusupova and Yusupov 2014; Aviner et al. 2017; Kornprobst et al. 2016).

Since the sucrose gradient centrifugation can distinguish different ribosomal subcomplex by their centrifugation properties, this approach yielded fundamental insights into the components of each ribosomal subcomplex (Yusupova and Yusupov 2014; Aviner et al. 2017; Kornprobst et al. 2016; Aitken and Lorsch 2012; Lapointe et al. 2022). In addition, ribosome-associated proteins were identified by purifying ribosomes using the sucrose gradient centrifugation (Reschke et al. 2013). Recent studies also highlighted the monosome-specific phosphorylation (Imami et al. 2018) and 43S PIC-associated proteins (Kito et al. 2023), which impact on translational efficiency of specific subsets of mRNAs. Therefore, sucrose gradient centrifugation is an effective purification approach in analyzing the subcomplex-specific regulation of the ribosome. However, there are several caveats and technical difficulties in this approach. For example, sucrose gradient centrifugation does not

distinguish ribosomes and other ribosome-independent complexes that have similar centrifugation properties to the ribosome, such as clathrin and vault (Simsek et al. 2017). In addition, it is hard to obtain ribosomes from multiple samples in parallel due to its long experimental durations (~24 h). As an alternative approach, epitope tagging and immuno-affinity purification of ribosomes have been reported in yeast (Inada et al. 2002), mouse (Shi et al. 2017; Simsek et al. 2017; Sanz et al. 2009), and zebrafish (Tryon et al. 2013). This approach enabled us to purify fully assembled translating ribosomes in a relatively short time (~3 h), and revealed ribosome-associated proteins and mRNAs. However, this approach requires an epitope-tagged ribosomal protein expressed either exogenously or endogenously, unless a reliable antibody against an endogenous ribosomal protein that locates the solvent-exposed side is available. In addition, this approach does not distinguish different ribosomal subcomplexes.

There are two approaches to generating a genetically modified zebrafish strain that expresses an epitope-tagged ribosomal protein. One is a transgenic approach to insert extra copies of an epitope-tagged ribosomal protein gene in the genome. The other is a knock-in approach to directly insert an epitope tag sequence into the endogenous ribosomal protein gene locus. To generate a transgenic strain, the Tol2 transposon system is commonly used (Kawakami et al. 2000). A transposase of Tol2 transposon catalyzes the integration of a DNA sequence containing the Tol2 recognition sequence to the zebrafish genome. By co-injecting a plasmid DNA harboring an exogenous gene cassette sandwiched between the Tol2 recognition sequences with an mRNA encoding Tol2 transposase into eggs, the exogenous gene cassette is integrated into the zebrafish genome at random locations. Hence, the expression of the exogenous gene cassette can be affected by the surrounding genomic sequence of the integration site. The corresponding protein abundance may be different from wild-type as the transgene serves as extra copies of the endogenous gene. The CRISPR-Cas9-mediated genome editing system is considered the most promising and versatile technology to create knock-in model organisms (Salsman and Dellaire 2017). This system uses the Cas9 nuclease that induces a double-stranded DNA break (Jansen et al. 2002) and a single-guide RNA (sgRNA) molecule that recognizes and binds at a specific target site (Jinek et al. 2012). Following a double-stranded DNA break formation, the site is repaired by endogenous repair mechanisms. In the presence of a repair template DNA containing an exogenous sequence and homology arms, the site is repaired by homology-directed repair (HDR) with the insertion of the exogenous sequence in the targeted locus (Bai et al. 2020; Boel et al. 2018; Richardson et al. 2016). Although the efficiency of precise insertion by HDR is low, this system can insert an epitope-tag sequence in an endogenous locus, thus minimizing the perturbation of the protein expression level.

To analyze post-translational modifications on ribosomal proteins during zebrafish development, multiple samples derived from different developmental time-points must be treated in parallel. Therefore, it will be beneficial to develop an affinity purification system of the ribosome in

zebrafish. For this purpose, a zebrafish strain that expresses an epitope-tagged ribosomal protein exogenously or endogenously is needed. Importantly, the excess of ribosomal proteins that are not incorporated into ribosomes triggers the p53-activating checkpoint signaling pathway (Bursac et al. 2014; Xu et al. 2016). To minimize the perturbation of ribosomal protein stoichiometry, a zebrafish strain that expresses an epitope-tagged ribosomal protein endogenously is more desirable than the transgene-based approach.

In the present study, I generated a zebrafish strain that expresses a FLAG-tagged ribosomal protein Rpl36/eL36 by using the CRISPR-Cas9-mediated genome editing system. I and Dr. Koshi Imami validated the utility of this strain for ribosome purification by four approaches: RNA electrophoresis, immunoblotting analysis, protein staining, and LC/MS/MS analysis. I found that this strain enables the efficient (20% of the input) and quick (about one hour) purification of fully assembled 80S ribosomes from zebrafish eggs and embryos. Furthermore, Dr. Koshi Imami identified about 400 proteins copurified with ribosomes from various developmental time-points. This number is comparable to the previous study in mice (Simsek et al. 2017). The copurified proteins included mRNA-associated proteins and translation elongation factors. This result suggested that the generated zebrafish strain allowed the purification of fully assembled and translation-engaging 80S ribosomes by a simple FLAG-immunoprecipitation strategy. With these results, I discuss the utility and application of this strain to analyze ribosome heterogeneity during zebrafish development. I also mention the limitation of this strain for ribosome purification.

Results

80S ribosomes were purified from zebrafish embryos by transiently overexpressing Rpl36-FLAG

To generate a zebrafish strain that expresses an epitope-tagged ribosomal protein endogenously, I considered which ribosomal proteins are suitable for epitope tagging. Generally, ribosomal proteins that locate the solvent-exposed side of the 80S ribosome are selected as targets for epitope tagging due to accessibility to affinity-capture reagents. Thus far, FLAG-tagged Rpl25/uL23 has been used to identify ribosome-associated mRNAs and proteins and to examine the ubiquitination status of ribosomal proteins in yeast (Inada et al. 2002; Sugiyama et al. 2019). In mice, Rpl10a/uL1, Rps25/eS25, Rpl36/eL36, Rps17/eS17, and Rpl22/eL22 were selected for epitope tagging to study ribosome-associated mRNAs and proteins (Shi et al. 2017; Simsek et al. 2017; Sanz et al. 2009). In zebrafish, GFP-tagged Rpl10a/uL1 was used to analyze ribosome-associated mRNAs (Tryon et al. 2013). From these candidates, I selected Rpl36/eL36 as a target for epitope tagging in this study for the following reasons. Since Rpl22/eL22 has an extra-ribosomal function, specific purification of ribosomes might be difficult due to the contamination of non-ribosomal binding proteins, such as Histone H1 (Warner and Mcintosh 2009). The amount of Rpl10a/uL1 and Rps25/eS25 are significantly substoichiometric in polysomes (Shi et al. 2017), suggesting the existence of ribosomes lacking these ribosomal proteins. As two paralogous genes encode Rps17/eS17 in zebrafish, there is a possibility that the tagged Rps17/eS17 paralog protein might not always be incorporated into functional ribosomes. It was difficult to design a reliable sgRNA in the *rpl25* gene locus.

FLAG-tagged Rpl36/eL36 was used to purify fully assembled ribosomes in mESCs (Simsek et al. 2017). I verified the utility of this strategy in zebrafish embryos by a transient expression experiment. To this end, an mRNA encoding C-terminally FLAG-tagged Rpl36/eL36 (Rpl36-FLAG) was injected into zebrafish eggs. Then the 24-hours post-fertilization (hpf) embryos were subjected to immunoprecipitation with a FLAG antibody (Figure 3A). To validate the purification of ribosomes, the immunoprecipitant was subjected to RNA electrophoresis, immunoblotting analysis with antibodies against ribosomal proteins, and protein staining. Electrophoresis of the immunoprecipitated RNA revealed that both 18S and 28S rRNAs, a component of the small ribosomal subunit and the large ribosomal subunit, respectively, were purified from Rpl36-FLAG overexpressed embryos (Figure 3B). Immunoblotting analysis showed that a large ribosomal subunit protein Rpl7a/eL8 and a small ribosomal subunit protein Rps10/eS10 were copurified with Rpl36-FLAG (Figure 3C). Protein staining showed that proteins that were less than 50 kDa, which is the size of most ribosomal proteins (Martini and Gould 1975), were copurified with Rpl36-FLAG (Figure 3D). These results indicate that transiently overexpressed Rpl36-FLAG is incorporated into 80S ribosomes, thus allowing for the purification of components of both the large and the small ribosomal subunits by FLAG-

immunoprecipitation. Hence, I conclude that Rpl36/eL36 is a suitable target for epitope tagging to purify assembled 80S ribosomes from zebrafish embryos.

A zebrafish strain that expresses FLAG-tagged Rpl36/eL36 endogenously was generated by the CRISPR-Cas9-mediated genome editing system

As it is difficult to express Rpl36-FLAG constitutively throughout development by the injection experiment, I sought to generate a mutant strain that expresses Rpl36-FLAG endogenously using the CRISPR-Cas9-mediated genome editing system. The detailed procedure is described in the Materials and Methods section, thus I briefly summarized it here. To induce a double-stranded DNA break at the genome sequence around the stop codon of the *rpl36* gene locus, I synthesized a corresponding sgRNA. To insert a FLAG-tag sequence into the genome via HDR, I designed a single-strand oligodeoxynucleotide (ssODN) with homology arms and a FLAG-tag sequence (Figure 4A). After incubating the sgRNA with the Cas9 protein, the sgRNA/Cas9 complex was co-injected into zebrafish eggs with the ssODN. To assess the insertion of a FLAG-tag sequence into the *rpl36* gene locus in germline cells, each raised fish was crossed with wild-type fish. Genomic DNA from 24 hpf embryos obtained from the mating was subjected to genotyping PCR using a specific primer pair that amplifies around the expected insertion sites, followed by TA cloning and Sanger sequencing (Figure 4B). As a result, a strain carrying a precisely edited *rpl36* gene locus with the FLAG-tag sequence was obtained (Figure 4C).

To examine the effect of the inserted FLAG-tag sequence for viability, I counted the number of progeny fish around 60 days post-fertilization (dpf) obtained by crossing *rpl36*-FLAG heterozygous fish. It was confirmed that the *rpl36*-FLAG allele was transmitted to progenies at the expected Mendelian ratio, suggesting that the inserted FLAG-tag sequence did not affect viability significantly (Figure 5A). Unless noticed, embryos obtained by crossing the *rpl36*-FLAG heterozygous fish were used in this study (hereafter called *rpl36*-FLAG embryos). Furthermore, I examined the incorporation efficiency of Rpl36-FLAG into 80S ribosomes by sucrose gradient centrifugation. As expected from the Rpl36-FLAG overexpression experiment, fractionation of *rpl36*-FLAG embryonic lysate showed that Rpl36-FLAG was incorporated in the functional 60S ribosomal subunit: Rpl36-FLAG was detected in 60S, 80S monosome, and polysome fractions like other ribosomal proteins (Figure 5B). Thus, I conclude that the Rpl36-FLAG is incorporated into 80S ribosomes.

The *rpl36*-FLAG strain allows the purification of ribosomes from 24 hpf zebrafish embryos

As with the Rpl36-FLAG overexpression experiment, I verified the utility of the established *rpl36*-FLAG strain for ribosome purification (Figure 6A). 24 hpf embryos obtained from crossing of wild-type fish or the *rpl36*-FLAG strain were subjected to FLAG-immunoprecipitation followed by three approaches: RNA electrophoresis (Figure 6B), immunoblotting analysis (Figure 6C), and protein

staining (Figure 6D). These results showed that components of both the small and the large ribosomal subunits were specifically detected in the FLAG-immunoprecipitant of *rpl36*-FLAG embryos. From these results, I conclude that the *rpl36*-FLAG strain is a powerful tool to purify assembled 80S ribosomes from 24 hpf embryos.

The *rpl36*-FLAG strain allows the purification of ribosomes from zebrafish embryos throughout development

To verify the versatility of the *rpl36*-FLAG strain for ribosome purification throughout development, I performed FLAG-immunoprecipitation using the same number of *rpl36*-FLAG embryos at various developmental time-points: 0 (zygote period), 6 (gastrula period), 12 (segmentation period), and 24 (pharyngula period) hpf. The obtained FLAG-immunoprecipitants were subjected to RNA electrophoresis (Figure 7A), immunoblotting analysis (Figure 7B), and protein staining (Figure 7C). These results showed that components of both ribosomal subunits were detected in the FLAG-immunoprecipitants at comparable levels throughout all developmental time-points investigated.

To more comprehensively and directly examine the purification of fully assembled 80S ribosomes, I asked Dr. Koshi Imami and Dr. Yasushi Ishihama for nano-scale reversed-phase liquid chromatography coupled with tandem mass spectrometry (nanoLC/MS/MS) analysis of the FLAG-immunoprecipitants. Their nanoLC/MS/MS analysis detected most of the ribosomal proteins of the small and the large ribosomal subunits in all developmental time-points (Figure 7D). Four ribosomal proteins were not detected: Rpl29/eL29 and Rpl41/eL41 due to a technical limitation, and Rps20/uS10 and Rpl27a/uL15 for unknown reasons. As expected, the large ribosomal subunit-associated factors were also identified, such as eIF6, which prevents ribosomal subunit association by binding to the large ribosomal subunit (Brina et al. 2015). However, their data resulted in the enrichment of components of both the small and the large ribosomal subunits to a similar degree throughout development, indicating that the majority of purified ribosomes were fully assembled 80S ribosomes. Therefore, I conclude that the *rpl36*-FLAG strain is a valuable tool to purify fully assembled 80S ribosomes throughout developmental time-points with simple procedure and high efficiency (20% of the input).

Translation-engaging ribosomes were purified by FLAG-immunoprecipitation using *rpl36*-FLAG embryos

To examine whether the 80S ribosomes purified from the *rpl36*-FLAG embryos were translating ribosomes, I assessed the copurified proteins identified by the nanoLC/MS/MS analysis. The nanoLC/MS/MS analysis identified not only the components of ribosomes but also various non-ribosomal proteins involved in translation. I further focused on Pabpc1, Ddx6, and eEF1a because of their well-characterized function in translation and the availability of specific antibodies (Figure 8A).

Pabpc1, one of the cytoplasmic poly(A)-binding proteins, is known to interact with the poly(A)-tail and regulate translation initiation rate and mRNA stability (Chen and Shyu 2011; Gray 2000). A DEAD-box RNA helicase Ddx6 was reported as a contributor to mRNA storage, translation inhibition, and mRNA degradation via interaction with various factors (Wang et al. 2015). Lastly, eEF1a, one of the eukaryotic translation elongation factors, is known to deliver aminoacyl-tRNAs to the ribosome (Dever et al. 2018). To validate the nanoLC/MS/MS analysis, FLAG-immunoprecipitants obtained from wild-type and *rpl36*-FLAG embryos at 24 hpf were subjected to immunoblotting analysis using antibodies against the three proteins. Immunoblotting analysis showed that these proteins were detected in the FLAG-immunoprecipitant of *rpl36*-FLAG embryos but not in the wild-type control, confirming copurification of these proteins with the FLAG-immunoprecipitated ribosomes (Figure 8B). These results indicated that mRNA-bound and translation-elongating ribosomes were purified by FLAG-immunoprecipitation. Taken together, I conclude that the *rpl36*-FLAG strain allows the purification of fully assembled and translation-engaging 80S ribosomes from zebrafish embryos by FLAG-immunoprecipitation.

Discussion

In this study, I generated a *rpl36*-FLAG strain for ribosome purification by the CRISPR-Cas9-mediated genome editing system and demonstrated that this strain allowed me to purify fully assembled and translation-engaging 80S ribosomes from zebrafish embryos at various developmental time-points by a simple FLAG-immunoprecipitation strategy (Figure 9).

The utility of the established ribosome purification system

The utility of the *rpl36*-FLAG strain for ribosome purification was validated by four approaches: RNA electrophoresis, immunoblotting analysis, protein staining, and nanoLC/MS/MS analysis. I and Dr. Koshi Imami revealed that components of ribosomal subunits and other translation-related proteins were detected in FLAG-immunoprecipitants. This result suggests that fully assembled and translation-engaging 80S ribosomes were successfully purified by the method I developed. In comparison to the standard ribosome purification methods employing sucrose gradient centrifugation, this method cannot provide any ribosomal subcomplex information but offers certain advantages, such as the simplicity of the experimental process, good reproducibility, and efficiency (20% of the input). To date, a transgenic zebrafish strain expressing an exogenous copy of EGFP-fused Rpl10a/uL1 was generated and utilized for purifying ribosome-associated mRNAs (Tryon et al. 2013). However, engineering an endogenous ribosomal gene locus with an epitope tag insertion has been challenging in zebrafish. The *rpl36*-FLAG strain I established here is the first example of tagging an endogenous ribosomal protein in zebrafish, enabling the purification of ribosomes with minimum perturbation of the stoichiometry of ribosomal proteins.

Application of the established ribosome purification system

The nanoLC/MS/MS analysis of FLAG-immunoprecipitants identified about 400 proteins copurified with ribosomes. This dataset and the follow-up immunoblotting experiment revealed the copurification of mRNA-associated proteins, such as Pabpc1 and Ddx6, indicating that mRNA-bound ribosomes were purified by the FLAG-immunoprecipitation. Therefore, by combining the FLAG-immunoprecipitation of *rpl36*-FLAG embryos with RNA-sequencing or real-time PCR, it will be possible to analyze the translational status of mRNAs as previously reported (Tryon et al. 2013). Moreover, the dataset included proteins related to phosphorylation, UFMylation, SUMOylation, and ubiquitination. Given that post-translational modifications on the ribosome are emerging as dynamic events in response to multiple stimuli and stress (Xue and Barna 2012; Simsek and Barna 2017), these copurified proteins may contribute to ribosome heterogeneity and generate functional diversity of ribosomes. Therefore, the *rpl36*-FLAG strain will accelerate the analysis of ribosome modifications, ribosome components, ribosome-associated proteins, and ribosome-associated mRNAs in

development.

Limitation of the established ribosome purification system

Although the *rpl36*-FLAG strain enables the purification of ribosomes rapidly, reliably, and efficiently by a simple FLAG-immunoprecipitation strategy, there are several caveats of this ribosome purification system. First, although enough (20% of the input), the efficiency of ribosome purification using this established system is limited. Given that very large polysomes are not effectively purified using the affinity resin in yeast (Inada et al. 2002), this system also may have technical difficulties in purifying specific ribosomal subcomplexes. Technical improvement to further upgrade ribosome purification efficiency is needed. Second, the solvent-exposed surface of the ribosome acts as a platform for interacting with various factors, such as mRNAs, tRNAs, synthesized nascent polypeptide chains (Yusupova and Yusupov 2014), folding factors (Deuerling et al. 2019; Gamerdinger et al. 2019), initiation factors (Aitken and Lorsch 2012), elongation factors (Dever et al. 2018), and termination factors (Hellen 2018) during the translation process. In addition to the interaction of the canonical translation factors, the solvent-exposed surface of the ribosome may provide an interface for yet uncharacterized ribosome-associated proteins. Epitope tagging for Rpl36/eL36, which locates the solvent-exposed side of the ribosome (Yusupova and Yusupov 2014), might perturb such interactions. In this aspect, it is uncertain whether the ribosome containing Rpl36-FLAG is functionally identical to the wild-type ribosome. Third, if ribosomes lacking Rpl36/eL36 are present in a tissue- or subcellular environment-specific manner, the present system cannot purify such ribosomes. Indeed, it is suggested that ribosomes lacking Rpl36/eL36 are temporarily present in rat neuropil (Fusco et al. 2021). In rat neuropil, newly synthesized Rpl36/eL36 is incorporated into mature ribosomes more frequently than other ribosomal proteins. As the incorporation occurs independently of the canonical ribosome biogenesis pathway, Rpl36/eL36 might be repaired or remodeled after the initial assembly of the large ribosomal subunit. Therefore, to purify ribosomes comprehensively, an additional strain that expresses epitope-tagged ribosomal proteins other than Rpl36/eL36 is awaited in the future.

Chapter 2: Znf598-mediated Rps10/eS10 ubiquitination contributes to the ribosome ubiquitination dynamics during zebrafish development

Introduction

Ubiquitin is a highly conserved 76 amino acid protein that is covalently and reversibly bonded to substrate proteins. Ubiquitin is attached to substrate proteins either in a monomeric form (monoubiquitination) or as a long chain of multiple ubiquitin molecules (polyubiquitination) (Dougherty et al. 2020; Komander and Rape 2012). A ubiquitin moiety contains seven lysine and an N-terminal methionine residues, which are targets for polyubiquitination. Hence, different types of ubiquitin chains are formed depending on the ubiquitin-conjugated site (Akutsu et al. 2016). Ubiquitination is catalyzed by a cascade of specific enzymes, including an activating enzyme (E1), a conjugating enzyme (E2), and a ligase (E3). E1 activates free ubiquitin in an ATP-dependent manner in the initial step of this enzymatic cascade. Following the activation by an E1, ubiquitin is transferred to an E2. Lastly, an E3 recognizes the ubiquitin-conjugating E2 and selects a target protein for specific catalysis of the ubiquitination (Dougherty et al. 2020; Komander and Rape 2012). In contrast, the removal of ubiquitin from a target protein, deubiquitination, is catalyzed by deubiquitinating enzymes (DUBs) (Clague et al. 2019; Tanguturi et al. 2020). It is known that there are around 20 DUBs in yeast and nearly 100 DUBs in mammalian cells, and each DUB targets specific proteins and ubiquitin chain types. Although ubiquitination was initially characterized as a signal for protein degradation via the proteasome system (Johnson et al. 1992), accumulating studies have shown its additional functions to regulate multiple processes by inducing structural changes, altering protein localization, and regulating protein-protein interactions (Song and Luo 2019). In addition, it has been estimated that ubiquitination occurs on more than 9000 distinct proteins, which is equal to ~50% of the human proteome, in mammalian cells (Kim et al. 2011; Rose et al. 2016). Furthermore, ubiquitination defects have been linked to several diseases, including neurodegenerative diseases (Tramutola et al. 2018; Walden and Muqit 2017) and several types of cancer (Borg and Dixit 2017; Liu et al. 2015). Owing to advancements in mass spectrometry and cryo-EM, we now know that several ribosomal proteins are targets for ubiquitination (Monem and Arribere 2023). Current research is elucidating multiple roles of ribosome ubiquitination, including ribosome degradation (An and Harper 2020; Li et al. 2022b; Sugiyama et al. 2019), quality control pathway to maintain proteostasis (Inada 2020; Joazeiro 2017, 2019), and modulation of translation in response to stress conditions (Matsuki et al. 2020).

Cell cycle-dependent ubiquitination on a ribosomal protein is the first example of ribosome ubiquitination discovered. In yeast, ribosomal protein Rpl28/uL15 is highly ubiquitinated during the S phase of the cell cycle, while this ubiquitination is reduced in the G1 phase of the cell cycle (Spence et al. 2000). Although the biological relevance of this ubiquitination has been unclear, this cell cycle-dependent ubiquitination event is highly conserved in humans.

Emerging studies have emphasized the significance of ribosome ubiquitination in the quality control of translationally arrested ribosomes and peptides, faulty mRNAs, and nonfunctional

translation machinery. When a ribosome slows aberrantly during translation, it collides with the trailing ribosome to form a specific structure called disome (Ikeuchi et al. 2019; Juszkiewicz et al. 2018). Ribosome collision and disome formation trigger the ribosome-associated quality control (RQC) pathway, which dissociates stalled ribosomes into ribosomal subunits and degrades nascent polypeptides (Inada 2020; Joazeiro 2017, 2019). The site-specific ubiquitination of the 40S ribosomal proteins Rps10/eS10 and Rps20/uS10 in the disome initiates the RQC pathway (Garzia et al. 2017; Juszkiewicz and Hegde 2017; Matsuo et al. 2017; Sundaramoorthy et al. 2017). These reactions are catalyzed by an E3 ubiquitin ligase ZNF598 (Hel2 in yeast), which recognizes the disome structure by an unknown mechanism (Juszkiewicz et al. 2018; Juszkiewicz and Hegde 2017; Matsuo et al. 2017; Sundaramoorthy et al. 2017; Garzia et al. 2017). Ubiquitinated forms of Rps10/eS10 and/or Rps20/uS10 are recognized by the ASC-1 complex (also known as RQT complex in yeast), in which an ATP-dependent RNA helicase ASCC3 (Slh1/Rqt2 in yeast) dissociates the stalled ribosome into ribosomal subunits (Matsuo et al. 2017; Juszkiewicz et al. 2020b; Matsuo et al. 2020; Narita et al. 2022; Sitron et al. 2017). Another E3 ubiquitin ligase, Ltn1, polyubiquitinates a nascent polypeptide in the split 60S ribosomal subunit, which is then degraded by the proteasome (Bengtson and Joazeiro 2010; Brandman et al. 2012; Shao and Hegde 2014). The Rps10/eS10 and/or Rps20/uS10 ubiquitination also promotes endonucleolytic cleavage of the mRNA with the stalled ribosome, known as no-go decay (NGD) (Ikeuchi et al. 2019; D'Orazio et al. 2019; Glover et al. 2020). In addition to the RQC and NGD pathways, an E3 ubiquitin ligase called RNF10 (Mag2 in yeast) ubiquitinates the 40S ribosomal proteins Rps2/uS5 and Rps3/uS3 in response to decoding and initiation/elongation abnormalities. This results in the degradation of 40S ribosomal subunits (Li et al. 2022b; Sugiyama et al. 2019; Garzia et al. 2021). Monoubiquitination of Rps3/uS3 by Mag2 is followed by polyubiquitination by Fap1, Rsp5, and Hel2, leading to 18S nonfunctional rRNA decay (18S NRD) (Sugiyama et al. 2019; Li et al. 2022b). More recently, it was revealed that dysfunctional eEF1a and eRF1, which induce ribosome stalling, are degraded by two E3 ubiquitin ligases, RNF14 and RNF25. These degradation events depend on Rps27a/eS31 ubiquitination by RNF25 (Oltion et al. 2023). Overall, these ribosome ubiquitination pathways maintain cellular proteostasis and protect the eukaryotic translation system against a variety of translational problems.

Ribosome ubiquitination is strongly induced under environmentally stressed conditions. In yeast, ER stress enhances the level of Rps7/eS7 ubiquitination. The Rps7/eS7 ubiquitination upregulates and downregulates the translational efficiency of *HAC1* mRNA and *HNT1* mRNA, respectively (Matsuki et al. 2020). Not limited to Rps7/eS7 ubiquitination, ER stressors induce other site-specific ubiquitination on ribosomal proteins, and this phenomenon is conserved among humans, flies, and yeast (Higgins et al. 2015). Although their biological relevance remains largely unknown, the lack of ubiquitination of Rps2/uS5 and Rps20/uS10 activates cell death in ER-stressed conditions (Higgins et al. 2015). This observation suggests that ribosome ubiquitination represents an important

regulatory mechanism in ER stress. In another example, 78 sites on 37 ribosomal proteins are heavily ubiquitinated under oxidative stress in yeast, and these ubiquitinated proteins are rapidly deubiquitinated during recovery from stress (Back et al. 2019). Forty-five of these sites are located on the head of the small subunit, which interacts with translational regulators, such as initiation factors and elongation factors, as well as mRNA and tRNA molecules (Schmitt et al. 2021). Hence, the oxidative stress-dependent ribosome ubiquitination events are supposed to be important regulators of translational control.

Because the ribosome can serve as an important amino acid source, it is degraded in specific physiological settings, such as nutrient stress and specific cell lineages. The ribosome degradation is mediated by the proteasome system or autophagy systems (An and Harper 2020). Both mechanisms are regulated by ribosome ubiquitination. For example, in yeast, an E3 ubiquitin ligase Ltn1 ubiquitinates Rpl23a/uL23 and prevents ribosome degradation in normal nutrient-rich conditions. In contrast, upon nutrient starvation, a DUB Ubp3 removes the ubiquitin from Rpl23a/uL23. This deubiquitination event leads to the selective sequestration of the 60S ribosomal subunits by autophagic membranes through an unknown mechanism (An and Harper 2020). During reticulocyte maturation, ribosomes are eliminated via the ubiquitin-proteasome system (Glowacki and Millette 1965). A hybrid E2-E3 enzyme UBE2O is thought as a major factor in this process. UBE2O recognizes ribosomal proteins in either their free or assembled state and targets them to proteasomes for degradation (Nguyen et al. 2017). UBE2O-deficient mice result in anemia characterized by small erythrocyte cells with low hemoglobin content, indicating that ribosome ubiquitination is a key aspect of reticulocyte maturation (Nguyen et al. 2017).

As mentioned above, the ubiquitination status of the ribosome changes dynamically in response to intracellular and extracellular stimuli and thus provides a clue to understanding the cellular condition. Therefore, a study of ribosome ubiquitination has the potential to expand our biological knowledge and establish a novel therapeutical tool. However, little is known about the dynamics of ribosome ubiquitination during the normal life cycle of multicellular animals due to the lack of studies using multicellular organisms. In the present study, by combining the ribosome purification system established in Chapter 1 with immunoblotting analysis, I detected the dynamic change of ribosome ubiquitination levels during zebrafish development. Furthermore, Dr. Koshi Imami and I revealed that Rps10/eS10 is one of the ribosomal proteins that is dynamically ubiquitinated during development. Given that the mutations on Rps10/eS10 ubiquitination sites reduced the overall ubiquitination pattern of ribosomes, I conclude that ribosomes are ubiquitinated in a hierarchical manner. Rps10/eS10 ubiquitination has a critical role in forming the unique ubiquitination pattern of ribosomes directly and indirectly. With these results, I discuss the potential mechanisms that induce this ubiquitination pattern of ribosomes during development. I also mention the potential biological relevance of this ribosome ubiquitination in development.

Results

Ribosome ubiquitination was detected under physiological and translational stress conditions in zebrafish embryos

To assess the utility of the ribosome purification system established in Chapter 1 for analyzing ribosome ubiquitination, I performed immunoblotting analysis using an anti-Ubiquitin antibody on cell lysates and FLAG-immunoprecipitants obtained from 24 hpf wild-type and *rpl36*-FLAG embryos (Figure 10A). In these experiments, the purification efficiency of ribosomes was confirmed by protein staining. While the ubiquitination pattern was comparable between the two strains in cell lysates (input), several ubiquitination signals were specifically detected in the FLAG-immunoprecipitant from *rpl36*-FLAG embryos (Figure 10A). Because the FLAG-immunoprecipitant contained not only components of ribosomes but also ribosome- or mRNA-associated proteins as mentioned in Chapter 1 (Figure 8), I wondered if the ubiquitination signals in the FLAG-immunoprecipitant were derived from ribosomal proteins. Therefore, I performed FLAG-immunoprecipitation using the high-salt wash buffer to minimize the copurification of ribosome- and mRNA-associated proteins, followed by immunoblotting analysis using an anti-Ubiquitin antibody (Figure 10B and C). As expected, in physiological salt concentration (150 mM NaCl), Ddx6 and Pabpc1, mRNA-associated proteins, and eEF1a that binds ribosomes, were detected in FLAG-immunoprecipitant. However, when the FLAG-immunoprecipitant was washed vigorously (400 mM NaCl), I found that Ddx6 and eEF1a were not copurified (Figure 10B). Notably, even in this high-salt wash condition, the ubiquitination signals of the FLAG-immunoprecipitant remained unchanged (Figure 10C). Although there was a possibility that some ubiquitination signals originated from proteins that were closely associated with the ribosome, such as Pabpc1 (Figure 10B), I assumed that the majority of signals were caused by the ubiquitination of core ribosomal proteins.

Accumulating studies have highlighted that ribosomes are subjected to ubiquitination upon translational stresses (Higgins et al. 2015; Juszkiewicz et al. 2018; Garzia et al. 2021; Oltion et al. 2023; Garshott et al. 2021; Simms et al. 2017). I thus further investigated whether this ribosome purification system could detect ribosome ubiquitination triggered by translation inhibitors known to enhance ribosome ubiquitination. A translation initiation inhibitor harringtonine (HTN) causes Rps2/uS5 and Rps3/uS3 ubiquitination, presumably due to ribosome stalling on the initiation codon (Garzia et al. 2021; Garshott et al. 2021). Following these reports, I treated *rpl36*-FLAG embryos at 23 hpf with different concentrations of HTN for an hour. The 24 hpf embryos were subjected to FLAG-immunoprecipitation followed by immunoblotting analysis with an anti-Ubiquitin antibody (Figure 11A). A significant dose-dependent increase in ubiquitination signals was caused by HTN treatment. I assumed that HTN caused ribosome stalling on the initiation codon, thereby inducing ribosome ubiquitination, as observed in mammalian cells (Garzia et al. 2021; Garshott et al. 2021). Likewise, I

next treated *rpl36*-FLAG embryos at 22 hpf with a translation elongation inhibitor cycloheximide (CHX) for two hours and then analyzed the FLAG-immunoprecipitants from the 24 hpf embryos with an anti-Ubiquitin antibody (Figure 11B). Treatment of elongation inhibitors with intermediate concentrations causes ribosome collisions and induces Rps10/eS10 and Rps3/uS3 ubiquitination (Juszkiewicz et al. 2018; Simms et al. 2017). In fact, I observed that ubiquitination signals were upregulated as CHX concentration increased, reaching the maximum intensity at 80-320 μg/mL. The signals decreased at the highest concentration (1280 μg/mL), probably because the majority of ribosomes stalled at this concentration and fewer collisions were induced, as observed in other organisms (Juszkiewicz et al. 2018).

As an alternative approach, I took advantage of a GGQ motif mutant of eukaryotic release factor (eRF1-AAQ) that stalls the ribosome on termination codons and induces Rps10/eS10 ubiquitination (Frolova et al. 1999; Juszkiewicz et al. 2018a). Eggs from the *rpl36*-FLAG strain were injected with mRNAs encoding C-terminally Hemagglutinin (HA)-tagged wild-type Etf1b (a zebrafish orthologue of eRF1) or Etf1b-AAQ mutant (Figure 11C). Then I analyzed the FLAG-immunoprecipitants obtained from the 6 hpf embryos with an anti-Ubiquitin antibody. As expected, ubiquitination signals increased at 6 hpf when eRF1-AAQ was injected, while there was little or no change in the presence of wild-type eRF1 (Figure 11D). These results indicate that, like other organisms, zebrafish embryos exhibit fluctuations in ribosome ubiquitination levels in response to translational stresses. The present FLAG-immunoprecipitation system is thus suitable for monitoring the dynamics of ribosome ubiquitination occurring in zebrafish embryos.

Ribosome ubiquitination levels change during zebrafish development

In order to detect and compare ribosome ubiquitination levels at different developmental time-points, I purified ribosomes from embryonic (0 hpf to 2 dpf) and larval (3 dpf to 7 dpf) stages and analyzed them with an anti-Ubiquitin antibody. I found that ribosome ubiquitination signals temporally changed during development (Figure 12A and B). Although it was most noticeable in the signal above 25 kDa (Figure 12A, arrowhead), this tendency was present in all the signals detected between 25 kDa and 50 kDa (Figure 12A, bracket). To quantify the ribosome ubiquitination levels among different developmental time-points, I normalized the ubiquitination signals between 25-50 kDa by the corresponding signals detected in protein staining (Figure 12B). Immediately after spawning (0 hpf), the level of ribosome ubiquitination was low; but as development proceeded, it gradually increased. The ubiquitination level reached the maximum intensity at 24 hpf and then decreased toward 7 dpf (Figure 12B). These findings indicate that during development, the level of ribosome ubiquitination fluctuates.

To understand the characteristics of the ubiquitination signals in detail, I investigated which ribosomal subunit was linked with the detected ubiquitination signals. As the ribosome is bound to

239 Mg^{2+} ions that help in stabilizing the negative charges of rRNA residues (Dastidar and Nair 2022), EDTA treatment dissociates the 80S ribosome into the 40S and 60S ribosomal subunits. Hence, in the presence of EDTA, only 60S ribosomal subunits should be purified in the present ribosome purification system because the FLAG-tag was attached to the 60S ribosomal protein Rpl36/eL36. Based on this logic, I reasoned that the ubiquitination signal(s) that remained in the presence of EDTA represents the ubiquitination of the 60S ribosomal subunit. Conversely, the ubiquitination signal(s) that disappeared in the presence of EDTA should represent the ubiquitination of the 40S ribosomal subunit (Figure 13A). I performed FLAG-immunoprecipitation using the EDTA-containing and $MgCl_2$-free buffer to dissociate 80S ribosomes into 40S and 60S ribosomal subunits. As expected, components of the 60S ribosomal subunit were selectively purified in the presence of EDTA (Figure 13B). The amount of the purified 60S ribosomal subunits reduced to approximately 25%-50% compared to the yield in the absence of EDTA, suggesting that the ribosomes purified in the absence of EDTA contained 80S ribosomes forming polysomes. I thus compared the ubiquitination signals linked with the purified 60S ribosomal subunits (+EDTA) to that of serial dilutions of 80S ribosomes (-EDTA) and found that most of the signals were not detected in the purified 60S ribosomal subunits (Figure 13C). Only the signal around 50 kDa remained in the +EDTA condition, indicating that this signal was derived from the 60S ribosomal subunit (Figure 13C, arrowhead). Remarkably, EDTA *per se* did not reduce ubiquitination signals artificially, because the signals were retained when the FLAG-immunoprecipitant was prepared in the EDTA-free condition and then incubated with EDTA (Figure 13D). Hence, most ubiquitination signals were associated with the 80S ribosome in a 40S ribosomal subunit-dependent manner. These findings suggest that during zebrafish development, components of the 40S ribosomal subunit are differently ubiquitinated.

Znf598 promotes ribosome ubiquitination during development

Several E3 ubiquitin ligases ubiquitinate ribosomal proteins in the 40S ribosomal subunit (Garzia et al. 2017, 2021; Juszkiewicz et al. 2018; Li et al. 2022b; Oltion et al. 2023; Panasenko and Collart 2012; Sugiyama et al. 2019). Unfortunately, the initial nanoLC/MS/MS analysis in Chapter 1 detected no E3 ubiquitin ligases known to ubiquitinate ribosomal proteins probably due to technical limitations. Emerging work has highlighted that an E3 ubiquitin ligase ZNF598 ubiquitinates Rps10/eS10 and Rps20/uS10, components of the 40S ribosomal subunit, and revealed its critical role in the RQC pathway (Sundaramoorthy et al. 2017; Garzia et al. 2017). Since Dr. Yuichiro Mishima had already generated a *znf598* mutant zebrafish strain (Mishima et al. 2022), I utilized this strain to investigate whether Znf598 contributes to ribosome ubiquitination during zebrafish development. To purify ribosomes from the *znf598* mutant strain by FLAG-immunoprecipitation, I crossed the *rpl36*-FLAG strain with the *znf598* mutant strain and obtained fish carrying heterozygous *rpl36*-FLAG allele and homozygous *znf598* mutant allele. Crossing female and male of this genotype, I obtained maternal-

zygotic *znf598* (MZ*znf598*) mutant embryos expressing Rpl36-FLAG (hereafter called MZ*znf598*; *rpl36*-FLAG embryos). Then, to compare the ubiquitination status of ribosomes, I performed FLAG-immunoprecipitation using MZ*znf*598; *rpl36*-FLAG embryos and *rpl36*-FLAG embryos at 0 and 24 hpf followed by immunoblotting analysis with an anti-Ubiquitin antibody (Figure 14A). I normalized the ubiquitination signals by the corresponding protein abundance (Figure 14B). I found that although the initial ubiquitination levels at 0 hpf were comparable, the increase of the ubiquitination level at 24 hpf was attenuated in MZ*znf598*; *rpl36*-FLAG embryos (Figure 14A and B). To investigate whether overexpressing Znf598 increased the ubiquitination level of ribosomes, I injected mRNAs encoding C-terminally Myc-tagged wild-type Znf598 or catalytic domain-mutated Znf598 (the 13th and 16th cysteine residues were substituted with alanine residues; C13/16A) into *rpl36*-FLAG eggs (Figure 14C). The ubiquitination level was increased by overexpression of wild-type Znf598 but not by that of mutated Znf598, indicating that Znf598 ubiquitination activity was required for the upregulation of the ubiquitination level (Figure 14D and E). These results indicate that Znf598 enhances ribosome ubiquitination during zebrafish development.

Znf598 ubiquitinates the 139th and 140th lysine residues of Rps10/eS10 in zebrafish embryos

Next, I tried identifying ribosomal protein(s) that was ubiquitinated by Znf598 during zebrafish development. Due to the low ubiquitination levels of ribosomal proteins, the nanoLC/MS/MS analysis with FLAG-immunoprecipitants obtained from 0 to 24 hpf embryos in Chapter 1 was unable to identify ubiquitinated ribosomal proteins reliably. Therefore, I overexpressed Znf598 by mRNA injection experiment to maximize the ubiquitination level at 24 hpf and subsequently performed the FLAG-immunoprecipitation (Figure 15A). The FLAG-immunoprecipitants with or without Znf598 overexpression were subjected to nanoLC/MS/MS analysis by Dr. Koshi Imami. To identify the ubiquitinated ribosomal protein(s), he adopted a commonly used mass spectrometry technique (Peng et al. 2003). Briefly, when proteins are digested with trypsin protease, a di-glycyl motif derived from the C-terminus of Ubiquitin is covalently left on a lysine residue of a target peptide via an isopeptide bond. This signature of ubiquitinated peptide causes a mass shift at the lysine residue of 114.1 Da and is used to determine the ubiquitination sites on proteins. He detected the MS/MS spectrum of an Rps10/eS10 peptide with a di-glycine remnant at the 139th lysine residue in two independent Znf598 overexpression samples (Figure 15B). Furthermore, the quantity of the peptide was increased in the Znf598 overexpression samples compared to the control samples (Figure 15C). To examine whether Rps10/eS10 was indeed ubiquitinated at 24 hpf in a Znf598-dependent manner, I purified ribosomes and detected Rps10/eS10 by immunoblotting analysis in three conditions: *rpl36*-FLAG, *rpl36*-FLAG with Znf598 overexpression, and MZ*znf598*; *rpl36*-FLAG (Figure 15D and E). The major signal that appeared below 20 kDa (Figure 15E, left) was consistent with the predicted molecular weight of zebrafish Rps10/eS10 (18.9 kDa). Additionally, in *rpl36*-FLAG embryos, a minor signal above 25 kDa

was detected, which I ascribed to monoubiquitinated Rps10/eS10. Overexpression of Znf598 increased this minor signal and induced an additional slower migrating signal attributable to Rps10/eS10 attached with two ubiquitin molecules. By contrast, these additional signals were not detected in MZ*znf598*; *rpl36*-FLAG embryos. The same result was observed with exogenously expressed Rps10/eS10 with an HA-tag at the C-terminus (Figure 16A and B). These results indicate that Rps10/eS10 is ubiquitinated at 24 hpf in a Znf598-dependent manner.

The nanoLC/MS/MS analysis detected the 139th lysine residue in Rps10/eS10 as a potential ubiquitination site by Znf598 in zebrafish. However, because trypsin proteolysis cannot occur at the modified lysine residues (Burke et al. 2015), there was a technical limitation to detect Rps10/eS10 peptides with di-glycine remnants both at the 139th and 140th lysine residues. Given that both the 138th and 139th lysine residues (corresponding to the 139th and 140th lysine residues in zebrafish) are ubiquitinated in a ZNF598-dependent manner in mammals (Sundaramoorthy et al. 2017; Garzia et al. 2017), follow-up examination was needed to identify ubiquitination site(s) precisely. To validate ubiquitination site(s) in zebrafish Rps10/eS10 further, I took advantage of the Rps10-HA overexpression experiment (Figure 16A and B). I substituted the 139th and/or 140th lysine residue with an arginine residue in Rps10-HA and overexpressed the resultants in *rpl36*-FLAG embryos. The obtained FLAG-immunoprecipitants were analyzed with an anti-HA antibody. I found that the ubiquitinated signal of Rps10-HA was not detectable in K139R single and K139/140R double mutants (Figure 16C). In contrast, the K140R single mutant reduced the ubiquitinated signal only marginally. From these results, I conclude that the 139th lysine residue in Rps10/eS10 is a major ubiquitination site by Znf598 in zebrafish embryos, although I cannot rule out the possibility that the 140th lysine residue serves as an additional ubiquitination site.

Rps10/eS10 ubiquitination is crucial for establishing the overall ribosome ubiquitination pattern during zebrafish development

To further examine the contribution of Rps10/eS10 ubiquitination to the overall ribosome ubiquitination pattern during development, I generated a zebrafish strain with mutated ubiquitination sites in Rps10/eS10 by the CRISPR-Cas9-mediated genome editing system. I synthesized a sgRNA that recognizes the genome sequence at the exon 5 of the *rps10* gene locus and designed a ssODN harboring substitution of lysine 139 and 140 codons with arginine codons. Similar to the *rpl36*-FLAG strain, the sgRNA/Cas9 complex was co-injected into zebrafish eggs with the ssODN. The precise editing in germline cells was assessed by genotyping PCR followed by TA cloning and Sanger sequencing. As a result, a strain carrying a precisely edited *rps10* gene was obtained (*rps10* K139/140R) (Figure 17A). Homozygous *rps10* K139/140R fish reached adulthood, and I obtained a homozygous *rps10* K139/140R strain with a heterozygous *rpl36*-FLAG allele. In order to examine whether Znf598 is unable to ubiquitinate Rps10/eS10 in the *rps10* K139/140R strain, I purified

ribosomes from *rpl36*-FLAG and *rps10* K139/140R; *rpl36*-FLAG embryos at 24 hpf with or without Znf598 overexpression and analyzed with an anti-Rps10 antibody. Consistent with the experiments using Rps10-HA (Figure 16C), the ubiquitinated signals of endogenous Rps10/eS10 were not detected in ribosomes purified from the *rps10* K139/140R; *rpl36*-FLAG embryos even with Znf598 overexpression (Figure 17B and C). Hence, I conclude that Rps10/eS10 ubiquitination by Znf598 does not occur in the *rps10* K139/140R strain. The established *rps10* K139/140R strain provides an opportunity to investigate the role of Rps10/eS10 ubiquitination in forming the characteristic ribosome ubiquitination pattern during development.

To analyze the contribution of Rps10/eS10 ubiquitination on the overall ubiquitination pattern of the ribosome, I purified ribosomes using 24 hpf embryos obtained from three strains; *rpl36*-FLAG, *rps10* K139/140R; *rpl36*-FLAG, and MZ*znf598*; *rpl36*-FLAG strains. Then, the ribosomes were analyzed with an anti-Ubiquitin antibody. Similar to the ribosomes purified from MZ*znf598*; *rpl36*-FLAG embryos, multiple ubiquitination signals were attenuated in ribosomes purified from *rps10* K139/140R; *rpl36*-FLAG embryos compared to ribosomes containing wild-type Rps10/eS10 (Figure 18A). Considering the molecular weight of the ubiquitinated Rps10/eS10 forms detected in the Rps10/eS10 immunoblotting analysis (Figure 17C), two ubiquitination signals were attributable to ubiquitinated forms of Rps10/eS10 (Figure 18A, black arrowheads). Indeed, the signal probably derived from the Rps10/eS10 with two ubiquitin molecules was not detected in *rps10* K139/140R; *rpl36*-FLAG and MZ*znf598*; *rpl36*-FLAG embryos. The signal probably derived from the monoubiquitinated Rps10/eS10 was reduced but still present in both *rps10* K139/140R; *rpl36*-FLAG and MZ*znf598*; *rpl36*-FLAG embryos, likely due to an overlap with other ubiquitinated protein(s). Notably, intensities of three additional signals were also reduced in *rps10* K139/140R; *rpl36*-FLAG and MZ*znf598*; *rpl36*-FLAG embryos (Figure 18A, white arrowheads). These results suggest that the level of Rps10/eS10 ubiquitination dynamically changes during development, and this ubiquitination is required for further ubiquitination events on other ribosomal proteins.

The overall ubiquitination pattern on ribosomes is formed in a hierarchical manner

It is plausible to speculate that there are additional ribosomal proteins that are ubiquitinated dependent on Znf598-mediated Rps10/eS10 ubiquitination. In mammalian cells, some hierarchical rule of ribosome ubiquitination events was reported. For example, ubiquitination levels of Rps20/uS10 and Rps3/uS3 are reduced in the absence of Rps10/eS10 ubiquitination (Garshott et al. 2020; Meyer et al. 2020). Similarly, the ubiquitination of Rps3/uS3 is necessary for the ubiquitination of Rps2/uS5 (Meyer et al. 2020). From these previous studies, I focused on Rps20/uS10, Rps3/uS3, and Rps2/uS5 to further analyze the hierarchical ubiquitination events. To investigate the ubiquitination levels of these ribosomal proteins, HA-tagged Rps20/uS10, Rps3/uS3, and Rps2/uS5 were overexpressed in *rpl36*-FLAG and *rps10* K139/140R; *rpl36*-FLAG embryos. The 24 hpf embryos were subjected to

FLAG-immunoprecipitation followed by immunoblotting analysis with an anti-HA antibody (Figure 19A-C). I observed that the exogenously overexpressed ribosomal proteins were incorporated into 80S ribosomes at the comparable level between *rpl36*-FLAG and *rps10* K139/140R; *rpl36*-FLAG embryos. Furthermore, these ribosomal proteins were ubiquitinated in *rpl36*-FLAG embryos at 24 hpf. However, their ubiquitinated signals were barely detectable in *rps10* K139/140R; *rpl36*-FLAG embryos, indicating that Rps20/uS10, Rps3/uS3, and Rps2/uS5 ubiquitination was dependent on Rps10/eS10 ubiquitination (Figure 19A-C). Although I could not characterize the identity of each attenuated ubiquitination signal detected by an anti-Ubiquitin antibody in *rps10* K139/140R; *rpl36*-FLAG and MZ*znf598*; *rpl36*-FLAG embryos (Figure 18A), these signals may represent Rps20/uS10, Rps3/uS3, and Rps2/uS5 ubiquitination.

To further test the requirement of Znf598-mediated Rps10/eS10 ubiquitination for establishing the entire ubiquitination pattern of the ribosome, I performed two experiments. First, I compared the ubiquitination patterns in *rpl36*-FLAG and *rps10* K139/140R; *rpl36*-FLAG embryos under the Znf598-overexpressed condition. I purified ribosomes from *rpl36*-FLAG and *rps10* K139/140R; *rpl36*-FLAG embryos at 24 hpf with or without Znf598 overexpression and analyzed them with an anti-Ubiquitin antibody. Similar to the results in Figure 14E, multiple ubiquitination signals were enhanced by overexpression of Znf598 in *rpl36*-FLAG embryos. However, the increase of these signals was significantly suppressed in *rps10* K139/140R; *rpl36*-FLAG embryos (Figure 20A). Second, I investigated the ubiquitination levels under translationally stressed conditions in *rpl36*-FLAG, *rps10* K139/140R; *rpl36*-FLAG, and MZ*znf598*; *rpl36*-FLAG embryos (Figure 20B-E). When I treated embryos from the three strains with HTN at the highest concentration, which maximized the ubiquitination signals in Figure 11A, I found that HTN treatment increased ribosome ubiquitination levels in *rps10* K139/140R; *rpl36*-FLAG and MZ*znf598*; *rpl36*-FLAG embryos comparable to *rpl36*-FLAG embryos (Figure 20B). By contrast, under CHX treatment with the intermediate concentration, which maximally increased ubiquitination signals in Figure 11B, the enhancement of ribosome ubiquitination levels in both *rps10* K139/140R; *rpl36*-FLAG and MZ*znf598*; *rpl36*-FLAG embryos were attenuated (Figure 20C). Likewise, the increase of ribosome ubiquitination induced by eRF1-AAQ overexpression was suppressed in both *rps10* K139/140R; *rpl36*-FLAG and MZ*znf598*; *rpl36*-FLAG embryos albeit to different extents (Figure 20D and E). Taken together, these results further support my assumption that Rps10/eS10 ubiquitination is a prerequisite for multiple ubiquitination events promoted by Znf598.

The level of Rps10/eS10 ubiquitination dynamically changes during zebrafish development

Given the critical role of Znf598-mediated Rps10/eS10 ubiquitination for establishing the overall ribosome ubiquitination pattern at 24 hpf, I wondered if Rps10/eS10 ubiquitination *per se* fluctuates during development. To test this possibility, I purified ribosomes using *rpl36*-FLAG and *rps10*

K139/140R; *rpl36*-FLAG embryos from 0 to 24 hpf. Then the ribosomes were subjected to immunoblotting analysis with an anti-Rps10 antibody. At 0 hpf, the monoubiquitinated Rps10/eS10 signal was barely detectable; however, it gradually increased until 24 hpf in *rpl36*-FLAG embryos, mirroring the increase in the whole ribosome ubiquitination levels (Figure 21A and 12A). These Rps10/eS10 monoubiquitinated signals were completely abolished in *rps10* K139/140R; *rpl36*-FLAG embryos (Figure 21A). To examine the Rps10/eS10 ubiquitination level at various developmental time-points, I purified and analyzed the ribosomes from *rpl36*-FLAG embryos and larvae. The Rps10/eS10 monoubiquitination levels peaked between 1 and 3 dpf and gradually decreased toward 7 dpf (Figure 21B), similar to the whole ribosome ubiquitination levels (Figure 12A). Together, these results demonstrate that Rps10/eS10 ubiquitination by Znf598 occurs dynamically after fertilization and contributes directly and indirectly to establishing the overall ribosome ubiquitination pattern during zebrafish development.

Discussion

Advances in mass spectrometry have identified many ubiquitination events on ribosomal proteins (Monem and Arribere 2023). A growing body of literature has shown ribosome ubiquitination's ability to regulate multiple processes besides ribosome degradation (Back et al. 2019; Higgins et al. 2015; Matsuki et al. 2020; Silva et al. 2015; Spence et al. 2000; Takehara et al. 2021; Inada 2020; Joazeiro 2017, 2019). However, before this study, it was not clear to what extent the dynamics of ribosome ubiquitination occurred in physiological conditions in multicellular animals, because ribosome ubiquitination has been studied mainly in cultured cells and yeast under artificially stressed conditions. In this study, I and Dr. Koshi Imami detected ribosome ubiquitination in zebrafish embryos by combining the ribosome purification system with immunoblotting analysis using an anti-Ubiquitin antibody and nanoLC/MS/MS analysis (Figure 22A). My immunoblotting analysis showed a dynamic nature of ribosome ubiquitination during zebrafish development. Follow-up analysis revealed that an E3 ubiquitin ligase Znf598 contributes to the detected ubiquitination dynamics. Dr. Koshi Imami and I identified the 139th and 140th lysine residues of Rps10/eS10 as ubiquitination target sites of Znf598. Lastly, I found that Znf598-mediated Rps10/eS10 ubiquitination has a critical role in establishing the entire ribosome ubiquitination pattern directly and indirectly (Figure 22B). From these results, the present study demonstrated for the first time that Rps10/eS10 is dynamically ubiquitinated in the normal developmental process.

The possible molecular mechanism changing ribosome ubiquitination level during development

The ubiquitination level of ribosomes was at its lowest just after spawning, indicating that ribosomes in eggs are mostly stored without ubiquitination. Before fertilization, global translation is silenced, and ribosomes are kept in a dormant state (Leesch et al. 2023). The cotranslational ubiquitination pathways should not be at work in such a situation. Hence, the low level of ribosome ubiquitination in eggs may reflect the absence of cotranslational ribosome ubiquitination during oogenesis. Because ubiquitination events occur at a balance between ubiquitin ligases and DUBs (Clague et al. 2019), the activity of ribosome DUBs is another factor that might generate a low ubiquitination level in eggs. Indeed, several DUBs, such as USP10, OTUD1, USP21, and OTUD3, are related to deubiquitination events on ribosomes (Garshott et al. 2020; Meyer et al. 2020; Snaurova et al. 2022). The activity of these DUBs may predominate over ribosome ubiquitination activity during oogenesis, keeping the ribosome less ubiquitinated. In any case, my data indicate that the maternal ribosome starts from a low ubiquitination state in zebrafish embryogenesis.

In the present study, I revealed that multiple ribosome ubiquitination signals gradually increased after fertilization, and ubiquitination of Rps10/eS10 by Znf598 contributed to this process. As ZNF598 plays a pivotal role in RQC and its ubiquitination sites in Rps10/eS10 are highly conserved

(Juszkiewicz and Hegde 2017; Sundaramoorthy et al. 2017; Garzia et al. 2017), it is likely that the ribosome ubiquitination increases after fertilization in response to ribosome collisions. It is possible that after fertilization, translation activation induces ribosome collisions on stall-prone mRNAs. As collided ribosomes accumulate, Znf598-dependent ribosome ubiquitination should increase. Supporting this scenario, ribosome collision sites were detected in more than 1000 mRNA species at 4 hpf (Han et al. 2020). Alternatively, Znf598 may be developmentally regulated. Compared to the lysate of HEK293, ZNF598 accumulates at significantly lower levels in rabbit reticulocytes (Juszkiewicz et al. 2018), indicating that ZNF598 steady-state levels may vary depending on the cellular situation. Considering the sub-stoichiometric abundance of ZNF598 (Garzia et al. 2017) and Znf598 overexpression in zebrafish embryos increased ribosome ubiquitination at 24 hpf, the Znf598 protein amount can be a major determinant of ribosome ubiquitination levels in response to ribosome collisions. During oxidative stress, inhibition of a DUB promotes ribosome ubiquitination (Silva et al. 2015). Therefore, the degree of DUB(s) activation or expression is also a critical factor in determining ribosome ubiquitination levels. Future research must determine the frequency of ribosome collision and the balance between DUB(s) and Znf598 activities during zebrafish development.

A balance between Znf598-mediated ubiquitination and other molecular pathways that recognize collided ribosomes is another factor that potentially affects the ubiquitination levels of the ribosome. ZAKα is recruited to collided ribosomes and phosphorylates p38 and JNK, leading to cell death (Wu et al. 2020; Vind et al. 2020). Additionally, ZAKα recruits GCN1 to collided ribosomes (Wu et al. 2020), and GCN1 further binds to collided ribosomes to provide a scaffold for eIF2α phosphorylation, therefore attenuating global translation initiation and preventing further ribosome collision (Pochopien et al. 2021; Yan and Zaher 2021). EDF1 is an additional collided ribosome sensor and inhibits translation initiation via the GIGYF2-4EHP complex (Juszkiewicz et al. 2020a). Therefore, competition among Znf598, ZAKα, GCN1, and EDF1 on the collided ribosomes may impact the efficiency of ribosome ubiquitination. In addition, several factors are reported to reduce ribosome stalling, such as GTPBP2 and eIF5A (Ishimura et al. 2014; Schuller et al. 2017). I assume that during development, a delicate balance between these multiple factors is not static but rather dynamic and contributes to the changes in the ubiquitination levels of the ribosome.

A hierarchical relationship between the ribosome ubiquitination events during zebrafish development

Although Rps10/eS10 is one of the key ubiquitinated ribosomal proteins in zebrafish embryos, neither loss of Znf598 nor mutations of the ubiquitination sites in Rps10/eS10 abolished ubiquitination signals on the ribosome completely. Hence, Rps10/eS10 alone cannot explain the entire ubiquitination pattern of the ribosome during development. The identity of the remaining ubiquitinated protein(s) needs to be determined. My data showed that most of the ubiquitination signals were linked with the 40S

ribosomal subunit. Furthermore, the Znf598 mutant and the Rps10 K139/140R mutant not only abolished the Rps10/eS10 ubiquitination *per se* but also reduced the additional ubiquitination signals on the ribosome. These findings imply that further ubiquitination events on the 40S ribosomal subunit require Znf598-mediated Rps10/eS10 ubiquitination as a prerequisite. Indeed, I observed that ubiquitination levels of Rps20/uS10, Rps3/uS3, and Rps2/uS5 decreased in the Rps10 K139/140R mutant. Therefore, as reported in other organisms (Garshott et al. 2020; Meyer et al. 2020), ubiquitination of these ribosomal proteins depends on Znf598-mediated Rps10/eS10 ubiquitination in zebrafish embryos. I speculate that these ubiquitination events may fluctuate during zebrafish development, as observed with Rps10/eS10 ubiquitination. The K139/140R mutation of Rps10/eS10 attenuated multiple ribosome ubiquitination signals under CHX treatment and eRF1-AAQ overexpression, further supporting the presence of hierarchical ubiquitination events. Overall, my data indicate that Znf598-mediated Rps10/eS10 ubiquitination plays a key role in establishing the entire ubiquitination pattern on ribosomes during development. Currently, the identification of ubiquitinated proteins is accomplished with the following three distinct approaches prior to mass spectrometry analysis. The first approach uses cells expressing His-tagged Ubiquitin and His-Ubiquitin conjugates can be purified by affinity chromatography using Ni-NTA resin (Peng et al. 2003). Secondly, a specific antibody that recognizes di-glycyl remnants from digested peptides is used to concentrate Ubiquitin conjugates (Back et al. 2019). In the third approach, the protein signal of interest can be excised from a gel based on the protein staining (Takehara et al. 2021). By combining these methods with the approaches developed in the present study, the ubiquitination pattern on ribosomes will be clarified comprehensively in the future.

The potential biological relevance of Rps10/eS10 ubiquitination during zebrafish development

One remaining question is the biological relevance of the ribosome ubiquitination dynamics to development. Both the homozygous *znf598* mutant fish and the homozygous *rps10* K139/140R fish had morphologies similar to those of wild-type fish and had the ability to create offspring on their own. Hence, the requirement of Znf598-mediated Rps10/eS10 ubiquitination during zebrafish development is still unknown. The collided ribosome that is a target of Znf598-mediated ubiquitination is emerging as a major signaling hub not only for eliciting RQC (Ikeuchi et al. 2019; Juszkiewicz et al. 2018), but also for triggering various responses. Such examples include stimulation of mRNA decay (Ikeuchi et al. 2019; D'Orazio et al. 2019), activation of stress signaling (Wu et al. 2020; Yan and Zaher 2021; Wan et al. 2021), prevention of new translation initiation cycle on the mRNA with stalled ribosomes (Juszkiewicz et al. 2020a), and prevention of frameshifting by the collided ribosome (Juszkiewicz and Hegde 2017). Considering these observations, it can be easily imagined that multiple factors work corporately on the disome and compensate for the defect of Znf598-mediated Rps10/eS10 ubiquitination. It is known that cells lacking ZNF598 activity or containing ubiquitination-sites

mutation in Rps10/eS10 fail to stall ribosomes efficiently and permit read-through of poly(A) sequences with frameshifting (Juszkiewicz and Hegde 2017). Such defects in translational fidelity are linked with the accumulation of toxic translation intermediates and result in neurodegeneration (Kapur and Ackerman 2018). Thus, combining analysis of aggregated proteins (Koplin et al. 2010) in neurons with behavioral experiments may provide an important insight into the role of Znf598-mediated Rps10/eS10 ubiquitination during development.

UFMylation is one of the post-translational modifications in which a small ubiquitin-like modifier UFM1 is covalently attached to a lysine residue of substrates (Banerjee et al. 2020; Cappadocia and Lima 2018; Millrine et al. 2023). As known for the ubiquitination pathway, UFMylation is also catalyzed by a cascade of specific enzymes: E1-like UBA5, E2-like UFC1, and E3-like UFL1. UFL1 forms a complex with DDRGK1 and CDK5RAP3, both of which are the key components mediating the UFMylation of substrate proteins in the ER (Banerjee et al. 2020; Millrine et al. 2023). From Dr. Koshi Imami's nanoLC/MS/MS analysis in Chapter 2, I found that the intensity of a CDK5RAP3 peptide (up to 13.19-fold), UFL1 peptides (up to 2.28-fold), a DDRGK1 peptide (up to 2.18-fold), and a UFM1 peptide (up to 1.84-fold) increased in FLAG-immunoprecipitants obtained from Znf598 overexpression condition compared to that obtained from normal condition, although this analysis was performed without quantification method (Figure 23). Emerging studies have identified ribosomal protein Rpl26/uL24 as a target of UFMylation (Walczak et al. 2019; Wang et al. 2020), and revealed its impact on co-translational quality control of nascent polypeptides in aberrantly stalled ER-associated ribosomes (Ishimura et al. 2023; Scavone et al. 2023; Wang et al. 2023). Although the relationship between Znf598-mediated Rps10/eS10 ubiquitination and Rpl26/uL24 UFMylation remains unexplored, from our data, I speculate that Znf598-mediated Rps10/eS10 is the upstream event of Rpl26/uL24 UFMylation. Importantly, mutations in UFMylation-related genes result in abnormalities in erythroid differentiation (Cai et al. 2016; Tatsumi et al. 2011; Zhang et al. 2015), liver development (Yang et al. 2019), and neuronal development (Muona et al. 2016). Thus, the analysis of the expression pattern of these pathology-related genes in Rps10 K139/140R embryos will be an interesting area for future investigation.

General discussion

The variability of ribosome components and their biological relevance have been widely recognized in recent years (Emmott et al. 2019; Genuth and Barna 2018a; Norris et al. 2021; Genuth and Barna 2018b; Li and Wang 2020; Xue and Barna 2012). Post-translational modifications on ribosomal proteins are particularly important as one of the dynamic events in response to multiple stimuli and stresses (Simsek and Barna 2017). Ubiquitination is one of the post-translational modifications on ribosomes in which small Ubiquitin proteins are enzymatically bound to target ribosomal proteins (Monem and Arribere 2023). Besides ribosome degradation (An and Harper 2020), current research is elucidating multiple roles of ribosome ubiquitination, such as the quality control pathway to maintain proteostasis (Inada 2020; Joazeiro 2017, 2019) and modulation of translation in response to stress conditions (Matsuki et al. 2020). However, it is currently unclear to what extent this ubiquitination is essential for animal development. This is mainly due to the limited number of research conducted with embryos of various developmental time-points, for which there were difficulties in purifying ribosomes quickly, easily, and efficiently.

In Chapter 1, toward the establishment of a ribosome purification system, I sought to generate a zebrafish strain that expresses an epitope-tagged ribosomal protein endogenously by using the CRISPR-Cas9-mediated genome editing system. As a result, I succeeded in developing the *rpl36*-FLAG strain with little or no effect of a FLAG-tag for viability and ribosome assembly. With Dr. Koshi Imami's grateful support, I found this strain quite useful in that components of both small and large ribosomal subunits were purified from zebrafish embryos. Subsequent experiments further revealed that not only fully assembled but also translation-engaging ribosomes can be purified. There are several advantages of this ribosome purification system over the traditional centrifugation method to analyze ribosome heterogeneity. First, this system can provide more direct information about ribosome association, i.e. ubiquitination of ribosomal proteins, than the cosedimentation approach. Second, the purification procedure is simpler, faster (about one hour), and better in efficiency (20% of the input), so that a large number of different samples, such as embryos of various developmental time-points, can be processed at the same time.

In Chapter 2, to gain a better understanding of ribosome ubiquitination dynamics during normal development, I combined the ribosome purification system with immunoblotting analysis with the anti-Ubiquitin antibody. I concentrated on embryonic (0 hpf to 2 dpf) and larval stages (3 dpf to 7 dpf) for this analysis and found that immediately after spawning (0 hpf), the level of ribosome ubiquitination was low but that as development proceeded, it gradually increased. The ubiquitination level reached the maximum intensity at 24 hpf and then decreased toward 7 dpf. Further analysis with Dr. Koshi Imami identified the 139th and 140th lysine residues of Rps10/eS10 as ubiquitination targets by Znf598. Combining the genetic mutant with the ubiquitination analysis, I revealed for the first time

that the Rps10/eS10 ubiquitination level changes dynamically during development and that it is a prerequisite for establishing the entire ubiquitination pattern of the ribosome during development. This success, however, is only a first step as the biological relevance of the dynamics of ribosome ubiquitination during development remains elusive. To address this, it will be required to experimentally demonstrate what defect occurs in developing embryos having Rps10/eS10 with mutations at ubiquitination sites. At present, I did not see any developmental defects in the Rps10/eS10 mutant embryos, at least at the 'morphological' levels, and the mutant even produced healthy offspring. Further molecular analysis will be needed in the future, such as protein aggregation assay, RNA-sequencing, and ribosome footprint profiling (Figure 24).

In this doctoral thesis, I mainly focused on the dynamics of ribosome ubiquitination during early to late development. Another interesting period for analysis of ribosome ubiquitination in life is aging, a process characterized by the progressive loss of tissue and organ function. The main molecular characteristics of aging are genomic instability, loss of telomere function, epigenetic change, depletion of the stem cell pool, altered intercellular communication, and decline of proteostasis (Anisimova et al. 2018; Gonskikh and Polacek 2017). As manipulation of protein synthesis and translation-related signaling can extend lifespan (Gonskikh and Polacek 2017), changes in the translation machinery seem to play a central role in aging, which may affect the above mentioned multiple molecular mechanisms underlying aging. However, there is a limited number of studies that relate ribosome heterogeneity to aging. One example is RNA methyltransferase NSUN5, which is differentially regulated in aging. NSUN5 changes the methylation level of 28S/25S rRNA, which is shown to be implicated in the control of lifespan in flies, worms, and yeast by regulating translational control of distinct subsets of mRNAs (Schosserer et al. 2015). According to the free radical theory of aging, later termed as oxidative stress theory of aging, aging is the result of the accumulation of oxidative damage to macromolecules (lipids, DNA, and proteins) by reactive oxygen and nitrogen species (Russo et al. 2018). Given that oxidative stress promotes ribosome ubiquitination (Back et al. 2019; Silva et al. 2015; Yan et al. 2019), ribosome ubiquitination levels may be regulated in aging. It is thus interesting to address the ribosome ubiquitination in aging and in age-related diseases. Although some modifications to my ribosome purification system should be required to purify ribosomes from adult fish, I prospect that aging is an attractive field of ribosome ubiquitination research in the future.

Ribosome ubiquitination occurs under various conditions, but the ubiquitination targets are known to be strictly controlled in response to distinct stimuli (Back et al. 2019; Higgins et al. 2015; Spence et al. 2000; Takehara et al. 2021; Monem and Arribere 2023). For example, a translation elongation inhibitor induces Rps10/eS10 and Rps3/uS3 ubiquitination (Juszkiewicz et al. 2018; Simms et al. 2017) while a translation initiation inhibitor elicits Rps2/uS5 and Rps3/uS3 ubiquitination (Garshott et al. 2021; Garzia et al. 2021). Thus, I speculate that the target-specific regulated property of ribosome ubiquitination could provide us a clue to further understand the cellular status, leading to

opportunities to isolate more effective biomarkers. In addition, given its central role in translation, perturbation of ribosome biogenesis and mutations of several ribosomal proteins have been linked with various diseases (Kang et al. 2021; Jiao et al. 2023), cancers (Ferreira et al. 2020; Ebright et al. 2020), and aging (Anisimova et al. 2018; Gonskikh and Polacek 2017). Therefore, the ribosome is now an attractive therapeutic target. However, it is challenging to target the ribosome with little toxicity and side-effects because blocking translation affects not only defective cells but also normal cells, particularly those in the proliferation phase. Indeed, homoharringtonine is now the only direct and general ribosome inhibitor used in clinics for cancer treatment (Gilles et al. 2020). As discussed above, ribosome ubiquitination undergoes in a target-specific manner depending on cellular conditions. Thus, a future therapeutic target will be ribosome ubiquitination, instead of the ribosome in general. I hope that the present study will fuel ribosome ubiquitination research in animals and help in therapeutic application.

Materials and Methods

Zebrafish husbandry

The zebrafish AB strain was used as a wild-type strain and maintained according to the animal experiment protocol (2023-37) at Kyoto Sangyo University. Fishes were raised and maintained at 28.5°C under standard laboratory conditions with the cycle of 14 hour-light and 10 hour-dark. The natural breeding method was used to produce fertilized eggs, and embryos were grown in system water at 28.5°C.

Generation of *rpl36*-FLAG and *rps10* K139/140R strains

The zebrafish *rpl36*-FLAG and *rps10* K139/140R strains were generated by CRISPR-Cas9-mediated genome editing. CRISPRscan (Vejnar et al. 2016) was used to predict a single-guide RNA (sgRNA) targeting the exon 4 of the *rpl36* gene locus (ENSDARG00000100588) or exon 5 of the *rps10* gene locus (ENSDARG00000034897). The DNA template for sgRNA synthesis was prepared by PCR using the gene-specific sgRNA primer and the sgRNA tail primer as shown in Table S1. The template was transcribed with T7 RNA Polymerase (TAKARA) and purified using Probe-Quant G-25 microcolumns (Cytiva). As shown in Table S1, the single-stranded oligodeoxynucleotides (ssODNs) were synthesized by Eurofins Genomics. The recombinant Cas9 protein (TAKARA) and the sgRNA were incubated for 10 min at 37°C and then co-injected with the ssODN in the one-cell zebrafish embryos (0.45 μg/μL Cas9 protein, 90 ng/μL sgRNA, 0.125 pmol/μL ssODN). To screen an F0 fish carrying a precise insertion/substitution in the corresponding gene locus in germline cells, injected embryos were grown into adult fish and then each fish was crossed with wild-type fish. Seven to eight embryos at 24 hpf obtained from the mating were subjected to genomic DNA extraction followed by genotyping PCR using the appropriate set of primers (Table S1). After electrophoresis of the obtained PCR products, their sequence was determined by Sanger sequencing following TA cloning. The remained siblings with potential insertion/substitution were raised. Fin-clipping was used to genotype adult F1 fish, and Sanger sequencing was used to verify that the editing was successful.

Generation of MZ*znf598*; *rpl36*-FLAG and *rps10* K139/140R; *rpl36*-FLAG strains

The *znf598* mutant strain generated previously (Mishima et al. 2022) and the *rps10* K139/140R mutant strain generated in this study were crossed with the *rpl36*-FLAG strain. Heterozygous fish were crossed to generate homozygous *znf598* mutant or *rps10* K139/140R mutant in the *rpl36*-FLAG heterozygous background.

Plasmid construction

The primer sequences and plasmids used in this study are shown in Tables S1 and S2, respectively.

The ORFs of zebrafish *rpl36* (ENSDARG00000100588) and *rps20* (ENSDART00000052331.6) were amplified by RT-PCR and cloned into pCS2+ via EcoRI/XhoI restriction sites using DNA Ligation Kit (TAKARA). The ORF of zebrafish *znf598* (ENSDARG00000014945) was amplified by RT-PCR and cloned into pCS2+ via XhoI/XbaI restriction sites using DNA Ligation Kit (TAKARA). To generate *znf598* point mutation in ORF (*znf598* C13/16A), wild-type ORF was amplified using point mutated primers and cloned into pCS2+ via XhoI/XbaI restriction sites using DNA Ligation Kit (TAKARA). The ORFs of zebrafish *etf1b* (ENSDARG00000043976), *rps10* (ENSDARG00000034897), *rps3* (ENSDART00000185844.1), and *rps2* (ENSDART00000138107.3) were amplified by RT-PCR and cloned into pCS2+HA using NEBuilder HiFi DNA Assembly (New England BioLabs). The pCS2+HA was generated by inserting synthetic DNA fragments with HA-tag sequence into pCS2+ via EcoRI/XbaI restriction sites. To generate *etf1b* and *rps10* point mutations in ORFs (*etf1b*-AAQ, *rps10*-K139R, *rps10*-K140R, and *rps10*-K139/140R), wild-type ORFs were amplified using point mutated primers. DNA fragments were then assembled using NEBuilder HiFi DNA Assembly (New England BioLabs).

Polysome analysis

For polysome analysis, I followed the original protocol (Mishima et al. 2012) with some modifications. Zebrafish embryos at 24 hpf were dechorionated with 1 mg/mL pronase (Sigma). Sixty dechorionated embryos were homogenized in buffer A (20 mM HEPES-KOH pH 7.5, 100 mM KCl, 10 mM $MgCl_2$, 0.25% NP-40, 250 mM sucrose, 2 mM DTT, 10 µg/mL cycloheximide, 100 U/mL RNase inhibitor [Promega], Complete Protease Inhibitor EDTA-free in nuclease-free water). Lysates were incubated for 5 min on ice and centrifuged for 5 min at 12,000 rpm at 4°C. Clarified lysates were loaded onto a continuous 10%–45% *(w/v)* sucrose gradient prepared in buffer B (20 mM HEPES-KOH pH 7.5, 100 mM KCl, 10 mM $MgCl_2$, 2 mM DTT, 10 µg/mL cycloheximide, 100 U/mL RNase inhibitor [TAKARA]). Gradients were centrifuged in a P40ST rotor (himac) for 180 min at 36,000 rpm at 4°C. Polysome gradients were analyzed using a gradient station (BioComp) coupled to a TriaxTM Flow Cell detector (FC-2). Each fraction was collected and precipitated by ethanol (75% final). Pellets were dissolved in Sample Buffer Solution (Fujifilm-Wako). Samples were incubated for 30 min at 92°C and proceed to SDS-PAGE followed by immunoblotting analysis.

Immunoblotting analysis

Samples were incubated with Sample Buffer Solution (Fujifilm-Wako) for 10 min at 92°C. The SDS-PAGE and immunoblotting experiments were carried out according to standard protocols. Signals were developed using ImmunoStar LD (Fujifilm-Wako) or Luminata Forte (Millipore) and detected using Amersham Imager 680 (GE Healthcare). Antibodies used in this study are shown in Table S3.

Immunoprecipitation

To conduct the immunoprecipitation assay, I followed the original protocol (Simsek et al. 2017) with some modifications. For immunoprecipitation by an anti-FLAG antibody, 15-45 zebrafish embryos were homogenized in the lysis buffer A (25 mM Tris-HCl pH 7.6, 150 mM NaCl, 15 mM $MgCl_2$, 1 mM DTT, 8% glycerol, 1% triton X-100, 50 μM PR-619, 100 U/mL RNase inhibitor [TAKARA], Complete Protease Inhibitor EDTA-free in nuclease-free water). Lysates were incubated for 5 min on ice and centrifuged for 5 min at 2,000 g at 4°C. Supernatants were incubated with Anti-DYKDDDDK tag Antibody Beads (Fujifilm-Wako) for 15 min on rotation at 4°C.

Anti-DYKDDDDK tag Antibody Beads were prepared by washing with wash buffer (25 mM Tris-HCl pH 7.6, 150 mM NaCl, 15 mM $MgCl_2$, 1 mM DTT, 8% glycerol, 1% triton X-100) three times. Four micro-litter of slurry beads were used per embryo.

After 15 min incubation at 4°C with rotation, beads were washed twice with buffer B (25 mM Tris-HCl pH 7.6, 150 mM NaCl, 15 mM $MgCl_2$, 1 mM DTT, 1% triton X-100, 50 μM PR-619) and once with buffer C (25 mM Tris-HCl pH 7.6, 150 mM NaCl, 15 mM $MgCl_2$, 1% triton X-100, 50 μM PR-619). Samples were eluted from the beads by incubating with 0.5 mg/mL FLAG peptide (MEDICAL&BIOLOGICAL LABORATORIES CO., LTD) in buffer C at 25°C for 30 min.

For EDTA-treated samples (related to Figure 13B and C), 50 mM EDTA was used in place of 15 mM $MgCl_2$ in buffers A, B, C, and wash buffer.

For post-purification EDTA-treated samples (related to Figure 13D), FLAG-immunoprecipitants obtained in the EDTA-free conditions were separated and incubated continuously with or without 50 mM EDTA for 25 min at 4°C and for 30 min at 25°C.

For mass spectrometry analysis, beads were washed twice using buffer D (25 mM Tris-HCl pH 7.6, 150 mM NaCl, 15 mM $MgCl_2$) after washing with buffer B. Following manipulation was performed by Dr. Koshi Imami. Beads were resuspended in PTS buffer (12 mM sodium deoxycholate (SDC), 12 mM sodium N-lauroylsarcosinate (SLS) in 100 mM Tris-HCl pH 8.0) followed by incubation for 30 min at 37°C under constant agitation. After the incubation, the supernatant was reduced with 10 mM dithiothreitol (DTT) at 37°C for 30 min and alkylated with 50 mM iodoacetamide (IAA) at room temperature for 30 min in the dark room. The samples were diluted 5 times with 50 mM ammonium bicarbonate (ABC). For Figure 7D and 8A, proteins were digested by 0.5 μg lysyl endopeptidase (LysC) (Fujifilm-Wako) and 0.5 μg Trypsin (Promega) at room temperature overnight. For Figure 15B, 15C, and 23, proteins were digested by LysC, Trypsin, or Glu-C (Promega). Next day, 500 μL ethyl acetate (Fujifilm-Wako) was added to the sample and digestion was quenched by adding 0.5% trifluoroacetic acid (TFA) (final concentration). The samples were shaken for 1 min and centrifugated at 15,000 g for 2 min at room temperature. The organic phase containing SDC and SLS was discarded. The resulting peptide solution was evaporated in a SpeedVac. The residue was resuspended in 0.1% TFA and desalted with SDB-XC Stage tips (Rappsilber et al. 2007) prior to

nanoLC/MS/MS analysis.

For high-salt washes experiments (related to Figure 10B and C), after 15 min incubation at 4°C rotation, beads were washed twice with buffer B containing 400 mM NaCl (25 mM Tris-HCl pH 7.6, 400 mM NaCl, 15 mM $MgCl_2$, 1 mM DTT, 1% triton X-100, 50 µM PR-619). Afterwards, beads were washed once with buffer C containing 400 mM NaCl (25 mM Tris-HCl pH 7.6, 400 mM NaCl, 15 mM $MgCl_2$, 1% triton X-100, 50 µM PR-619). Samples were then eluted off the beads using 0.5 mg/mL FLAG peptide in buffer C containing 400 mM NaCl for 30 min at 25°C. RNA was extracted from a portion of the samples, and ribosomal RNAs were quantified by agarose gel electrophoresis, to compensate for differences in the quantities of ribosomes recovered from low and high-salt conditions. The equal amounts of ribosomes estimated from the RNA analysis were subjected to immunoblotting analysis and protein staining.

nanoLC-MS/MS analysis (performed by Dr. Koshi Imami)

Nano-scale reversed-phase liquid chromatography coupled with tandem mass spectrometry (nanoLC/MS/MS) was performed on an Orbitrap Exploris 480 (related to Figure 7D and 8A) or an Orbitrap Fusion Lumos mass spectrometer (related to Figure 15B, 15C, and 23) (Thermo Fisher Scientific) connected to a Thermo Ultimate 3000 RSLCnano pump equipped with a self-pulled analytical column (150 mm length × 100 µm i.d.) (Ishihama et al. 2002) packed with ReproSil-Pur C18-AQ materials (3 µm or 1.9 µm; Dr. Maisch GmbH). The mobile phases comprised (A) 0.5% acetic acid and (B) 0.5% acetic acid and 80% ACN.

For the Orbitrap Exploris 480 system (related to Figure 7D and 8A), peptides were separated on self-pulled needle columns (250 mm, 100 µm ID) packed with Reprosil-Pur 120 C18-AQ1.9 µm at 50°C in a column oven. The flow rate was 400 nL/min. The flow gradient was set as follows: 5% B in 5 min, 5–19% B in 55.3 min, 19–29% B in 21 min, 29–40% B in 8.7 min, and 40–99% B in 0.1 min, followed by 99% B for 4.9 min. The electrospray voltage was set to 2.2 kV in the positive mode. The mass spectrometric analysis was carried out with the FAIMS Pro interface (Thermo Fisher Scientific). The compensation voltage (CV) was set to −40, −60, and −80 and the cycle time of each CV experiment was set to 1 s. The mass range of the survey scan was from 375 to 1,500 *m/z* with a resolution of 60,000, 300% normalized automatic gain control (AGC) target and auto maximum injection time. The first mass of the MS/MS scan was set to 120 *m/z* with a resolution of 15,000, standard AGC, and auto maximum injection time. Fragmentation was performed by HCD with a normalized collision energy of 30%. The dynamic exclusion time was set to 20 s.

The Orbitrap Fusion Lumos instrument was operated in the data-dependent mode with a full scan in the Orbitrap followed by MS/MS scans using HCD (related to Figure 15B, 15C, and 23). Peptides were eluted from the analytical column at a flow rate of 500 nL/min, with the following gradient: 5–10% B for 5 min, 10–40% B for 60 min, 40–99% B for 5 min, and 99% for 5 min. The applied voltage

for ionization was 2.4 kV. The full scans were performed with a resolution of 120,000, the standard AGC target mode, and a maximum injection time of 50 ms. The MS scan range was *m/z* 300–1,500. The CV of the FAIMS Pro interface was set to −40, −60, and −80, and the cycle time of each CV experiment was set to 1 s. The MS/MS scans were collected in the ion trap with the rapid mode, the standard AGC target mode, and a maximum injection time of 35 ms. The isolation window was set to 1.6, and the normalized HCD collision energy was 30. Dynamic exclusion was applied for 20 s.

Processing of proteome data (performed by Dr. Koshi Imami)

All raw data files were analyzed and processed by maxquant (version 1.6.15.0 or 1.6.17.0) (Cox and Mann 2008), and the database search was performed with Andromeda (Cox et al. 2011), which is a peptide search engine integrated into the MaxQuant environment. Searches were conducted against a zebrafish UniProt database (version 2021-3; 46,849 protein entries) spiked with common contaminants and enzyme sequences. Search parameters included two missed cleavage sites and variable modifications such as methionine oxidation; protein N-terminal acetylation; deamidation of glutamine and asparagine residues; and diglycine of lysine residue (only ubiquitination analysis related to Figure 15B and C). Cysteine carbamidomethylation was set as a fixed modification. The enzyme was set as trypsin/P, which also cleaves at carboxyl side of the amino acids lysine or arginine, also if a proline follows, lysC (cleaves after lysine), or Glu-C (cleaves after glutamic acid). The peptide mass tolerance was 4.5 ppm, and the MS/MS tolerance was 20 ppm. The false discovery rate (FDR) was set to 1% at the peptide spectrum match level and protein level. The ‘match between runs’ function was performed. All necessary information regarding proteomic analyses, including protein and peptide lists, were deposited in a publicly accessible repository (jPOST) (Moriya et al. 2019; Okuda et al. 2017) with the dataset identifier, PXD039560.

Microinjection

To conduct microinjection, I used IM300 Microinjector (NARISHIGE) and followed the original protocol (Mishima and Tomari 2016). Approximately 1000 pL of the solution was injected per embryo within 15 min after spawning. Embryos were developed in system water at 28.5°C.

Protein staining

Following SDS-PAGE, the gel was immersed in Oriole solution (BioRad) for 90 min while being constantly agitated. For five minutes, the gel was rinsed twice with distilled water. Amersham Imager 680 was used to detect the signals (GE Healthcare).

RNA extraction

RNA samples were extracted from zebrafish embryos or FLAG-immunoprecipitants using TRI

Reagent (Molecular Research Center). Ethachinmate (Nippon gene) was used in ethanol precipitation to recover a small quantity of RNA.

In vitro mRNA transcription

mRNA was synthesized from a linearized plasmid DNA template using the SP6 Scribe Standard RNA IVT Kit and the ScriptCap m7G Capping System (CELLSCRIPT) or mMessage mMachine SP6 (Thermo Fisher Scientific), followed by purification with the RNeasy Mini Kit (QIAGEN).

Harringtonine and cycloheximide treatment

Embryos were incubated with the drugs at the indicated concentrations and duration at 28.5℃. 23 hpf embryos were given an hour of treatment with harringtonine (HTN) (LKT Laboratories, Inc.) at concentrations of 50, 100, 200, or 400 µg/mL. 22 hpf embryos were given two hours of treatment with cycloheximide (CHX) (Fujifilm-Wako) at concentrations of 1.25, 5, 20, 80, 320, or 1280 µg/mL.

Quantification of ubiquitination signals

Signals were quantified using the ROI manager function of the Image J software (http://imageJ.nih.gov/ij/). Background signal was measured with the empty lane and subtracted from quantified values. Relative ubiquitination levels were calculated by dividing a ubiquitin signal by a corresponding protein staining signal. Three biological replicates were used in the experiments, and averages were computed.

Figures and Legends

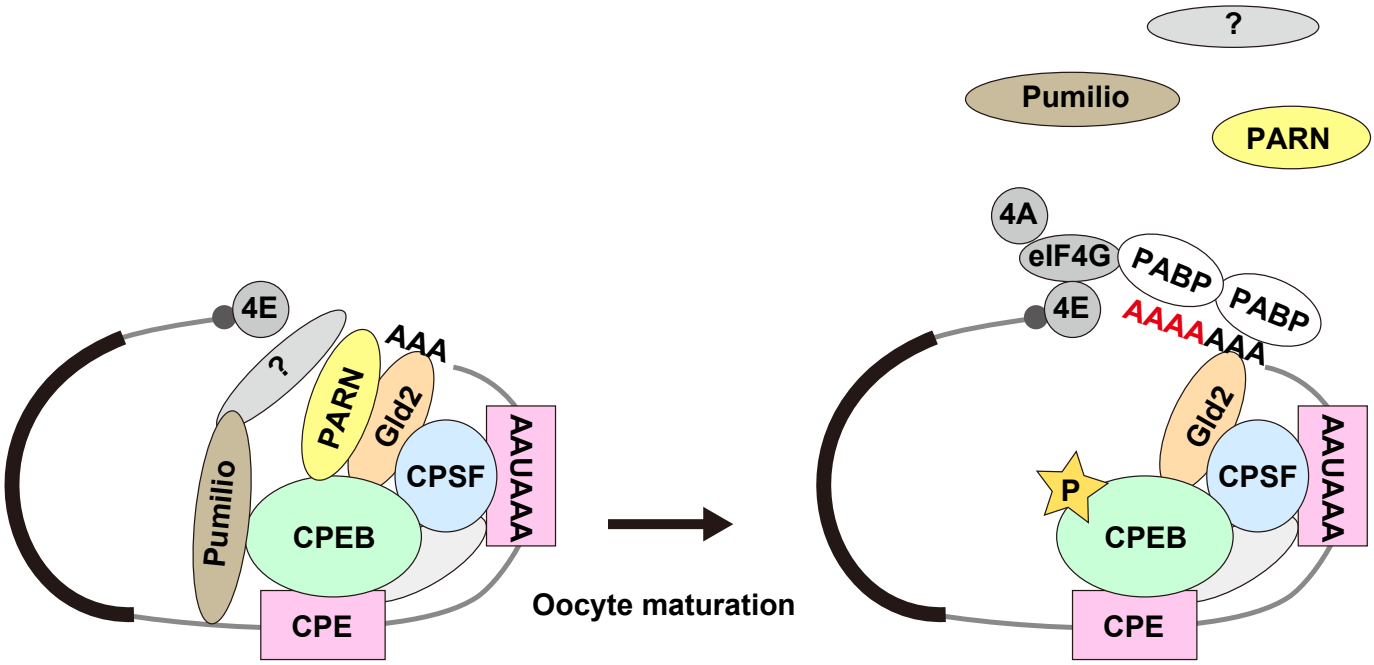

Figure 1. Translational control during Xenopus oocyte maturation

In immature oocytes, maternal cyclin B1 mRNA is bound by CPEB and CPSF. CPEB is also bound by PARN, Gld2, and Pumilio. PARN shortens the poly(A)-tail to 20-40 nucleotides. Pumilio also prevents poly(A)-tail elongation by interacting with an uncharacterized deadenylase. In response to progesterone, Aurora A phosphorylates CPEB. This event causes the dissociation of PARN and Pumilio from the CPEB-cyclin B1 mRNA complex. As a result, Gld2 elongates the poly(A)-tail to 80-250 nucleotides. The elongated poly(A)-tail recruits PABP, which activates translation initiation via interacting with eukaryotic initiation factor eIF4G.

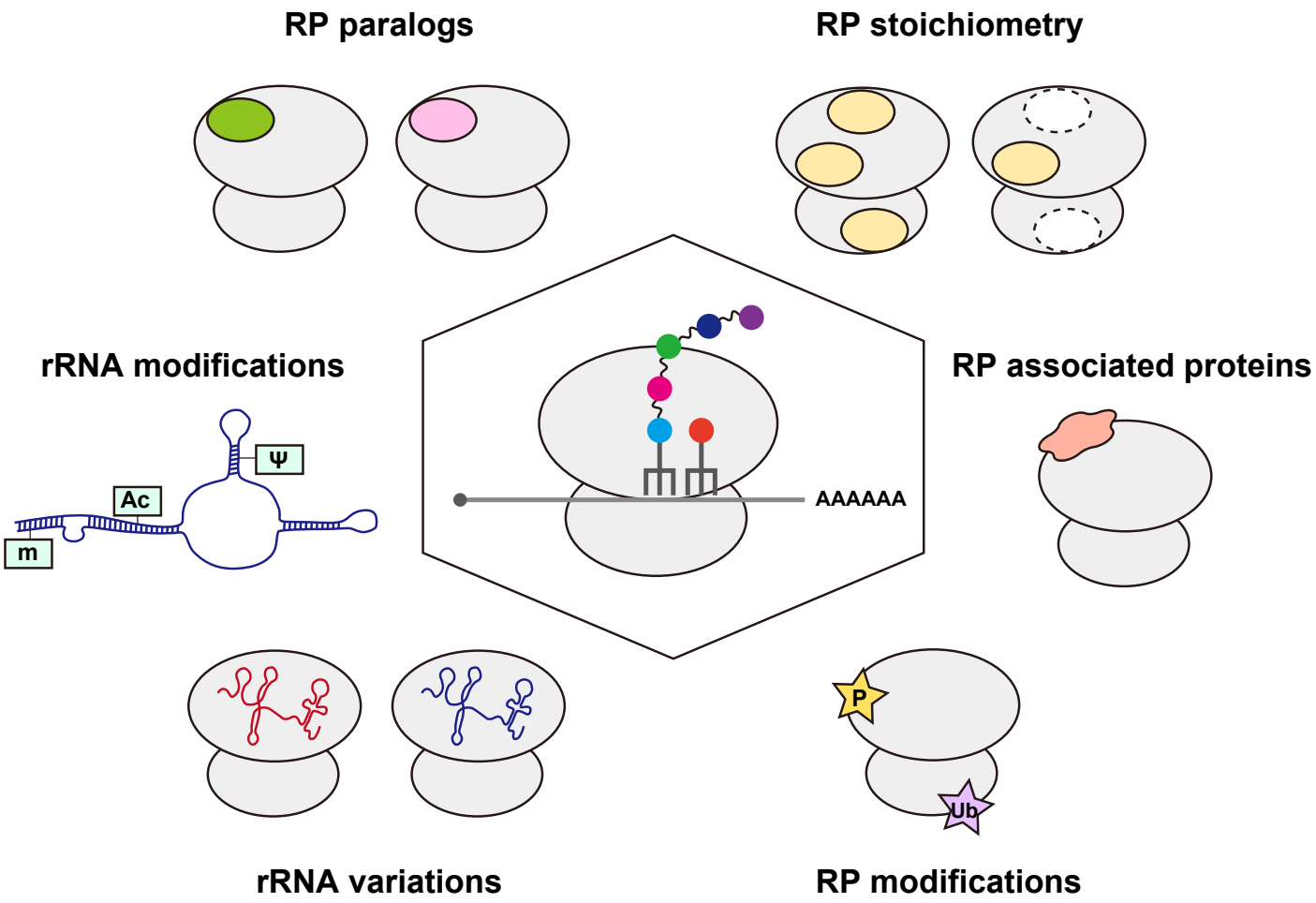

Figure 2. Types of ribosome heterogeneity (Norris et al., 2020)

A schematic representation of the different types of ribosome heterogeneity. Ribosome heterogeneity can occur at the level of core ribosomal proteins (RPs), ribosome-associated proteins, posttranslational modifications on RPs, rRNA sequences, and rRNA modifications.

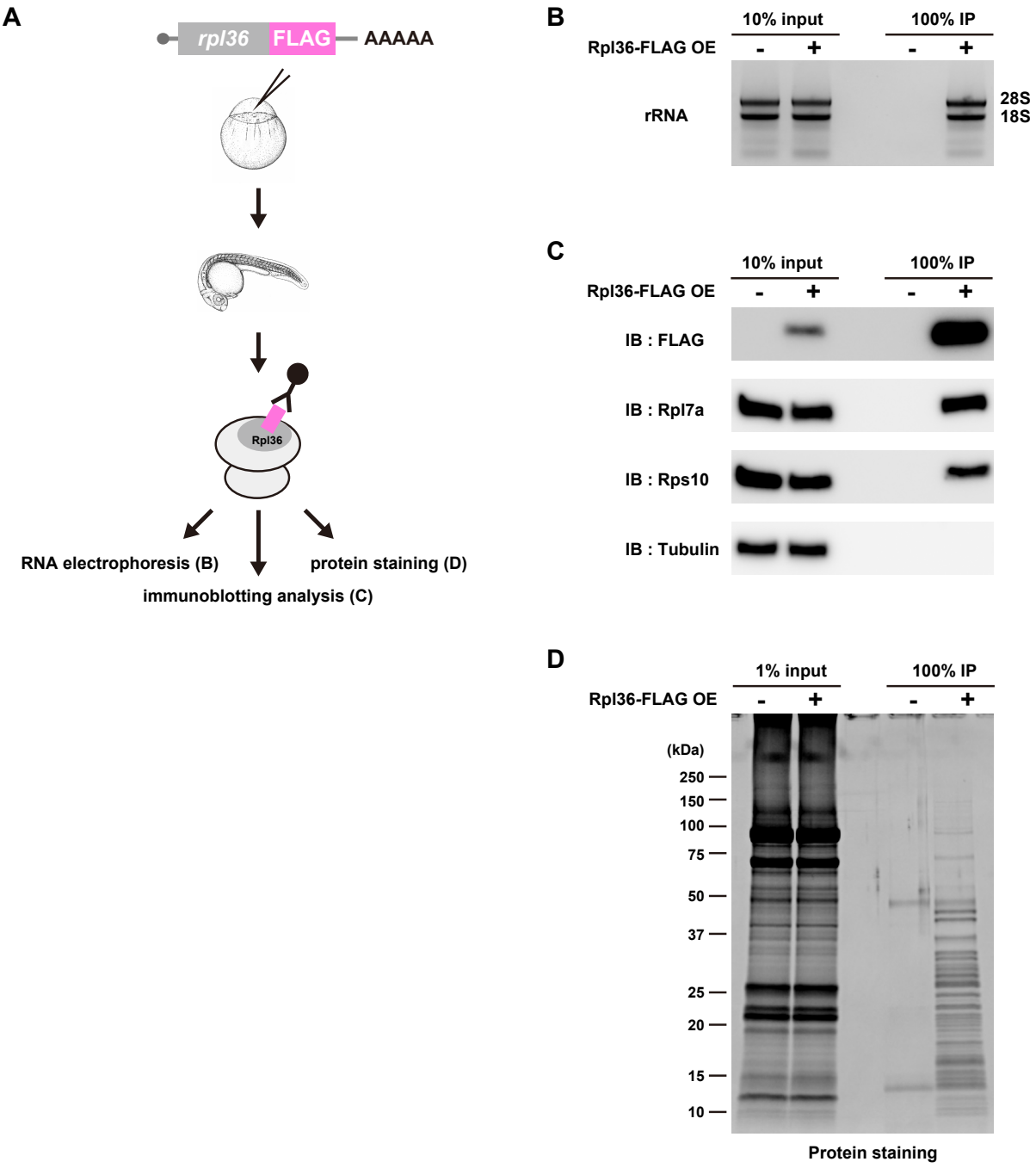

Figure 3. Exogenously overexpressed Rpl36-FLAG allows the purification of the assembled ribosomes.

(A) A schematic of experimental design.

(B-D) Validation of ribosome purification using exogenously overexpressed Rpl36-FLAG. Total lysates (input) and FLAG-immunoprecipitants (IP) in the presence (+) or absence (-) of Rpl36-FLAG overexpression were subjected to RNA electrophoresis (B), immunoblotting analysis using antibodies against the indicated proteins (C), and protein staining (D).

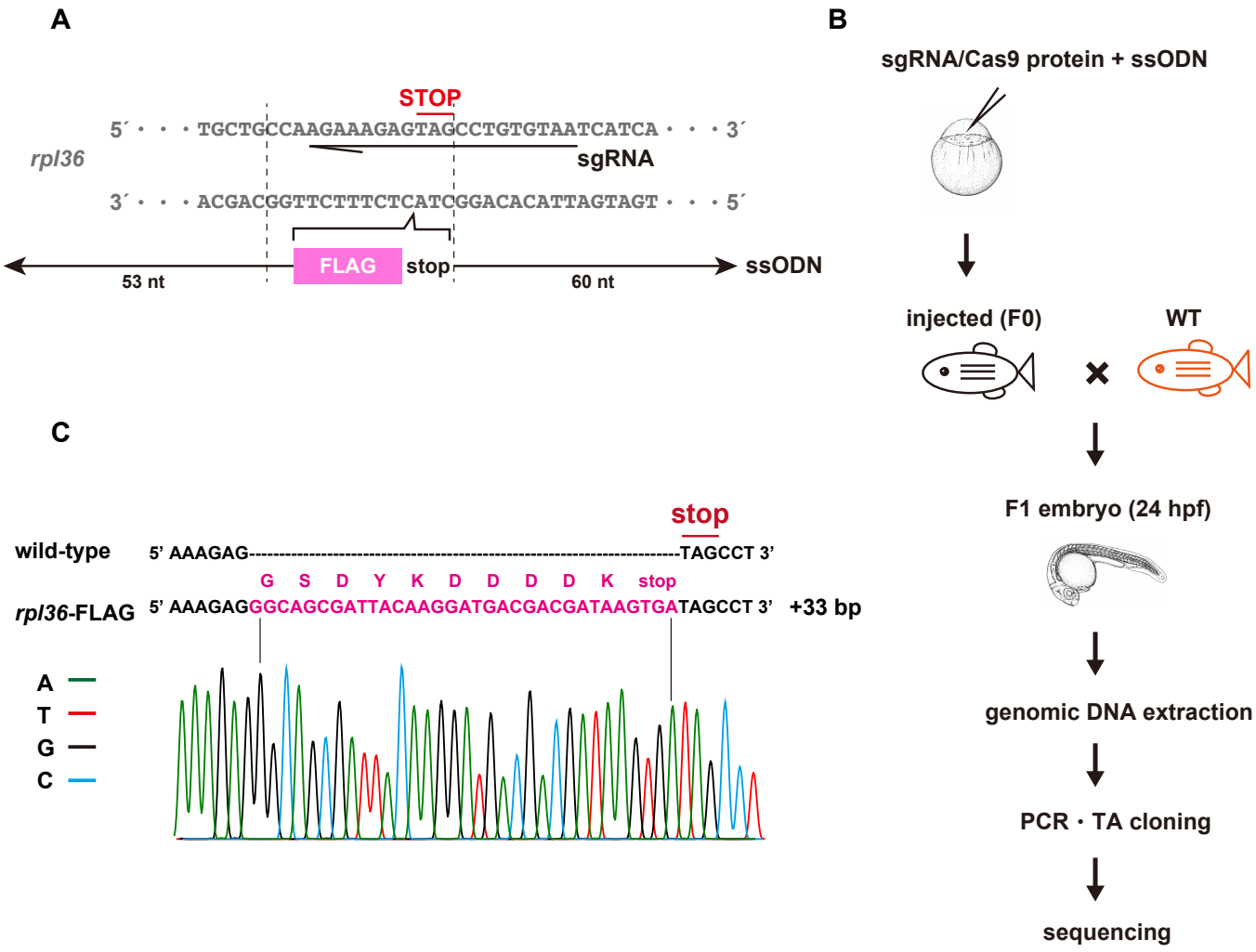

Figure 4. Generation of an *rpl36*-FLAG strain

(A) Scheme of the designed sgRNA and ssODN.

(B) A schematic of experimental design.

(C) Scheme of a FLAG-tagged *rpl36* gene locus. Genome sequences around the stop codon of wild-type and *rpl36*-FLAG strains are shown. The sequence chromatogram of *rpl36*-FLAG embryos is indicated below.

A

	Number	%
+/+	43	20.2
+/-	115	54.0
-/-	55	25.8
Total	213	

B

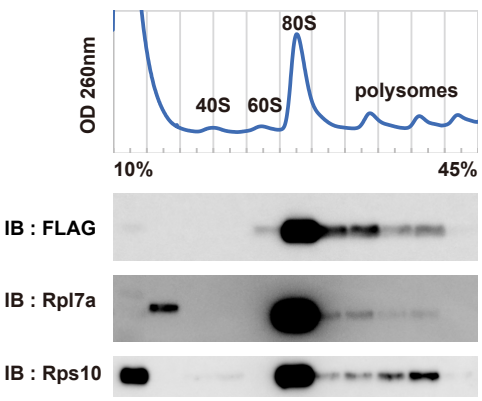

Figure 5. Insertion of the FLAG-tag sequence into the *rpl36* gene has little or no effect on viability and incorporation of Rpl36-FLAG into ribosomes

(A) Number and percentage of the offspring at around 60 dpf produced by mating *rpl36*-FLAG heterozygotes.

(B) Representative polysome profiles of *rpl36*-FLAG embryos at 24 hpf. The distribution patterns of ribosomal proteins are indicated below.

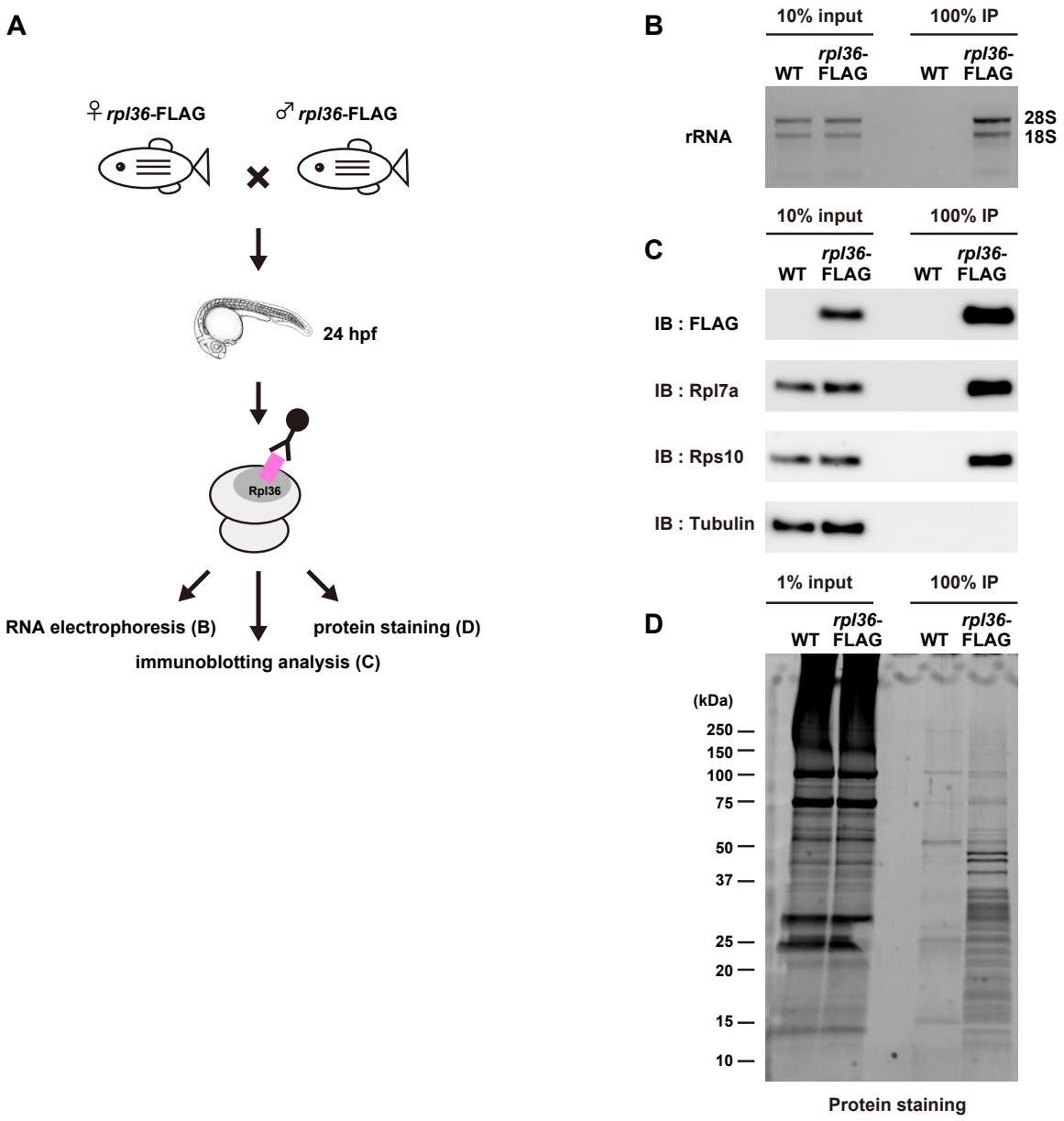

Figure 6. The *rpl36*-FLAG strain allows for purification of ribosomes from 24 hpf zebrafish embryos

(A) A schematic of experimental design.

(B-D) Validation of the ribosome purification system with wild-type (WT) and *rpl36*-FLAG embryos at 24 hpf. Total lysates (input) and FLAG-immunoprecipitants (IP) were subjected to RNA electrophoresis (B), immunoblotting analysis using antibodies against the indicated proteins (C), and protein staining (D).

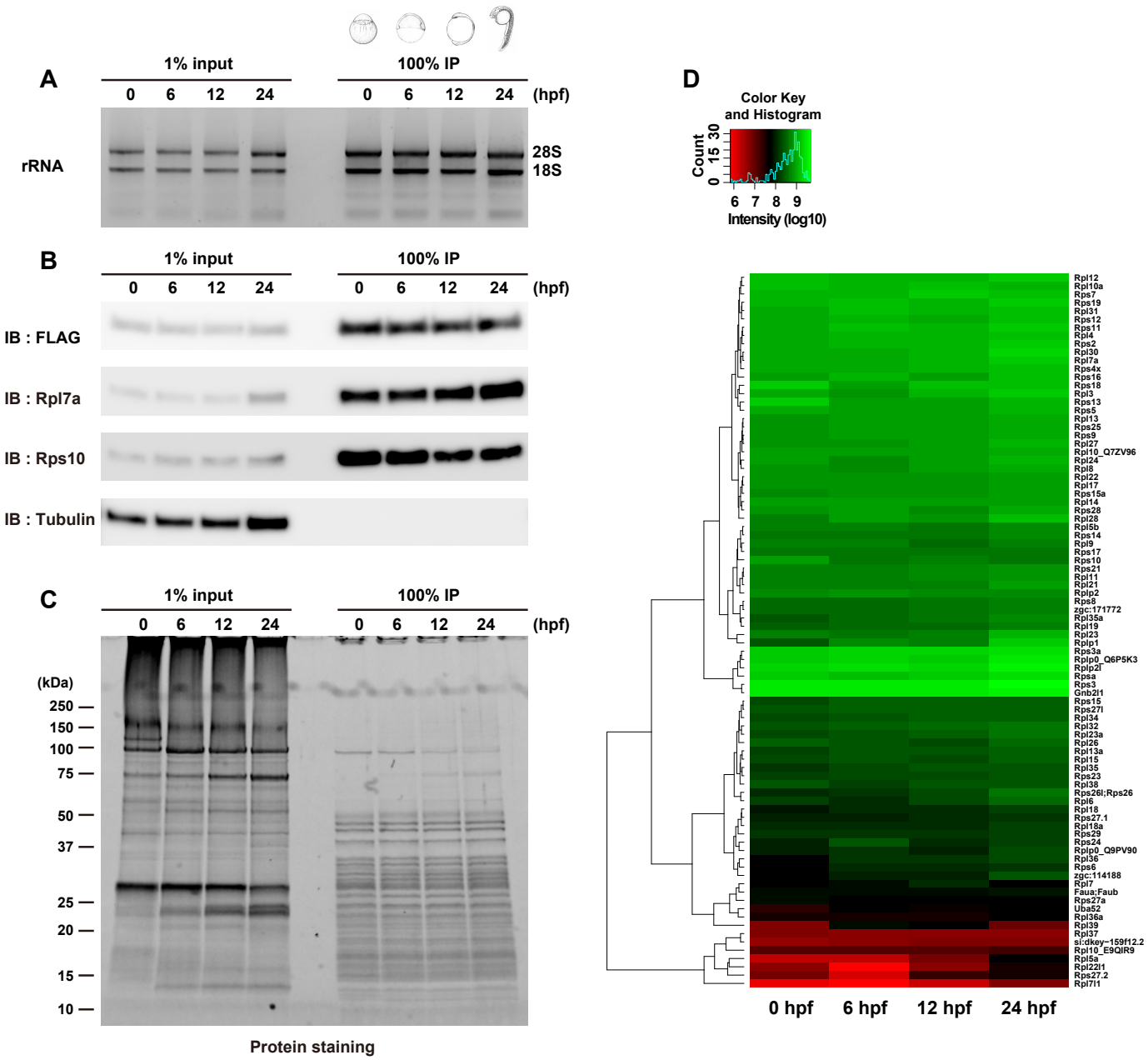

Figure 7. The *rpl36*-FLAG strain allows the purification of ribosomes from zebrafish embryos throughout development

(A-C) Validation of the ribosome purification system using embryos of various developmental time-points. The developmental time-points are indicated above as hours post-fertilization (hpf). Total lysates (input) and FLAG-immunoprecipitants (IP) were subjected to RNA electrophoresis (A), immunoblotting analysis using antibodies against the indicated proteins (B), and protein staining (C).

(D) Heat map showing ribosomal proteins identified by nanoLC/MS/MS analysis. The log10 scale is used to display the mean signal intensity of two biological replicates. The developmental time-points are indicated below as hours post-fertilization (hpf).

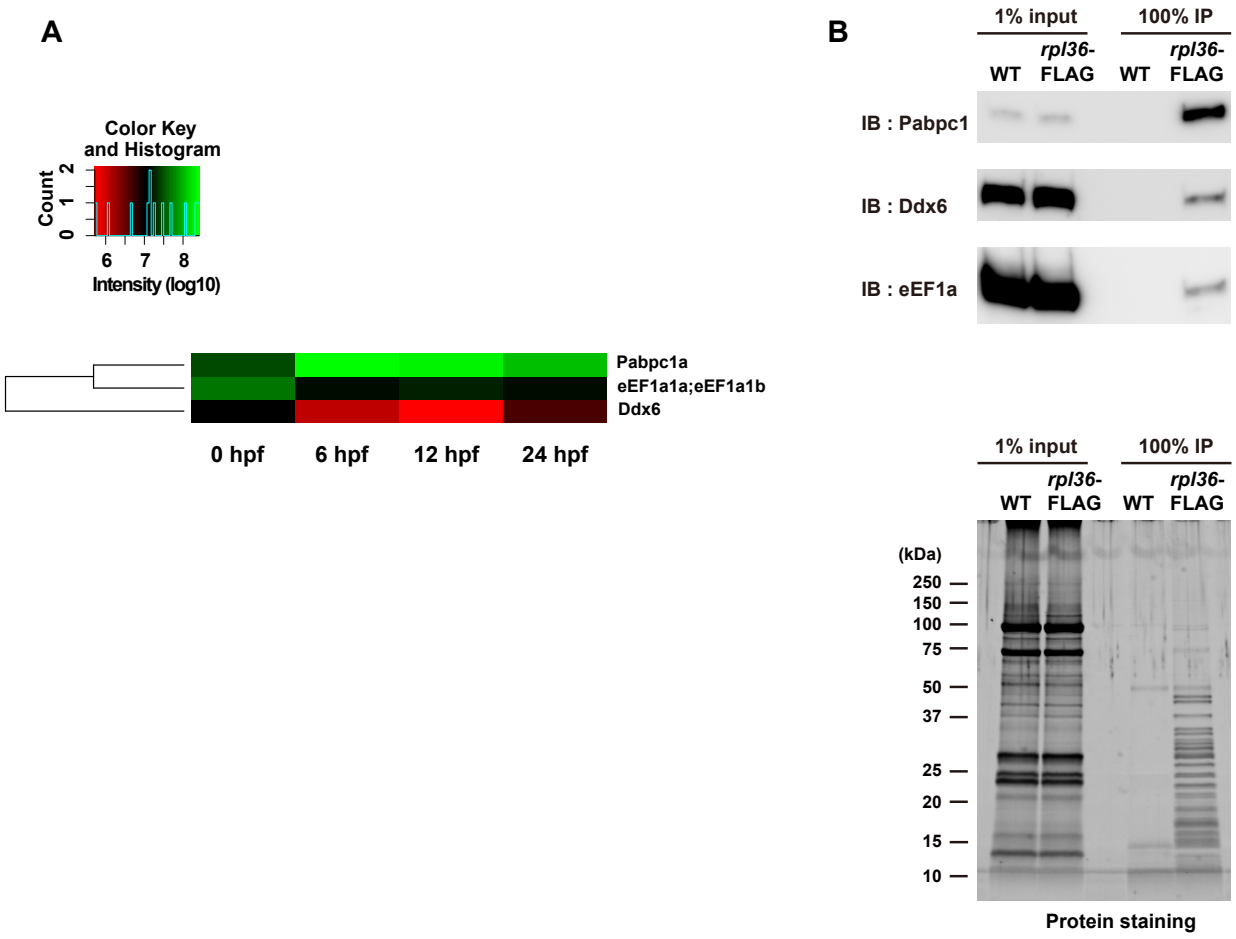

Figure 8. Translating ribosomes were purified by FLAG-immunoprecipitation using *rpl36*-FLAG embryos

(A) Heat map showing a part of the copurified proteins identified by the nanoLC/MS/MS analysis. The log10 scale is used to display the mean signal intensity of two biological replicates. The developmental time-points are indicated below as hours post-fertilization (hpf).

(B) Analysis of the copurified proteins detected by the nanoLC/MS/MS analysis in (A). Total lysates (input) and FLAG-immunoprecipitants (IP) obtained from wild-type (WT) and *rpl36*-FLAG embryos at 24 hpf were subjected to immunoblotting analysis using antibodies against the indicated proteins (upper) and protein staining (lower).

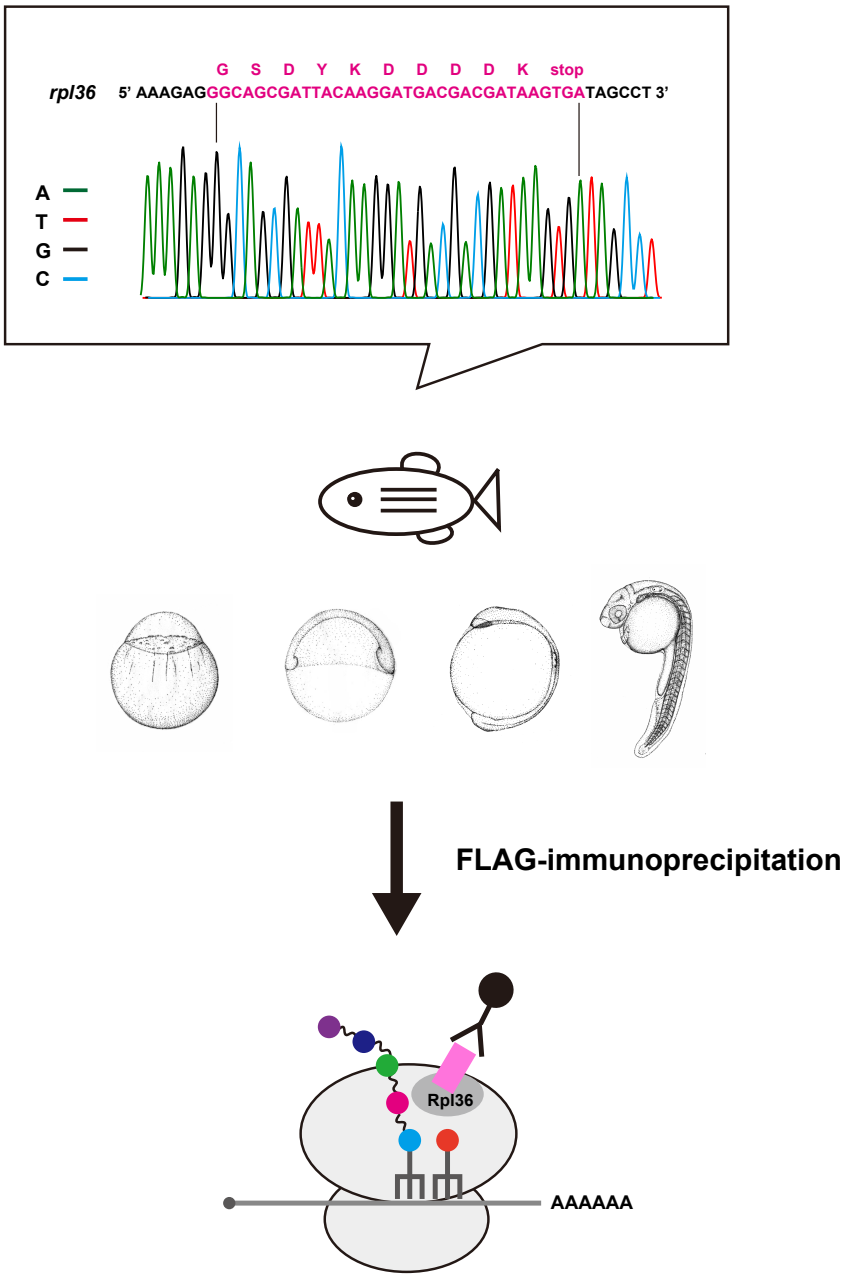

Figure 9. Summary of Chapter 1

A zebrafish strain that expresses FLAG-tagged Rpl36/eL36 endogenously was established. The Rpl36-FLAG was incorporated into the large ribosomal subunit, thus allowing me to purify fully assembled and translation-engaging 80S ribosomes.

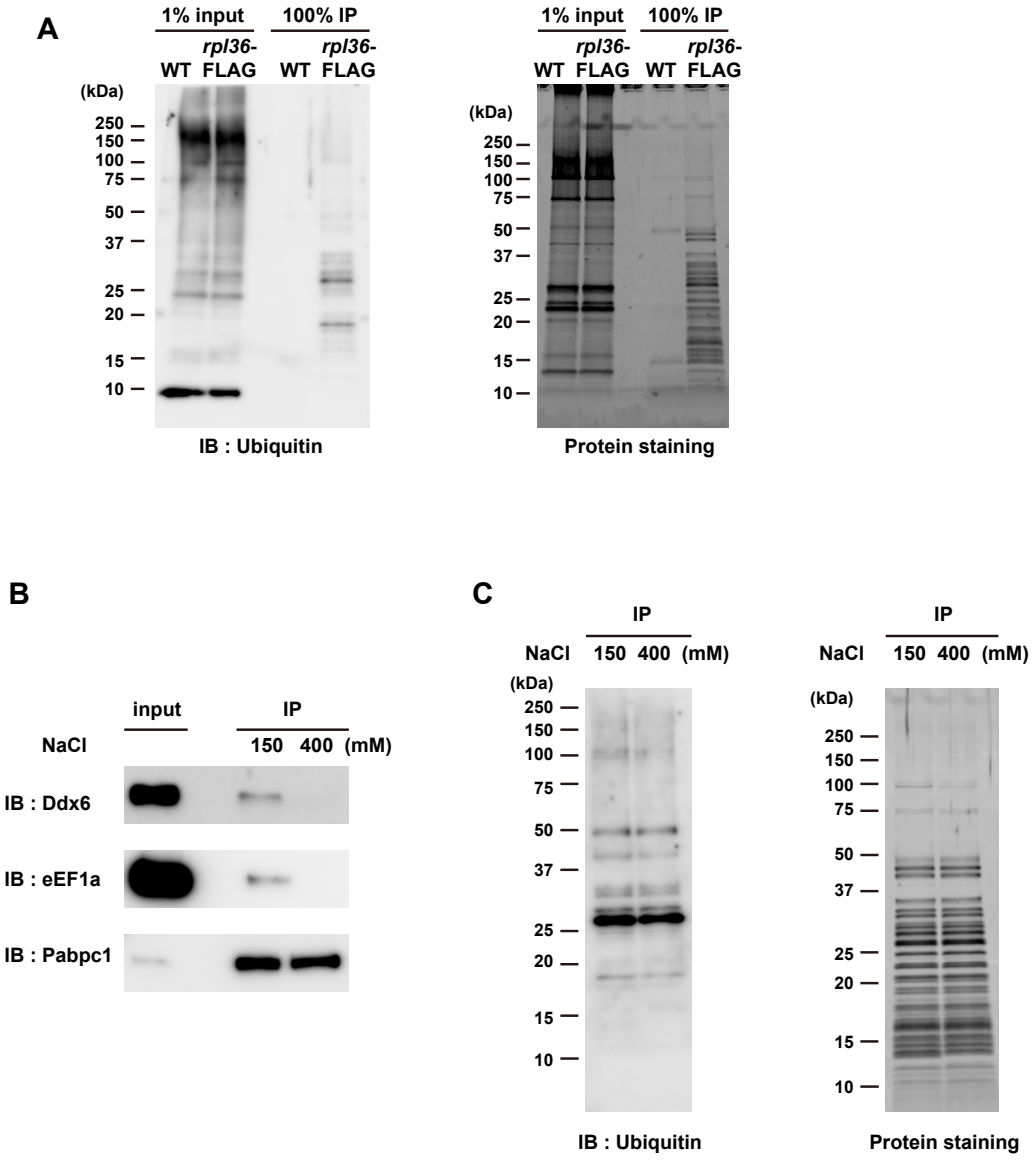

Figure 10. Ribosome ubiquitination was detected under the physiological condition

(A) Detection of ribosome ubiquitination. Total lysates (input) and FLAG-immunoprecipitants (IP) obtained from wild-type (WT) and *rpl36*-FLAG embryos at 24 hpf were subjected to immunoblotting analysis with an anti-Ubiquitin antibody (left) and protein staining (right).

(B) Detection of copurified proteins under normal (150 mM NaCl) and high salt (400 mM NaCl) wash conditions. Total lysate (input) and FLAG-immunoprecipitants (IP) were subjected to immunoblotting analysis using antibodies against the indicated proteins. Salt concentrations are indicated above.

(C) Comparison of ribosome ubiquitination levels under normal (150 mM NaCl) and high salt (400 mM NaCl) wash conditions. FLAG-immunoprecipitants in (B) were subjected to immunoblotting analysis with an anti-Ubiquitin antibody (left) and protein staining (right). Salt concentrations are indicated above.

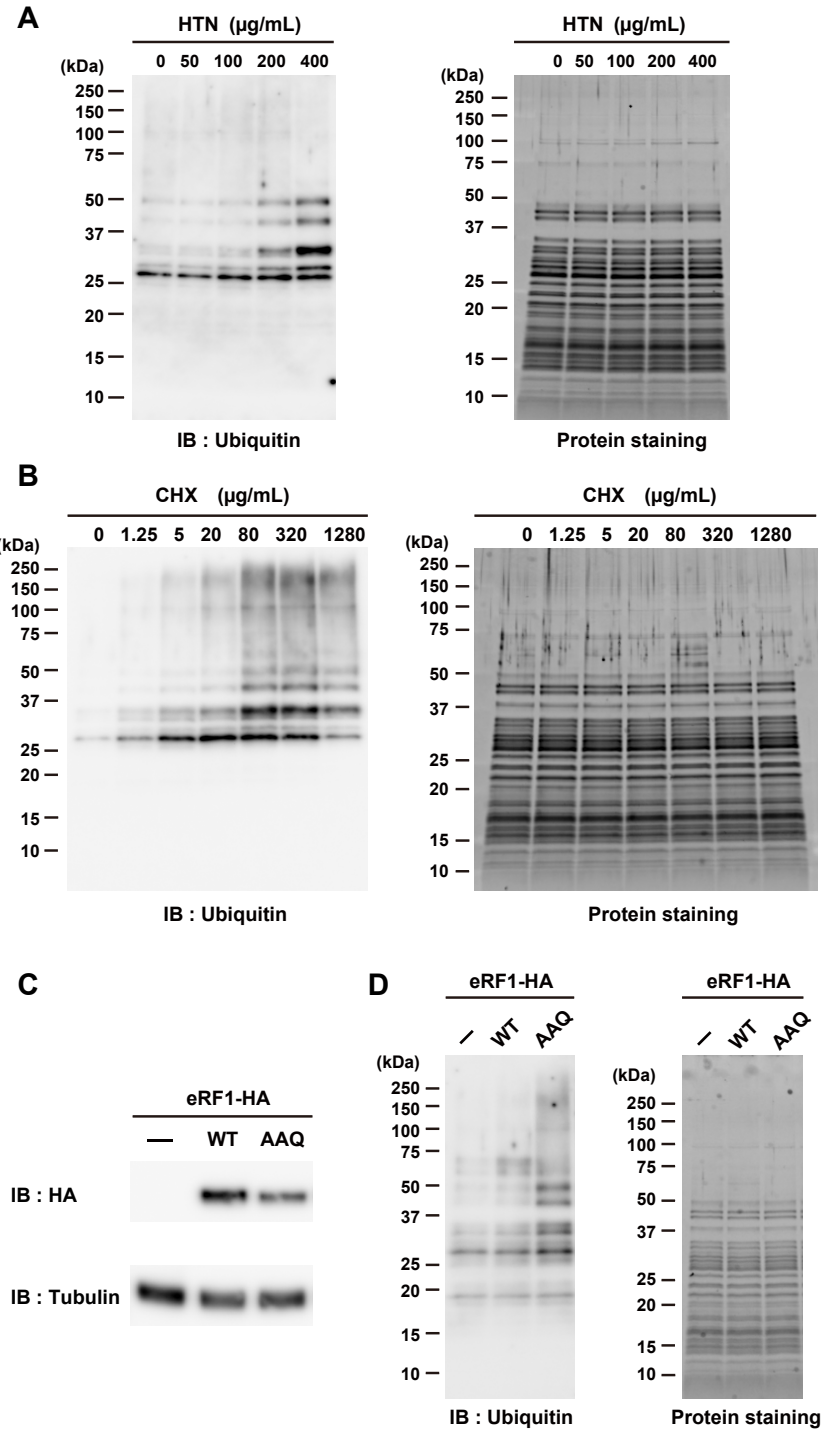

Figure 11. Ribosome ubiquitination was detected under translational stress conditions

(A) Analysis of ribosome ubiquitination under harringtonine (HTN) treatment. FLAG-immunoprecipitants were subjected to immunoblotting analysis with an anti-Ubiquitin antibody (left) and protein staining (right). HTN concentrations are indicated above.

(B) Analysis of ribosome ubiquitination under cycloheximide (CHX) treatment. FLAG-immunoprecipitants were subjected to immunoblotting analysis with an anti-Ubiquitin antibody (left) and protein staining (right). CHX concentrations are indicated above.

(C-D) Analysis of ribosome ubiquitination in the presence of mutant release factor eRF1-AAQ. Total lysates were subjected to immunoblotting analysis of eRF1-HA and Tubulin (C). FLAG-immunoprecipitants were subjected to immunoblotting analysis with an anti-Ubiquitin antibody (D, left) and protein staining (D, right).

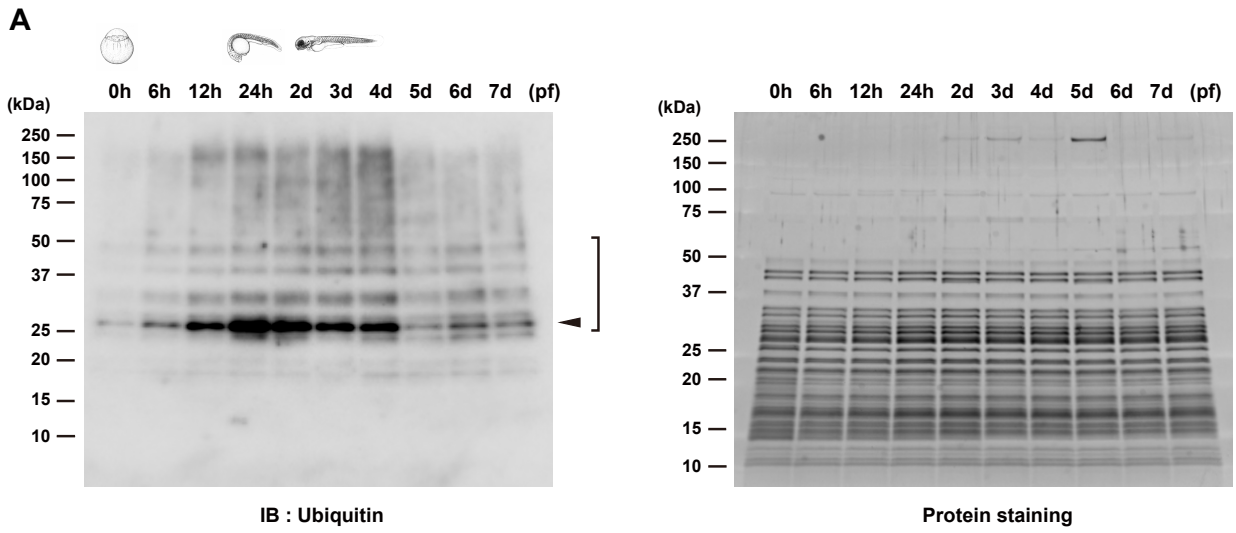

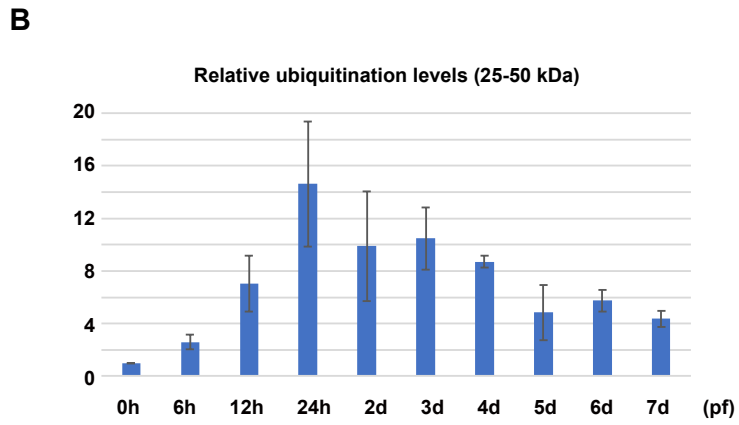

Figure 12. Ribosome ubiquitination levels change during zebrafish development

(A) Detection of ribosome ubiquitination during development. FLAG-immunoprecipitants from various developmental time-points were subjected to immunoblotting analysis with an anti-Ubiquitin antibody (left) and protein staining (right). The arrowhead indicates the most noticeable ubiquitination signal. Ubiquitination signals between 25 kDa and 50 kDa were reproducibly detected (bracket). The developmental time-points are indicated above as hours post-fertilization (hpf) or days post-fertilization (dpf).

(B) A bar graph shows relative ubiquitination levels relative to 0 hpf. Ubiquitination signals between 25 kDa and 50 kDa in (A, left) were normalized by corresponding protein amounts in (A, right). The average of three independent experiments is indicated. The error bars indicate the standard deviation.

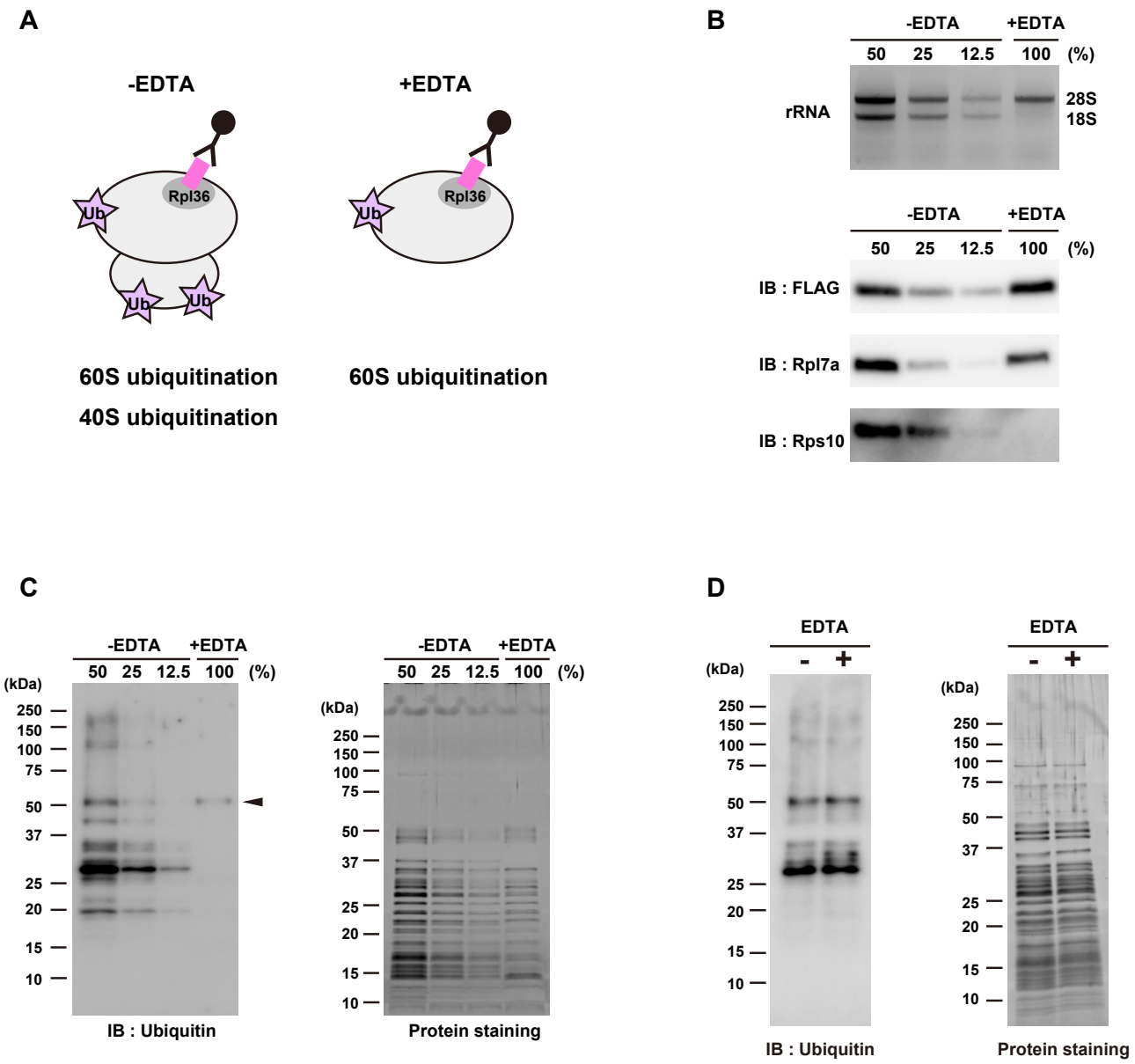

Figure 13. The 40S ribosomal subunit is differently ubiquitinated during development

(A) A schematic of experimental design.

(B) Validation of the 60S ribosomal subunit purification. FLAG-immunoprecipitants in the presence (+) or absence (-) of EDTA were subjected to RNA electrophoresis (upper) and immunoblotting analysis of ribosomal proteins (lower). The -EDTA samples were serially diluted as indicated above.

(C) Detection of ribosome ubiquitination in the presence (+) or absence (-) of EDTA. FLAG-immunoprecipitants in (B) were subjected to immunoblotting analysis with an anti-Ubiquitin antibody (left) and protein staining (right). The arrowhead indicates a ubiquitination signal derived from the 60S ribosomal subunit.

(D) Comparison of ribosome ubiquitination levels with or without EDTA incubation after purification. FLAG-immunoprecipitants obtained from EDTA-free conditions were incubated with or without EDTA and subjected to immunoblotting analysis with an anti-Ubiquitin antibody (left) and protein staining (right).

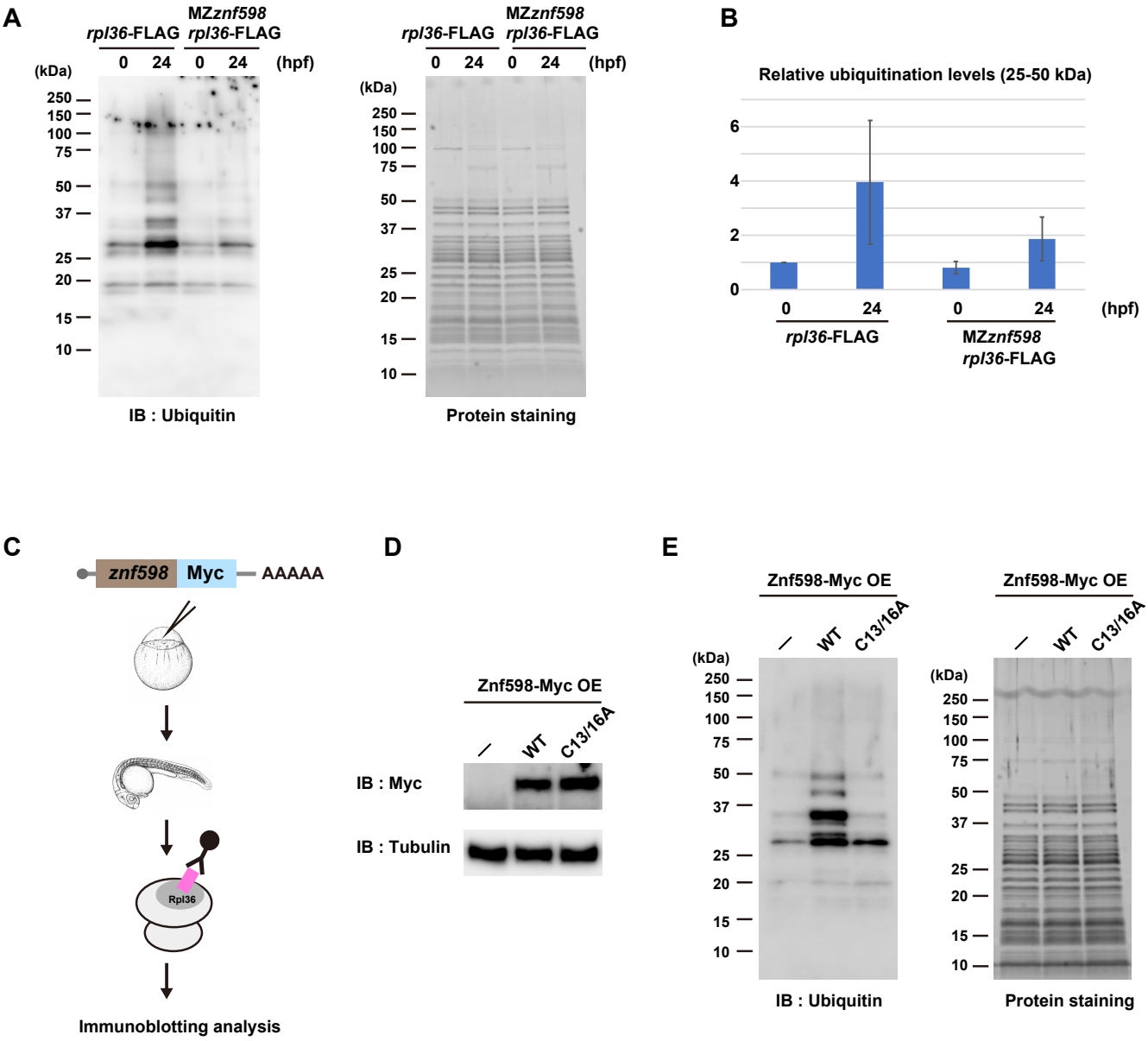

Figure14. Znf598 promotes ribosome ubiquitination during development

(A) Comparison of ribosome ubiquitination levels of *rpl36*-FLAG and MZ*znf598*; *rpl36*-FLAG embryos. FLAG-immunoprecipitants from 0 and 24 hpf embryos were subjected to immunoblotting analysis with an anti-Ubiquitin antibody (left) and protein staining (right). The developmental time-points are indicated above as hours post-fertilization (hpf).

(B) A bar graph shows ubiquitination levels relative to that of *rpl36*-FLAG embryos at 0 hpf. Ubiquitination signals between 25 kDa and 50 kDa in (A, left) were normalized by corresponding protein amounts in (A, right). The average of three independent experiments is indicated. The error bars indicate the standard deviation.

(C) A schematic of experimental design.

(D-E) Comparison of ribosome ubiquitination levels with or without Znf598 overexpression. Total lysates were subjected to immunoblotting analysis of Znf598-Myc and Tubulin (D). FLAG-immunoprecipitants were subjected to immunoblotting analysis with an anti-Ubiquitin antibody (E, left) and protein staining (E, right).

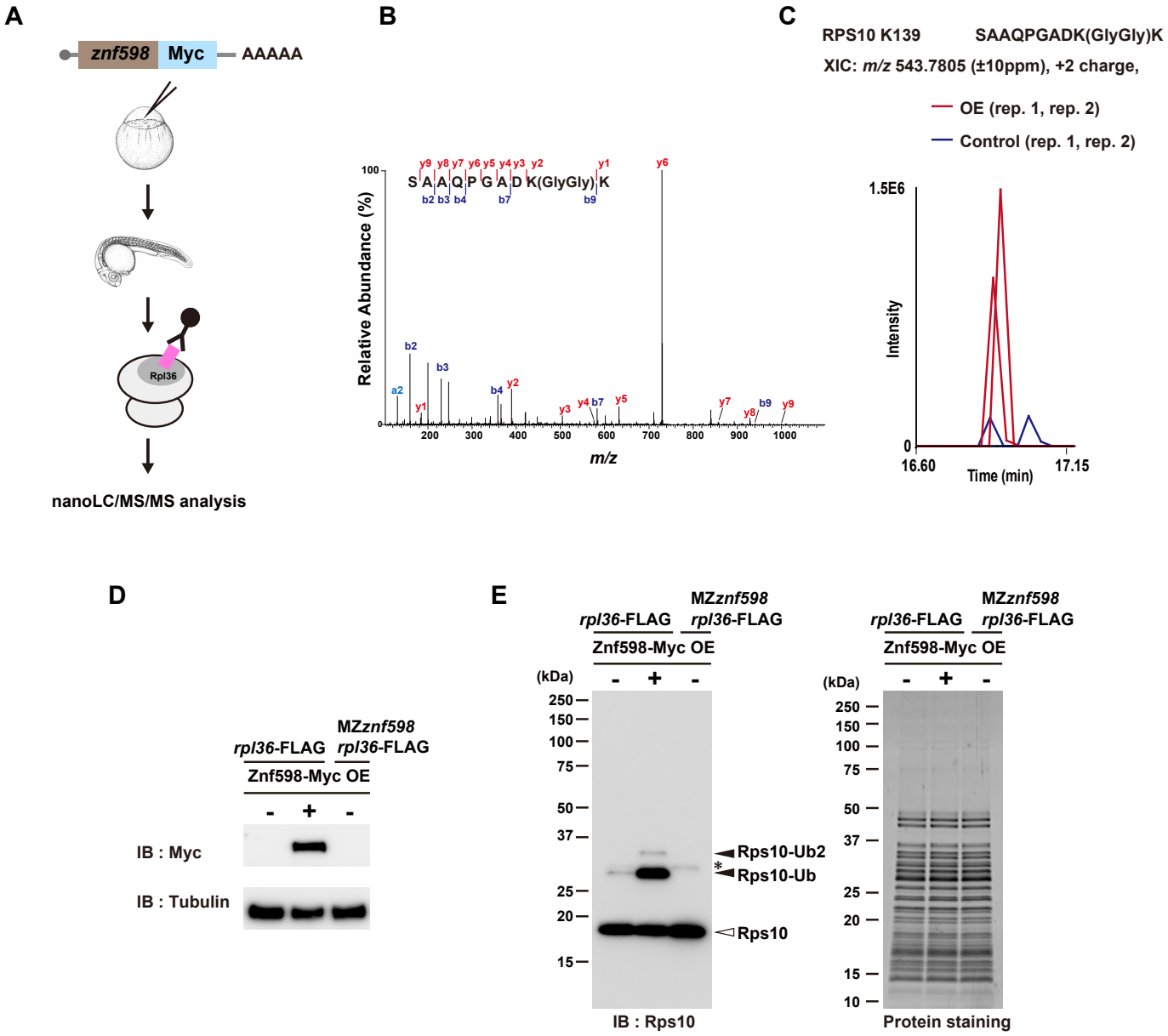

Figure 15. Znf598 ubiquitinates Rps10/eS10 in zebrafish

(A) A schematic of experimental design.

(B) A representative MS/MS spectrum of Rps10/eS10 di-glycyl K139.

(C) MS-based quantification of a peptide of Rps10/eS10 containing di-glycyl K139 under Znf598 OE (red) and control (blue) conditions.

(D-E) Detection of Rps10/eS10 ubiquitination. Total lysates were subjected to immunoblotting analysis of Znf598-Myc and Tubulin (D). FLAG-immunoprecipitants were subjected to immunoblotting analysis with an anti-Rps10 antibody (E, left) and protein staining (E, right). White and black arrowheads indicate non-ubiquitinated or ubiquitinated Rps10/eS10 signals, respectively. The asterisk indicates a non-specific signal.

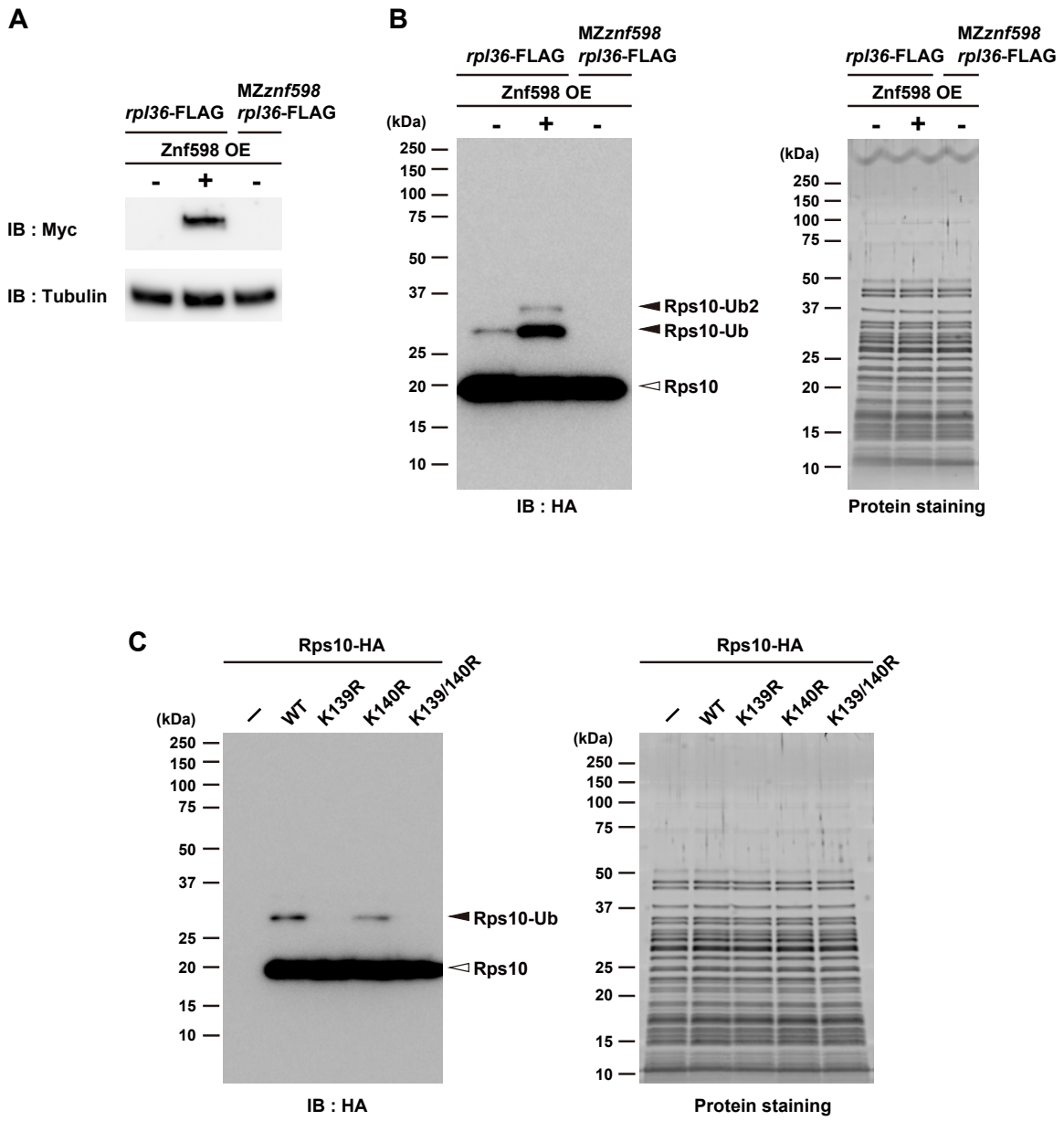

Figure 16. Znf598 ubiquitinates the 139th and 140th lysine residues of Rps10/eS10 in zebrafish embryos

(A-B) Detection of Rps10-HA ubiquitination. Total lysates were subjected to immunoblotting analysis of Znf598-Myc and Tubulin (A). FLAG-immunoprecipitants were subjected to immunoblotting analysis with an anti-HA antibody (B, left) and protein staining (B, right). White and black arrowheads indicate non-ubiquitinated or ubiquitinated Rps10-HA signals, respectively.

(C) Validation of Rps10/eS10 ubiquitination sites. FLAG-immunoprecipitants were subjected to immunoblotting analysis with an anti-HA antibody (left) and protein staining (right). White and black arrowheads indicate non-ubiquitinated or ubiquitinated Rps10-HA signals, respectively.

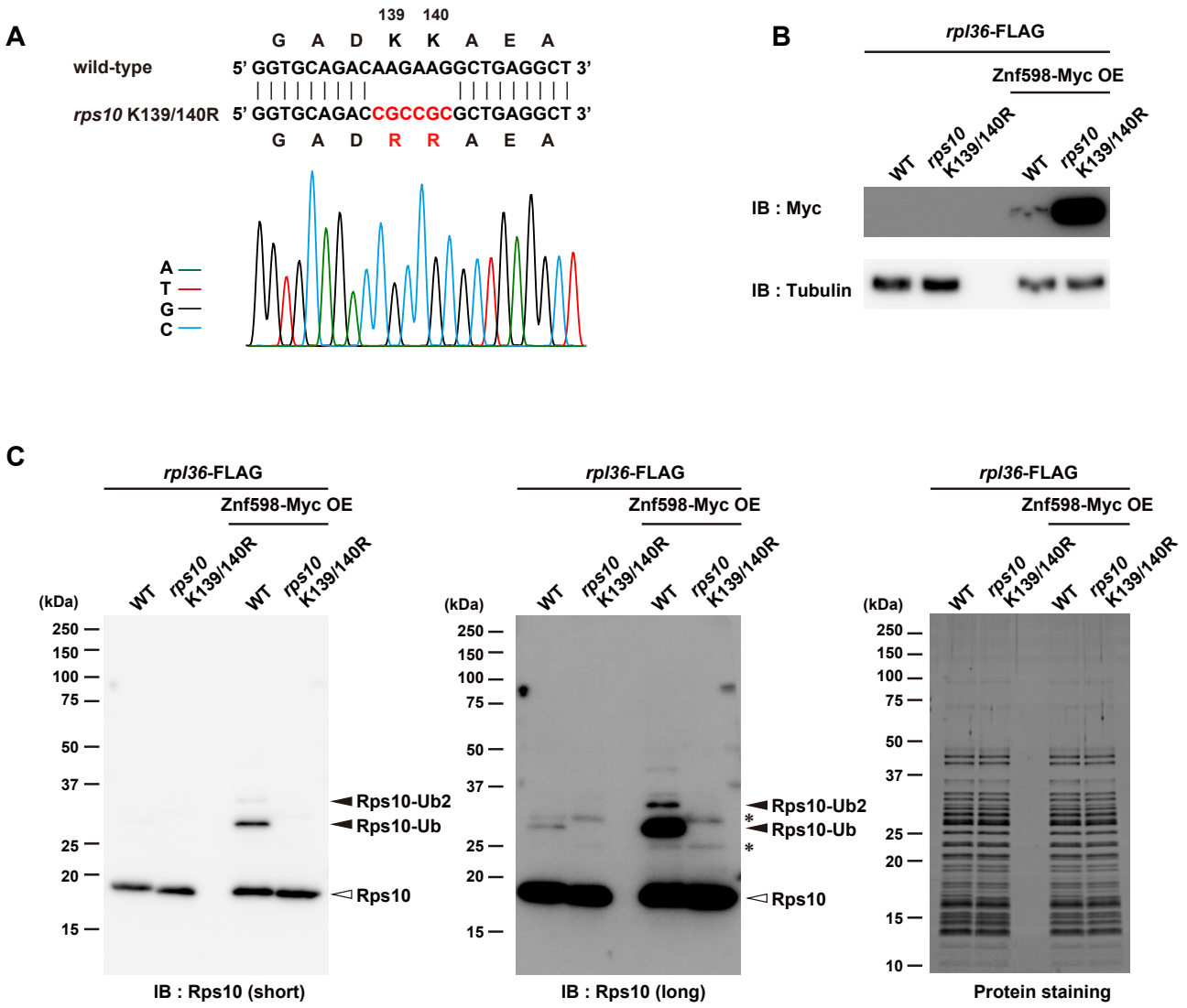

Figure 17. Generation of a Rps10/eS10 ubiquitination-sites mutant

(A) Sequence alignment of the *rps10* gene obtained from wild-type and the *rps10* K139/140R strain. The sequencing chromatogram of the *rps10* K139/140R embryos is indicated below.

(B-C) Detection of Rps10/eS10 ubiquitination with or without Znf598 overexpression in *rpl36*-FLAG and *rps10* K139/140R; *rpl36*-FLAG embryos. Total lysates were subjected to immunoblotting analysis of Znf598-Myc and Tubulin (B). FLAG-immunoprecipitants were subjected to immunoblotting analysis with an anti-Rps10 antibody (C, left and middle) and protein staining (C, right). White and black arrowheads indicate non-ubiquitinated or ubiquitinated Rps10/eS10 signals, respectively. Asterisks indicate non-specific signals.

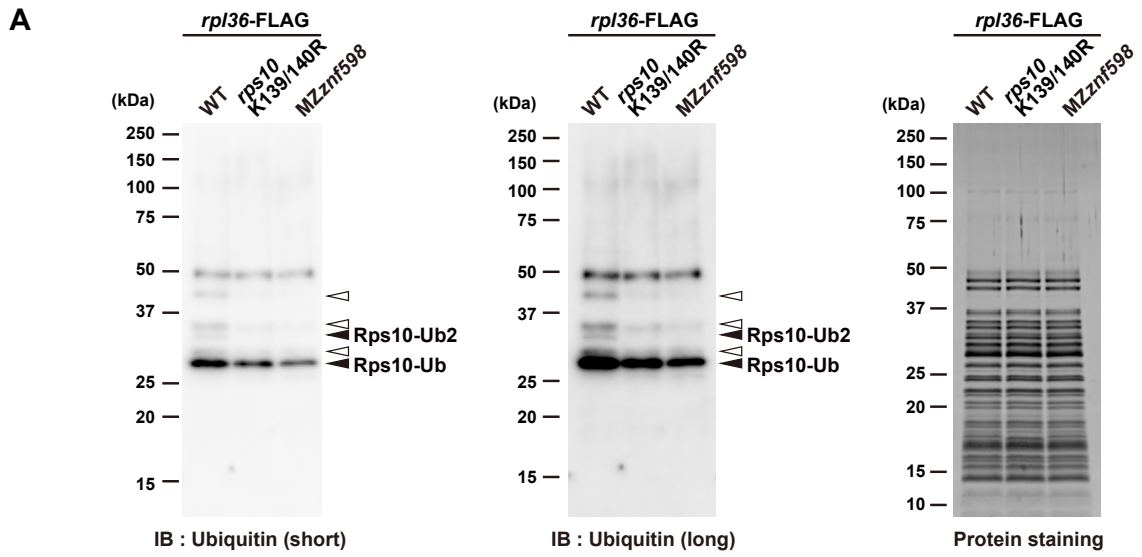

Figure 18. Rps10/eS10 ubiquitination is crucial for establishing the overall ribosome ubiquitination pattern

(A) Comparison of ribosome ubiquitination pattern in *rpl36*-FLAG, *rps10* K139/140R; *rpl36*-FLAG, and MZ*znf598*; *rpl36*-FLAG embryos. FLAG-immunoprecipitants were subjected to immunoblotting analysis with an anti-Ubiquitin antibody (left and middle) and protein staining (right). Black arrowheads indicate putative ubiquitinated Rps10/eS10 signals. White arrowheads indicate reduced ubiquitination signals in *rps10* K139/140R; *rpl36*-FLAG and MZ*znf598*; *rpl36*-FLAG embryos.

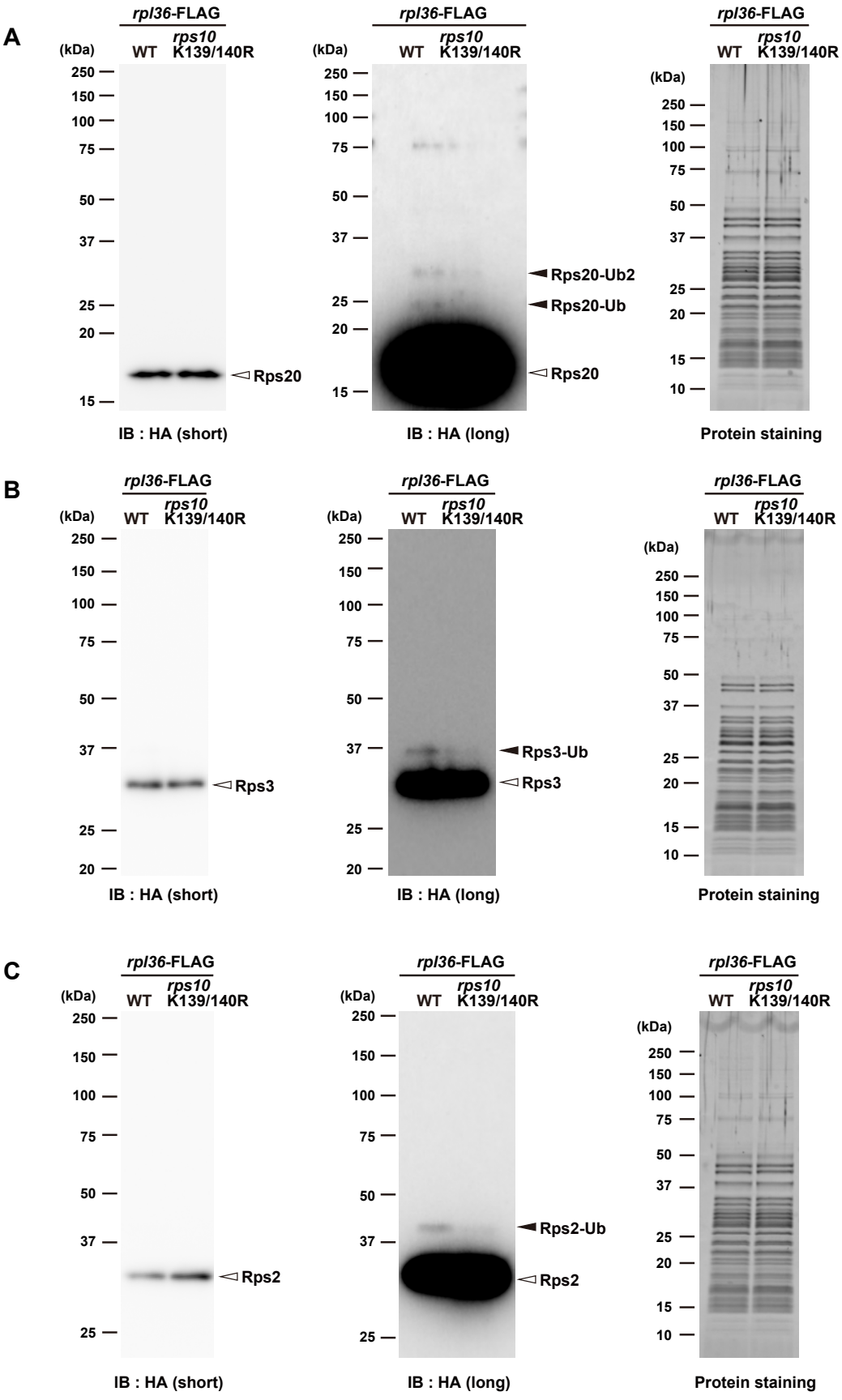

Figure 19. Rps20/uS10, Rps3/uS3, and Rps2/uS5 ubiquitination depend on Rps10/eS10 ubiquitination

(A-C) Comparison of Rps20-HA (A), Rps3-HA (B), and Rps2-HA (C) ubiquitination levels in *rpl36*-FLAG and *rps10* K139/140R; *rpl36*-FLAG embryos. FLAG-immunoprecipitants were subjected to immunoblotting analysis with an anti-HA antibody (left and middle) and protein staining (right). White and black arrowheads indicate non-ubiquitinated or ubiquitinated signals, respectively.

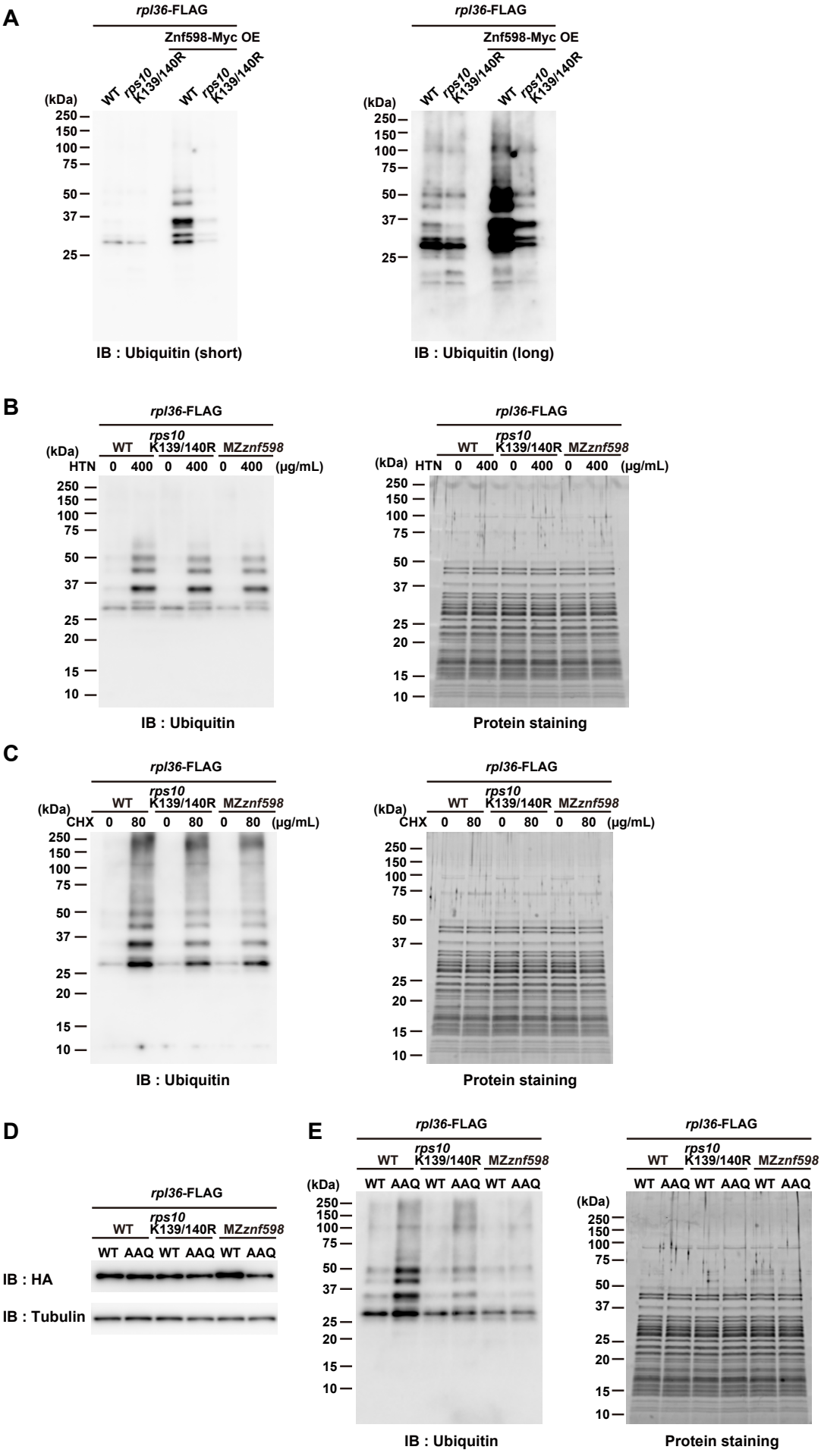

Figure 20. Figure legend on the next page

Figure 20. Rps10/eS10 ubiquitination is a prerequisite for multiple ubiquitination events promoted by Znf598

(A) Comparison of ribosome ubiquitination levels under Znf598 overexpression in *rpl36*-FLAG and *rps10* K139/140R; *rpl36*-FLAG embryos. FLAG-immunoprecipitants in Figure 17C were subjected to immunoblotting analysis with an anti-Ubiquitin antibody.

(B-C) Comparison of ribosome ubiquitination levels under harringtonine (HTN) (B) and cycloheximide (CHX) (C) treatment in *rpl36*-FLAG, *rps10* K139/140R; *rpl36*-FLAG, and MZ*znf598*; *rpl36*-FLAG embryos. FLAG-immunoprecipitants were subjected to immunoblotting analysis with an anti-Ubiquitin antibody (left) and protein staining (right). Concentrations of drugs are indicated above.

(D-E) Comparison of ribosome ubiquitination levels under eRF1-AAQ overexpressed conditions in *rpl36*-FLAG, *rps10* K139/140R; *rpl36*-FLAG, and MZ*znf598*; *rpl36*-FLAG embryos. Total lysates were subjected to immunoblotting analysis of eRF1-HA and Tubulin (D). FLAG-immunoprecipitants were subjected to immunoblotting analysis with an anti-Ubiquitin antibody (E, left) and protein staining (E, right).

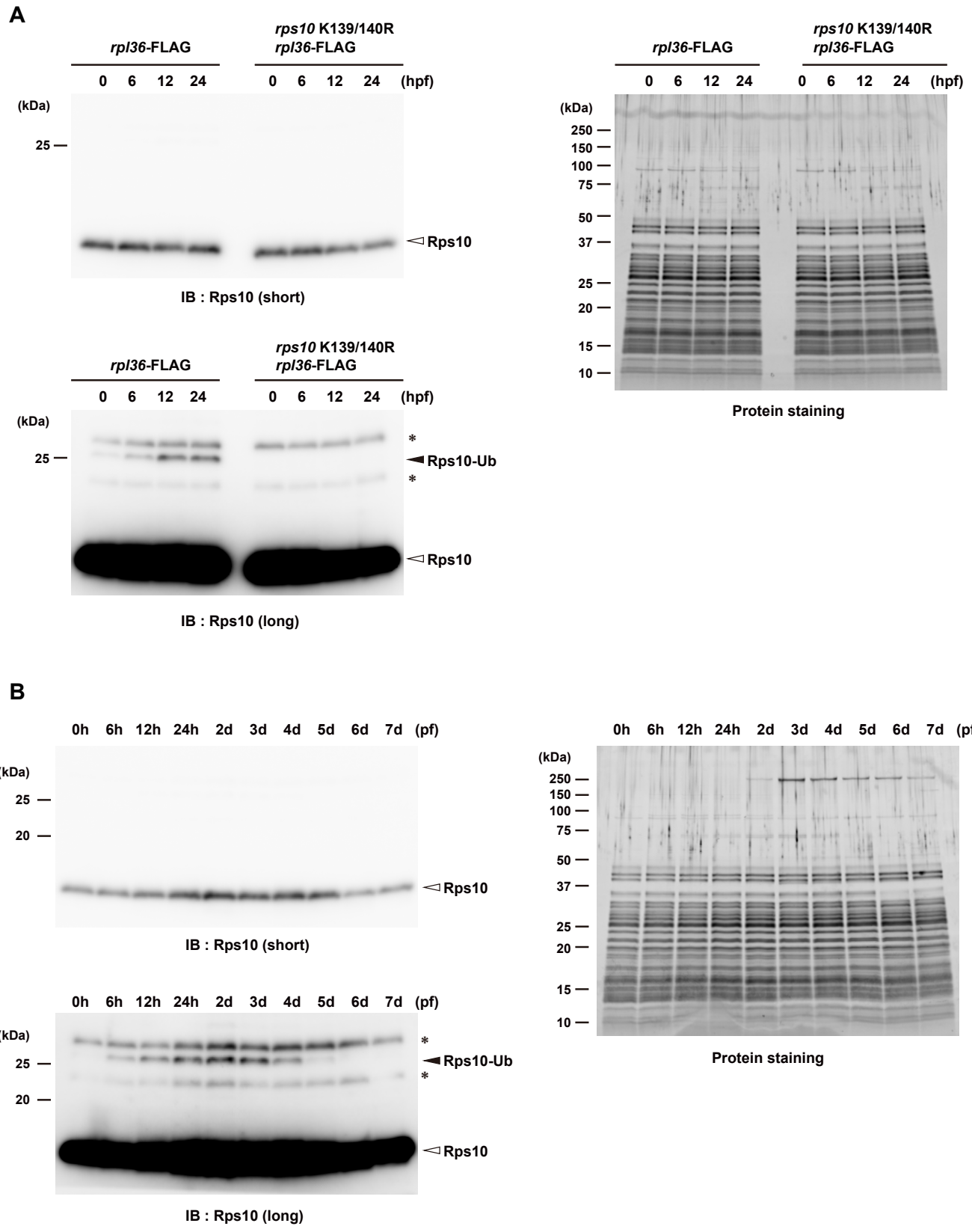

Figure 21. Figure legend on the next page

Figure 21. Rps10/eS10 ubiquitination level temporally changes during development

(A) Detection of Rps10/eS10 ubiquitination from 0 to 24 hpf embryos. FLAG-immunoprecipitants were subjected to immunoblotting analysis with an anti-Rps10 antibody (left) and protein staining (right). The developmental time-points are indicated above as hours post-fertilization (hpf). White and black arrowheads indicate non-ubiquitinated or ubiquitinated Rps10/eS10 signals, respectively. Asterisks indicate non-specific signals.

(B) Detection of Rps10/eS10 ubiquitination during development. FLAG-immunoprecipitants were subjected to immunoblotting analysis with an anti-Rps10 antibody (left) and protein staining (right). The developmental time-points are indicated above as hours post-fertilization (hpf) or days post-fertilization (dpf). White and black arrowheads indicate non-ubiquitinated or ubiquitinated Rps10/eS10 signals, respectively. Asterisks indicate non-specific signals.

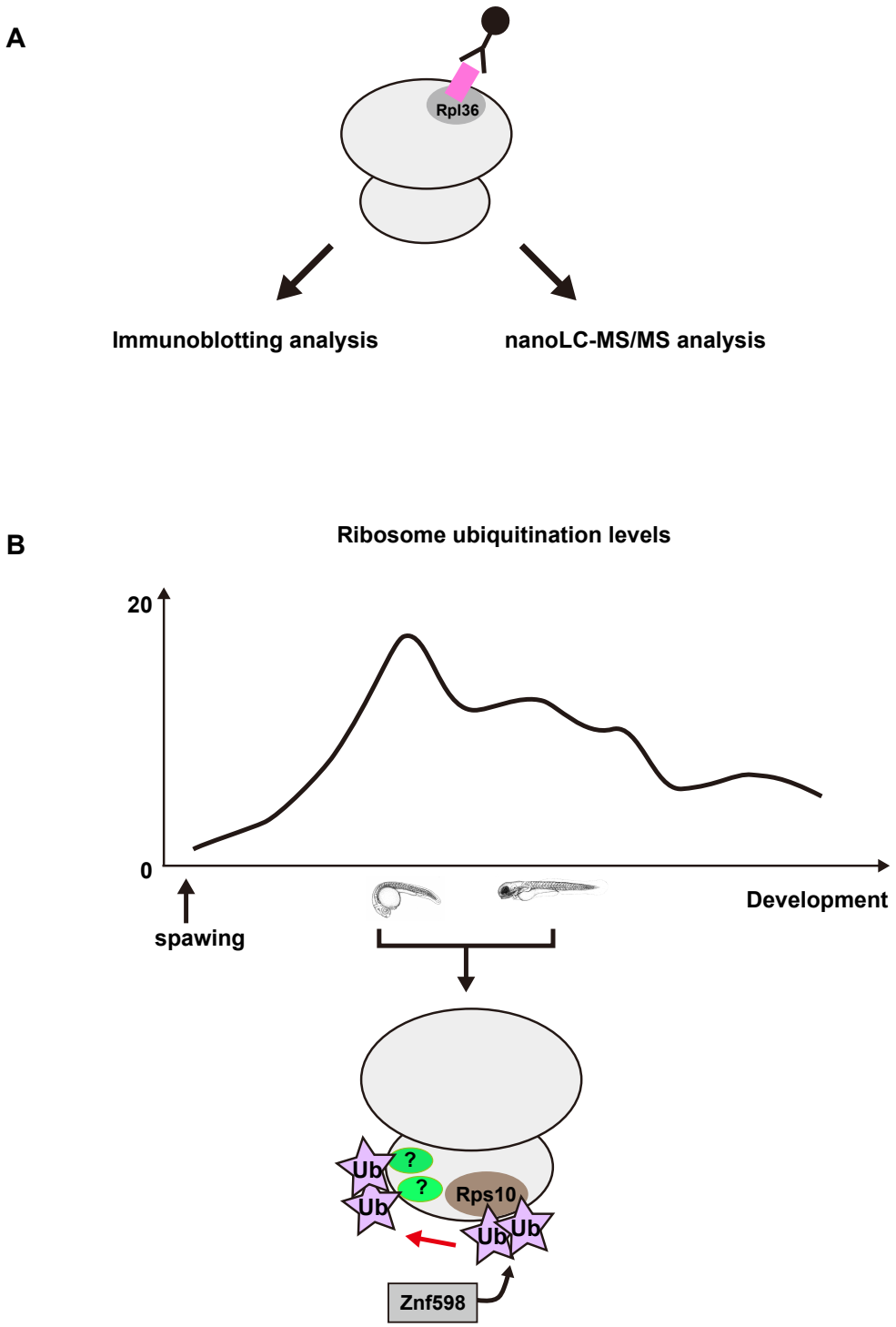

Figure 22. Summary of Chapter 2

(A) To analyze ribosome ubiquitination during zebrafish development, the ribosome purification system is combined with immunoblotting analysis and nanoLC/MS/MS analysis (performed by Dr. Koshi Imami). (B) Ubiquitination levels on ribosomes dynamically change during zebrafish development. In this process, Znf598-mediated Rps10/eS10 ubiquitination plays an important role in establishing the entire ubiquitination pattern on ribosomes directly and indirectly.

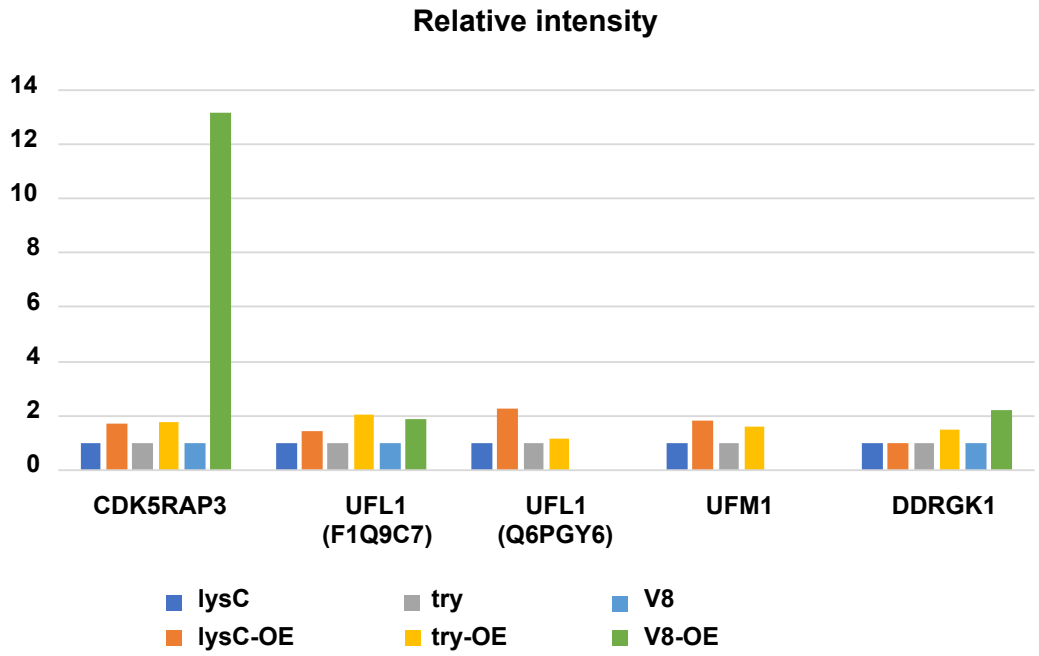

Figure 23. UFMylation-related proteins are efficiently copurified with ribosomes under the Znf598 overexpression condition

A bar graph shows the relative intensity of the indicated peptides under the Znf598 overexpression condition (OE). To compensate for the different amounts of ribosomes in each protease sample with or without Znf598 overexpression, the intensity of these peptides is normalized by the average intensity of identified all ribosomal protein peptides. The average of two independent experiments is indicated. Three proteases were used in this analysis: lysyl endopeptidase (lysC), trypsin (try), and endoproteinase GluC (V8).

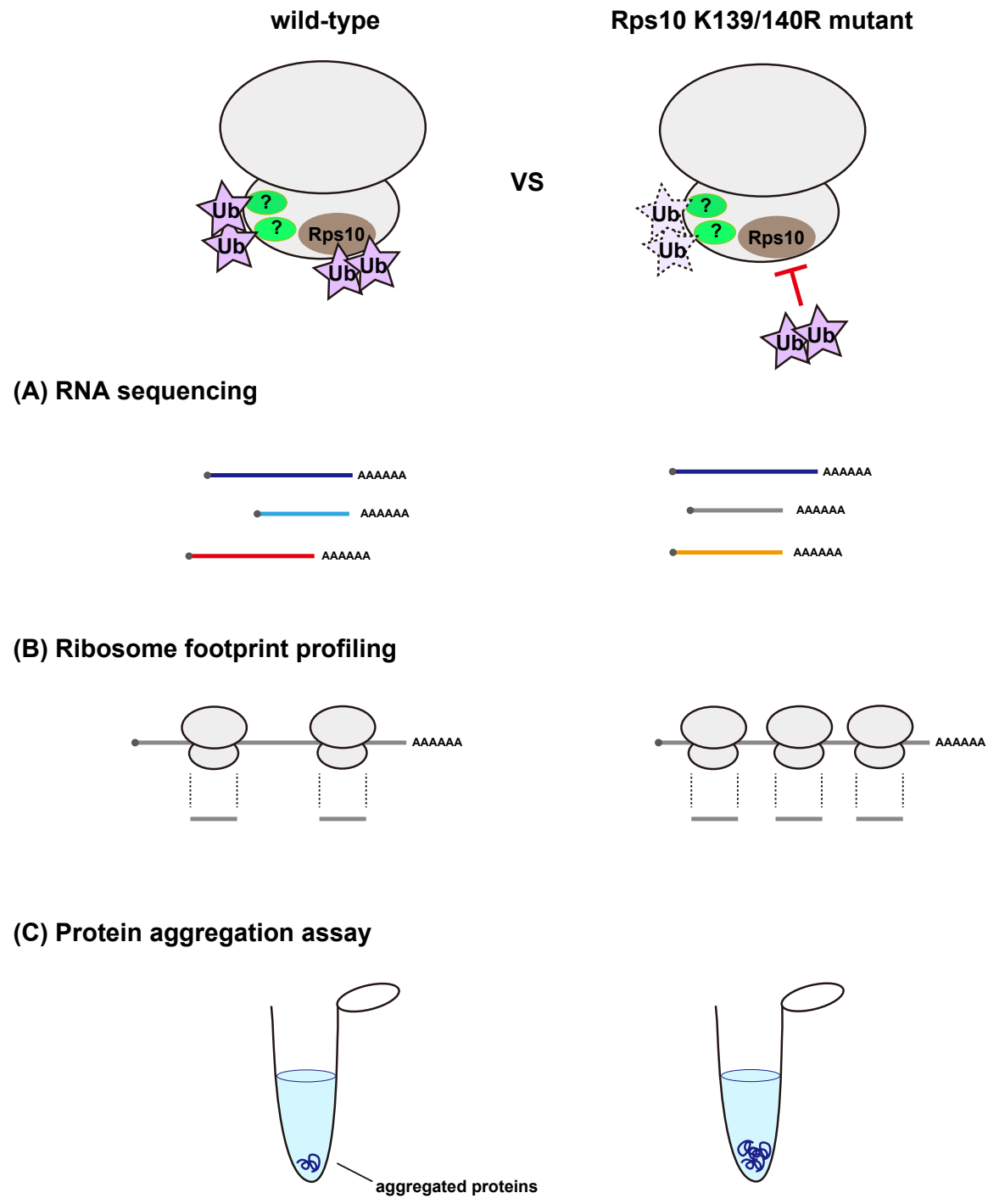

Figure 24. Future studies for examining the biological relevance of Rps10/eS10 ubiquitination during development

(A) To comprehensively compare the gene expression level between wild-type and Rps10/eS10 mutant embryos, RNA sequencing is a powerful tool. Genes related to erythroid differentiation, liver differentiation, and neuronal development are potential candidates affected in the mutant.

(B) Ribosome footprint profiling allows direct, high-resolution measurements of ribosome position and occupancy on endogenous genes in living cells. Thus, by combining ribosome footprint profiling with RNA sequencing, the efficiency of translation and ribosomal frameshifting can be compared between wild-type and Rps10/eS10 mutant embryos.

(C) If translational fidelity is declined in Rps10/eS10 mutant embryos, the level of aggregated proteins may be increased. Isolation and identification of aggregated proteins by sedimentation may provide further insights in such a scenario.

Tables

Supplemental Table S1. List of oligonucleotides and primers

Single-strand DNA oligonucleotide for generation of the rpl36-FLAG strain via CRISPR/Cas9	CACAAGAGTCAAAAATACTCGTTTTTAC ACAAACAATTTTATTTTTGATGATTACAC AGGCTATCACTTATCGTCGTCATCCTTGT AATCGCTGCCCTCTTTCTTGGCAGCAGC TTTCCTCATGGCGGCCAGTGTGTTGCTG AGCTCTTCCCTCTTTCTC
Single-strand DNA oligonucleotide for generation of the rps10 K139/140R strain via CRISPR/Cas9	CAGCATGTTTACCTTTTGCCTTTCTCATG CAGCATTATGTTAAACACAACCCTTTATT CAACAGCCGGTGCAGACCGCCGCGCTG AGGCTGGTGCAGGTGCAGCCACAGAGT TCCAGTTTG
Forward primer for rpl36-FLAG sgRNA	TAATACGACTCACTATAGGACACAGGCT ACTCTTTCTGTTTTAGAGCTAGAA
Forward primer for rps10 K139/140R sgRNA	TAATACGACTCACTATAGGGTGCAGACA AGAAGGCTGGTTTTAGAGCTAGAA
Reverse primer for rpl36-FLAG and rps10K139/140R sgRNA	AAAAGCACCGACTCGGTGCCACTTTTTC AAGTTGATAACGGACTAGCCTTATTTTAA CTTGCTATTTCTAGCTCTAAAAC
Forward primer for genotyping of the rpl36-FLAG strain	ACATCCGCGCTAAGAGAAAG
Reverse primer for genotyping of the rpl36-FLAG strain	TCAAGCACAAGAGTCAAAAATACTC
Forward primer for genotyping of the rps10 K139/140R strain	TGGCGAGGGAGACAGAGATGCT
Reverse primer for genotyping of the rps10 K139/140R strain	CCAGCCTCAGCGCGGCG
Forward primer for rpl36	CCGGAATTCAGAGCAGAGATGGTTGTCA GAT
Reverse primer for rpl36	CCGCTCGAGCTATCACTTATCGTCGTCAT CCTTGTAATCGCTGCCCTCTTTCTTGGCA GCAGCTT
Forward primer for eRF1b-WT	GGATCCCATCGATTCGAATTCATGGCGG ACGACCCCAGC

Reverse primer for eRF1b-WT	ACGACTCACTATAGTTCTAGACTAGGCG TAGTCTGGGACGTC
Forward primer for eRF1b-AAQ mutation	GCACGGTAGAGCAGCACAGTCCGCTCTT CGTTTTGCTCG
Reverse primer for eRF1b-AAQ mutation	GAAGAGCGGACTGTGCTGCTCTACCGTG CTTTTTGGGCAG
Forward primer for znf598-WT	GCCTCTCGAGATGGAGTCTG
Reverse primer for znf598-WT	TGCTCTAGACTACAAGTCCTCTTCAGAA ATGAGCTTTTGCTCGCTTCCGCCGCTGAT AATCTTGCTTATGG
Forward primer for znf598-C13/16A mutation	CCGCTCGAGATGGAGTCTGCCCTGAAGA AAGACACGGAGAGCACCGCTGTGCTGG CCTGCCAGGACATCGAC
Reverse primer for znf598-C13/16A mutation	TGCTCTAGACTACAAGTCCTCTTCAGAA ATGAGCTTTTGCTCGCTTCCGCCGCTGAT AATCTTGCTTATGG
Forward primer for rps10-WT	GATCCCATCGATTCGAATTCGATGTTGAT GCCCAAGAAGAAC
Reverse primer for rps10-WT	GTCGTATGGGTACATCTGTGGCTGCTGTC CTCGG
Forward primer for rps10-K139R mutation	CGGTGCAGACCGCAAGGCTGAGGCTGG TGCAGG
Reverse primer for rps10-K139R mutation	CCTCAGCCTTGCGGTCTGCACCGGGCTG AGCTG
Forward primer for rps10-K140R mutation	TGCAGACAAGCGCGCTGAGGCTGGTGC AGGTGC
Reverse primer for rps10-K140R mutation	CAGCCTCAGCGCGCTTGTCTGCACCGGG CTGAG
Forward primer for rps10-K139/140R mutation	CGGTGCAGACCGCCGCGCTGAGGCTGG TGCAGGTGC
Reverse primer for rps10-K139/140R mutation	CAGCCTCAGCGCGGCGGTCTGCACCGG GCTGAGCTG
Forward primer for rps20	CCGGAATTCAATGGCATTTAAAGACACT GGC
Reverse primer for rps20	CCGCTCGAGTTAGGCGTAGTCGGGCACG TCGTAGGGATAAGCATCTGCAATTGTGA

	CCTC
Forward primer for rps3	GATCCCATCGATTCGAATTCAAGATGGC GGTGCAAATCTC
Reverse primer for rps3	GTCGTATGGGTACATTGCTGTGGGCACT GGGG
Forward primer for rps2	GGATCCCATCGATTCCTCGAGCAAATGG CGGACGACGCCGGTGGTA
Reverse primer for rps2	GTCGTATGGGTACATGGAGGTTCCCTGA GGAAGAGC

Supplemental Table S2. List of plasmids

pCS2+Rpl36-FLAG
pCS2+eTF1b-HA
pCS2+eTF1b-HA-AAQ
pCS2+Znf598-Myc
pCS2+Znf598-Myc-C13/16A
pCS2+Rps10-HA
pCS2+Rps10-HA-K139R
pCS2+Rps10-HA-K140R
pCS2+Rps10-HA-K139/140R
pCS2+Rps20-HA
pCS2+Rps3-HA
pCS2+Rps2-HA

Supplemental Table S3. List of antibodies

Rabbit polyclonal anti-DDDDK tag (1:10000)	MEDICAL&BIOLOGICAL LABORATORIES CO., LTD	Cat# PM020-7
Mouse monoclonal anti-HA tag (1:10000)	MEDICAL&BIOLOGICAL LABORATORIES CO., LTD	Cat# M180-7
Mouse monoclonal anti-Myc tag (1:10000)	MEDICAL&BIOLOGICAL LABORATORIES CO., LTD	Cat# M192-3
Rabbit monoclonal anti-DDX6 (1:1000)	Cell Signaling	Cat# 8988
Rabblt polyclonal anti-Ef1a (1:1000)	GeneTex	Cat# GTX124538
Rabbit polyclonal anti-PABP1	Cell Signaling	Cat# 4992

(1:1000)		
Rabbit polyclonal anti-Rpl7a (1:4000)	GeneTex	Cat# GTX124314
Rabbit polyclonal anti-Rps10 (1:2500)	GeneTex	Cat# GTX127397
Rabbit polyclonal anti-Tubulin (1:10000)	MEDICAL&BIOLOGICAL LABORATORIES CO., LTD	Cat# PM054-7
Goat anti-rabbit secondary HRP-conjugated (1:5000)	MEDICAL&BIOLOGICAL LABORATORIES CO., LTD	Cat# 458
Goat anti-mouse secondary HRP-conjugated (1:5000)	MEDICAL&BIOLOGICAL LABORATORIES CO., LTD	Cat# 330
Ubiquitin mouse mAb (1:20000)	Cell Signaling	Cat#14049

References

Aebersold R, Mann M. 2016. Mass-spectrometric exploration of proteome structure and function. *Nature* **537**: 347–355.

Aitken CE, Lorsch JR. 2012. A mechanistic overview of translation initiation in eukaryotes. *Nat Struct Mol Biol* **19**: 568–576.

Akutsu M, Dikic I, Bremm A. 2016. Ubiquitin chain diversity at a glance. *J Cell Sci* **129**: 875–880.

An H, Harper JW. 2020. Ribosome Abundance Control Via the Ubiquitin–Proteasome System and Autophagy. *J Mol Biol* **432**: 170–184.

Anisimova AS, Alexandrov AI, Makarova NE, Gladyshev VN, Dmitriev SE. 2018. Protein synthesis and quality control in aging. *Aging* **10**: 4269–4288.

Avilés-Pagán EE, Orr-Weaver TL. 2018. Activating embryonic development in Drosophila. *Semin Cell Dev Biol* **84**: 100–110.

Aviner R, Hofmann S, Elman T, Shenoy A, Geiger T, Elkon R, Ehrlich M, Elroy-Stein O. 2017. Proteomic analysis of polyribosomes identifies splicing factors as potential regulators of translation during mitosis. *Nucleic Acids Res* **45**: 5945–5957.

Back S, Gorman AW, Vogel C, Silva GM. 2019. Site-Specific K63 Ubiquitinomics Provides Insights into Translation Regulation under Stress. *J Proteome Res* **18**: 309–318.

Bai H, Liu L, An K, Lu X, Harrison M, Zhao Y, Yan R, Lu Z, Li S, Lin S, et al. 2020. CRISPR/Cas9-mediated precise genome modification by a long ssDNA template in zebrafish. *BMC Genomics* **21**: 1–12.

Banerjee S, Kumar M, Wiener R. 2020. Decrypting UFMylation: How Proteins Are Modified with UFM1. *Biomolecules* **10**: 1442.

Bashan A, Yonath A. 2008. Correlating ribosome function with high-resolution structures. *Trends Microbiol* **16**: 326–335.

Bazzini AA, del Viso F, Moreno-Mateos MA, Johnstone TG, Vejnar CE, Qin Y, Yao J, Khokha MK, Giraldez AJ. 2016. Codon identity regulates mRNA stability and translation efficiency during the maternal-to-zygotic transition. *EMBO J* **35**: 2087–2103.

Bengtson MH, Joazeiro CAP. 2010. Role of a ribosome-associated E3 ubiquitin ligase in protein quality control. *Nature* **467**: 470–473.

Boel A, De Saffel H, Steyaert W, Callewaert B, De Paepe A, Coucke PJ, Willaert A. 2018. CRISPR/Cas9-mediated homology-directed repair by ssODNs in zebrafish induces complex mutational patterns resulting from genomic integration of repair-template fragments. *Dis Model Mech* **11**: dmm035352.

Borg NA, Dixit VM. 2017. Ubiquitin in Cell-Cycle Regulation and Dysregulation in Cancer. *Annu Rev Cancer Biol* **1**: 59–77.

Brandman O, Stewart-Ornstein J, Wong D, Larson A, Williams CC, Li GW, Zhou S, King D, Shen PS, Weibezahn J, et al. 2012. A Ribosome-Bound Quality Control Complex Triggers Degradation of Nascent Peptides and Signals Translation Stress. *Cell* **151**: 1042–1054.

Brina D, Miluzio A, Ricciardi S, Biffo S. 2015. eIF6 anti-association activity is required for ribosome biogenesis, translational control and tumor progression. *Biochim Biophys Acta BBA - Gene Regul Mech* **1849**: 830–835.

Burke MC, Wang Y, Lee AE, Dixon EK, Castaneda CA, Fushman D, Fenselau C. 2015. Unexpected Trypsin Cleavage at Ubiquitinated Lysines. *Anal Chem* **87**: 8144–8148.

Bursac S, Brdovcak MC, Donati G, Volarevic S. 2014. Activation of the tumor suppressor p53 upon impairment of ribosome biogenesis. *Biochim Biophys Acta - Mol Basis Dis* **1842**: 817–830.

Buschauer R, Matsuo Y, Sugiyama T, Chen Y-H, Alhusaini N, Sweet T, Ikeuchi K, Cheng J, Matsuki Y, Nobuta R, et al. 2020. The Ccr4-Not complex monitors the translating ribosome for codon optimality. *Science* **368**: eaay6912.

Cai Y, Singh N, Li H. 2016. Essential role of Ufm1 conjugation in the hematopoietic system. *Exp Hematol* **44**: 442–446.

Cappadocia L, Lima CD. 2018. Ubiquitin-like Protein Conjugation: Structures, Chemistry, and Mechanism. *Chem Rev* **118**: 889–918.

Carpenter S, Ricci EP, Mercier BC, Moore MJ, Fitzgerald KA. 2014. Post-transcriptional regulation of gene expression in innate immunity. *Nat Rev Immunol* **14**: 361–376.

Chen C-YA, Shyu A-B. 2011. Mechanisms of deadenylation-dependent decay: Mechanisms of deadenylation-dependent decay. *Wiley Interdiscip Rev RNA* **2**: 167–183.

Clague MJ, Urbé S, Komander D. 2019. Breaking the chains: deubiquitylating enzyme specificity begets function. *Nat Rev Mol Cell Biol* **20**: 338–352.

Cox J, Mann M. 2008. MaxQuant enables high peptide identification rates, individualized p.p.b.-range mass accuracies and proteome-wide protein quantification. *Nat Biotechnol* **26**: 1367–1372.

Cox J, Neuhauser N, Michalski A, Scheltema RA, Olsen JV, Mann M. 2011. Andromeda: A Peptide Search Engine Integrated into the MaxQuant Environment. *J Proteome Res* **10**: 1794–1805.

Dalla Venezia N, Vincent A, Marcel V, Catez F, Diaz J-J. 2019. Emerging Role of Eukaryote Ribosomes in Translational Control. *Int J Mol Sci* **20**: 1226.

Dastidar SG, Nair D. 2022. A Ribosomal Perspective on Neuronal Local Protein Synthesis. *Front Mol Neurosci* **15**: 1–14.

De La Cruz J, Karbstein K, Woolford JL. 2015. Functions of ribosomal proteins in assembly of eukaryotic ribosomes in vivo. *Annu Rev Biochem* **84**: 93–129.

Deuerling E, Gamerdinger M, Kreft SG. 2019. Chaperone Interactions at the Ribosome. *Cold Spring Harb Perspect Biol* **11**: a033977.

Dever TE, Dinman JD, Green R. 2018. Translation Elongation and Recoding in Eukaryotes. *Cold Spring Harb Perspect Biol* **10**: a032649.

D'Orazio KN, Wu CCC, Sinha N, Loll-Krippleber R, Brown GW, Green R. 2019. The endonuclease cue2 cleaves mRNAs at stalled ribosomes during no go decay. *eLife* **8**: 1–27.

Dougherty SE, Maduka AO, Inada T, Silva GM. 2020. Expanding role of ubiquitin in translational control. *Int J Mol Sci* **21**: 1–24.

Ebright RY, Lee S, Wittner BS, Niederhoffer KL, Nicholson BT, Bardia A, Truesdell S, Wiley DF, Wesley B, Li S, et al. 2020. Deregulation of ribosomal protein expression and translation promotes breast cancer metastasis. *Science* **367**: 1468–1473.

Emmott E, Jovanovic M, Slavov N. 2019. Ribosome Stoichiometry: From Form to Function. *Trends Biochem Sci* **44**: 95–109.

Ferreira R, Schneekloth JS, Panov KI, Hannan KM, Hannan RD. 2020. Targeting the RNA Polymerase I Transcription for Cancer Therapy Comes of Age. *Cells* **9**: 266.

Ferretti MB, Ghalei H, Ward EA, Potts EL, Karbstein K. 2017. Rps26 directs mRNA-specific translation by recognition of Kozak sequence elements. *Nat Struct Mol Biol* **24**: 700–707.

Frolova LY, Tsivkovskii RY, Sivolobova GF, Oparina NY, Serpinsky OI, Blinov VM, Tatkov SI, Kisselev LL. 1999. Mutations in the highly conserved GGQ motif of class I polypeptide release factors abolish ability of human eRF1 to trigger peptidyl-tRNA hydrolysis. *RNA* **5**: 1014–1020.

Fusco CM, Desch K, Dörrbaum AR, Wang M, Staab A, Chan ICW, Vail E, Villeri V, Langer JD, Schuman EM. 2021. Neuronal ribosomes exhibit dynamic and context-dependent exchange of ribosomal proteins. *Nat Commun* **12**: 6127.

Gabut M, Bourdelais F, Durand S. 2020. Ribosome and Translational Control in Stem Cells. *Cells* **9**: 1–31.

Gamerdinger M, Kobayashi K, Wallisch A, Kreft SG, Sailer C, Schlömer R, Sachs N, Jomaa A, Stengel F, Ban N, et al. 2019. Early Scanning of Nascent Polypeptides inside the Ribosomal Tunnel by NAC. *Mol Cell* **75**: 996-1006.e8.

Garshott DM, An H, Sundaramoorthy E, Leonard M, Vicary A, Harper JW, Bennett EJ. 2021. iRQC, a surveillance pathway for 40S ribosomal quality control during mRNA translation initiation. *Cell Rep* **36**: 109642.

Garshott DM, Sundaramoorthy E, Leonard M, Bennett EJ. 2020. Distinct regulatory ribosomal

ubiquitylation events are reversible and hierarchically organized. *eLife* **9**: 1–22.

Garzia A, Jafarnejad SM, Meyer C, Chapat C, Gogakos T, Morozov P, Amiri M, Shapiro M, Molina H, Tuschl T, et al. 2017. The E3 ubiquitin ligase and RNA-binding protein ZNF598 orchestrates ribosome quality control of premature polyadenylated mRNAs. *Nat Commun* **8**: 16056.

Garzia A, Meyer C, Tuschl T. 2021. The E3 ubiquitin ligase RNF10 modifies 40S ribosomal subunits of ribosomes compromised in translation. *Cell Rep* **36**: 109468.

Genuth NR, Barna M. 2018a. Heterogeneity and specialized functions of translation machinery: From genes to organisms. *Nat Rev Genet* **19**: 431–452.

Genuth NR, Barna M. 2018b. The Discovery of Ribosome Heterogeneity and Its Implications for Gene Regulation and Organismal Life. *Mol Cell* **71**: 364–374.

Genuth NR, Shi Z, Kunimoto K, Hung V, Xu AF, Kerr CH, Tiu GC, Oses-Prieto JA, Salomon-Shulman REA, Axelrod JD, et al. 2022. A stem cell roadmap of ribosome heterogeneity reveals a function for RPL10A in mesoderm production. *Nat Commun* **13**: 5491.

Gilbert WV. 2011. Functional specialization of ribosomes? *Trends Biochem Sci* **36**: 127–132.

Gilles A, Frechin L, Natchiar K, Biondani G, Loeffelholz O von, Holvec S, Malaval JL, Winum JY, Klaholz BP, Peyron JF. 2020. Targeting the Human 80S Ribosome in Cancer: From Structure to Function and Drug Design for Innovative Adjuvant Therapeutic Strategies. *Cells* **9**: 1–22.

Glover ML, Burroughs AM, Monem PC, Egelhofer TA, Pule MN, Aravind L, Arribere JA. 2020. NONU-1 Encodes a Conserved Endonuclease Required for mRNA Translation Surveillance. *Cell Rep* **30**: 4321-4331.e4.

Glowacki ER, Millette RL. 1965. Polyribosomes and the loss of hemoglobin synthesis in the maturing reticulocyte. *J Mol Biol* **11**: 116–127.

Gonskikh Y, Polacek N. 2017. Alterations of the translation apparatus during aging and stress response. *Mech Ageing Dev* **168**: 30–36.

Gray NK. 2000. Multiple portions of poly(A)-binding protein stimulate translation in vivo. *EMBO J*

19: 4723–4733.

Häfner SJ, Jansson MD, Altinel K, Andersen KL, Abay-Nørgaard Z, Ménard P, Fontenas M, Sørensen DM, Gay DM, Arendrup FS, Tehler D, Krogh N, Nielsen H, Kraushar ML, Kirkeby A, Lund AH. 2023. Ribosomal RNA 2′-O-methylation dynamics impact cell fate decisions. *Dev Cell* **58**: 1593-1609.e9.

Han P, Shichino Y, Schneider-Poetsch T, Mito M, Hashimoto S, Udagawa T, Kohno K, Yoshida M, Mishima Y, Inada T, et al. 2020. Genome-wide Survey of Ribosome Collision. *Cell Rep* **31**: 107610.

Hanson G, Coller J. 2018. Codon optimality, bias and usage in translation and mRNA decay. *Nat Rev Mol Cell Biol* **19**: 20-30.

Hellen CUT. 2018. Translation termination and ribosome recycling in eukaryotes. *Cold Spring Harb Perspect Biol* **10**: a032656.

Higgins R, Gendron JM, Rising L, Mak R, Webb K, Kaiser SE, Zuzow N, Riviere P, Yang B, Fenech E, et al. 2015. The Unfolded Protein Response Triggers Site-Specific Regulatory Ubiquitylation of 40S Ribosomal Proteins. *Mol Cell* **59**: 35–49.

Ikeuchi K, Tesina P, Matsuo Y, Sugiyama T, Cheng J, Saeki Y, Tanaka K, Becker T, Beckmann R, Inada T. 2019. Collided ribosomes form a unique structural interface to induce Hel2-driven quality control pathways. *EMBO J* **38**: 1–21.

Imami K, Milek M, Bogdanow B, Yasuda T, Kastelic N, Zauber H, Ishihama Y, Landthaler M, Selbach M. 2018. Phosphorylation of the Ribosomal Protein RPL12/uL11 Affects Translation during Mitosis. *Mol Cell* **72**: 84-98.e9.

Inada T. 2020. Quality controls induced by aberrant translation. *Nucleic Acids Res* **48**: 1084–1096.

Inada T, Winstall E, Tarun SZ, Yates JR, Schieltz D, Sachs AB. 2002. One-step affinity purification of the yeast ribosome and its associated proteins and mRNAs. *RNA* **8**: 948–958.

Ingolia NT. 2014. Ribosome profiling: New views of translation, from single codons to genome scale. *Nat Rev Genet* **15**: 205–213.

Ishihama Y, Rappsilber J, Andersen JS, Mann M. 2002. Microcolumns with self-assembled particle frits for proteomics. *J Chromatogr A* **979**: 233–239.

Ishimura R, Ito S, Mao G, Komatsu-Hirota S, Inada T, Noda NN, Komatsu M. 2023. Mechanistic insights into the roles of the UFM1 E3 ligase complex in ufmylation and ribosome-associated protein quality control. *Sci Adv* **9**: eadh3635.

Ishimura R, Nagy G, Dotu I, Zhou H, Yang XL, Schimmel P, Senju S, Nishimura Y, Chuang JH, Ackerman SL. 2014. Ribosome stalling induced by mutation of a CNS-specific tRNA causes neurodegeneration. *Science* **345**: 455–459.

Jansen Ruud, Embden JanDAV, Gaastra Wim, Schouls LeoM. 2002. Identification of genes that are associated with DNA repeats in prokaryotes. *Mol Microbiol* **43**: 1565–1575.

Jiao L, Liu Y, Yu X-Y, Pan X, Zhang Y, Tu J, Song Y-H, Li Y. 2023. Ribosome biogenesis in disease: new players and therapeutic targets. *Signal Transduct Target Ther* **8**: 15.

Jinek M, Chylinski K, Fonfara I, Hauer M, Doudna JA, Charpentier E. 2012. A Programmable Dual-RNA–Guided DNA Endonuclease in Adaptive Bacterial Immunity. *Science* **337**: 816–821.

Joazeiro CAP. 2019. Mechanisms and functions of ribosome-associated protein quality control. *Nat Rev Mol Cell Biol* **20**: 368–383.

Joazeiro CAP. 2017. Ribosomal stalling during translation: Providing substrates for ribosome-associated protein quality control. *Annu Rev Cell Dev Biol* **33**: 343–368.

Johannes G, Carter MS, Eisen MB, Brown PO, Sarnow P. 1999. Identification of eukaryotic mRNAs that are translated at reduced cap binding complex elF4F concentrations using a cDNA microarray. *Proc Natl Acad Sci U S A* **96**: 13118–13123.

Johnson ES, Bartel B, Seufert W, Varshavsky A. 1992. Ubiquitin as a degradation signal. *EMBO J* **11**: 497–505.

Juszkiewicz S, Chandrasekaran V, Lin Z, Kraatz S, Ramakrishnan V, Hegde RS. 2018. ZNF598 Is a Quality Control Sensor of Collided Ribosomes. *Mol Cell* **72**: 469-481.e7.

Juszkiewicz S, Hegde RS. 2017. Initiation of Quality Control during Poly(A) Translation Requires Site-Specific Ribosome Ubiquitination. *Mol Cell* **65**: 743-750.e4.

Juszkiewicz S, Slodkowicz G, Lin Z, Freire-pritchett P, Hegde RS. 2020a. Ribosome collisions trigger cis-acting feedback inhibition of translation initiation. *Elife* **9**: e60038.

Juszkiewicz S, Speldewinde SH, Wan L, Svejstrup JQ, Hegde RS. 2020b. The ASC-1 Complex Disassembles Collided Ribosomes. *Mol Cell* **79**: 603-614.e8.

Kang J, Brajanovski N, Chan KT, Xuan J, Pearson RB, Sanij E. 2021. Ribosomal proteins and human diseases: molecular mechanisms and targeted therapy. *Signal Transduct Target Ther* **6**: 323.

Kang MK, Han SJ. 2011. Post-transcriptional and post-translational regulation during mouse oocyte maturation. *BMB Rep* **44**: 147–157.

Kapur M, Ackerman SL. 2018. mRNA Translation Gone Awry: Translation Fidelity and Neurological Disease. *Trends Genet* **34**: 218–231.

Kawakami K, Shima A, Kawakami N. 2000. Identification of a functional transposase of the Tol2 element, an Ac-like element from the Japanese medaka fish, and its transposition in the zebrafish germ lineage. *Proc Natl Acad Sci U S A* **97**: 11403–11408.

Khajuria RK, Munschauer M, Ulirsch JC, Fiorini C, Ludwig LS, McFarland SK, Abdulhay NJ, Specht H, Keshishian H, Mani DR, et al. 2018. Ribosome Levels Selectively Regulate Translation and Lineage Commitment in Human Hematopoiesis. *Cell* **173**: 90-103.e19.

Kim JH, Richter JD. 2006. Opposing Polymerase-Deadenylase Activities Regulate Cytoplasmic Polyadenylation. *Mol Cell* **24**: 173–183.

Kim W, Bennett EJ, Huttlin EL, Guo A, Li J, Possemato A, Sowa ME, Rad R, Rush J, Comb MJ, et al. 2011. Systematic and Quantitative Assessment of the Ubiquitin-Modified Proteome. *Mol Cell* **44**: 325–340.

Kimmel CB, Ballard WW, Kimmel SR, Ullmann B, Schilling TF. 1995. Stages of embryonic development of the zebrafish. *Dev Dyn* **203**: 253–310.

Kito Y, Matsumoto A, Ichihara K, Shiraishi C, Tang R, Hatano A, Matsumoto M, Han P, Iwasaki S, Nakayama KI. 2023. The ASC-1 complex promotes translation initiation by scanning ribosomes. *EMBO J* **42**: e112869.

Kobayashi T. 2011. Regulation of ribosomal RNA gene copy number and its role in modulating genome integrity and evolutionary adaptability in yeast. *Cell Mol Life Sci* **68**: 1395–1403.

Komander D, Rape M. 2012. The Ubiquitin Code. *Annu Rev Biochem* **81**: 203–229.

Komili S, Farny NG, Roth FP, Silver PA. 2007. Functional Specificity among Ribosomal Proteins Regulates Gene Expression. *Cell* **131**: 557–571.

Kondrashov N, Pusic A, Stumpf CR, Shimizu K, Hsieh AC, Xue S, Ishijima J, Shiroishi T, Barna M. 2011. Ribosome-mediated specificity in Hox mRNA translation and vertebrate tissue patterning. *Cell* **145**: 383–397.

Koplin A, Preissler S, Llina Y, Koch M, Scior A, Erhardt M, Deuerling E. 2010. A dual function for chaperones SSB-RAC and the NAC nascent polypeptide-associated complex on ribosomes. *J Cell Biol* **189**: 57–68.

Kornprobst M, Turk M, Kellner N, Berninghausen O, Beckmann R, Hurt E, Thoms M, Berninghausen O, Beckmann R, Hurt E. 2016. Architecture of the 90S Pre-ribosome : A Structural View on the Birth of the Eukaryotic Ribosome. *Cell* **166**: 380–393.

Kronja I, Yuan B, Eichhorn SW, Dzeyk K, Krijgsveld J, Bartel DP, Orr-Weaver TL. 2014. Widespread changes in the posttranscriptional landscape at the Drosophila oocyte-to-embryo transition. *Cell Rep* **7**: 1495–1508.

Kuo B. 1996. Human ribosomal RNA variants from a single individual and their expression in different tissues. *Nucleic Acids Res* **24**: 4817–4824.

Lapointe CP, Grosely R, Sokabe M, Alvarado C, Wang J, Montabana E, Villa N, Shin B-S, Dever TE, Fraser CS, et al. 2022. eIF5B and eIF1A reorient initiator tRNA to allow ribosomal subunit joining. *Nature* **607**: 185–190.

Lee MT, Bonneau AR, Giraldez AJ. 2014. Zygotic Genome Activation During the Maternal-to-

Zygotic Transition. *Annu Rev Cell Dev Biol* **30**: 581–613.

Lee MT, Bonneau AR, Takacs CM, Bazzini AA, DiVito KR, Fleming ES, Giraldez AJ. 2013. Nanog, Pou5f1 and SoxB1 activate zygotic gene expression during the maternal-to-zygotic transition. *Nature* **503**: 360–364.

Leesch F, Lorenzo-Orts L, Pribitzer C, Grishkovskaya I, Roehsner J, Chugunova A, Matzinger M, Roitinger E, Belačić K, Kandolf S, et al. 2023. A molecular network of conserved factors keeps ribosomes dormant in the egg. *Nature* **613**: 712-720.

Li D, Wang J. 2020. Ribosome heterogeneity in stem cells and development. *J Cell Biol* **219**: 1–14.

Li H, Huo Y, He X, Yao L, Zhang H, Cui Y, Xiao H, Xie W, Zhang D, Wang Y, et al. 2022a. A male germ-cell-specific ribosome controls male fertility. *Nature* **612**: 725-731.

Li S, Ikeuchi K, Kato M, Buschauer R, Sugiyama T, Adachi S, Kusano H, Natsume T, Berninghausen O, Matsuo Y, et al. 2022b. Sensing of individual stalled 80S ribosomes by Fap1 for nonfunctional rRNA turnover. *Mol Cell* **82**: 3424-3437.e8.

Liu J, Shaik S, Dai X, Wu Q, Zhou X, Wang Z, Wei W. 2015. Targeting the ubiquitin pathway for cancer treatment. *Biochim Biophys Acta BBA - Rev Cancer* **1855**: 50–60.

Liu X, Bushnell DA, Kornberg RD. 2013. RNA polymerase II transcription: Structure and mechanism. *Biochim Biophys Acta BBA - Gene Regul Mech* **1829**: 2–8.

Liu Y, Beyer A, Aebersold R. 2016. On the Dependency of Cellular Protein Levels on mRNA Abundance. *Cell* **165**: 535–550.

Locati MD, Pagano JFB, Ensink WIMA, Olst MVAN, Van S, Nehrdich U, Zhu K, Spaink HP, Girard G, Rauwerda HAN, et al. 2017a. Linking maternal and somatic 5S rRNA types with different sequence-specific non-LTR retrotransposons. *RNA* **23**: 446–456.

Locati MD, Pagano JFB, Girard G, Ensink WA, Van Olst M, Van Leeuwen S, Nehrdich U, Spaink HP, Rauwerda H, Jonker MJ, et al. 2017b. Expression of distinct maternal and somatic 5.8S, 18S, and 28S rRNA types during zebrafish development. *RNA* **23**: 1188–1199.

Lu R, Markowetz F, Unwin RD, Leek JT, Airoldi EM, MacArthur BD, Lachmann A, Rozov R, Ma'ayan A, Boyer LA, et al. 2009. Systems-level dynamic analyses of fate change in murine embryonic stem cells. *Nature* **462**: 358–362.

Małecki JM, Odonohue MF, Kim Y, Jakobsson ME, Gessa L, Pinto R, Wu J, Davydova E, Moen A, Olsen JV, et al. 2021. Human METTL18 is a histidine-specific methyltransferase that targets RPL3 and affects ribosome biogenesis and function. *Nucleic Acids Res* **49**: 3185–3203.

Martin I, Kim JW, Lee BD, Kang HC, Xu JC, Jia H, Stankowski J, Kim MS, Zhong J, Kumar M, et al. 2014. Ribosomal protein s15 phosphorylation mediates LRRK2 neurodegeneration in parkinson's disease. *Cell* **157**: 472–485.

Martini OHW, Gould HJ. 1975. Molecular weight distribution of ribosomal proteins from several vertebrate species. *MGG Mol Gen Genet* **142**: 317–331.

Matsuki Y, Matsuo Y, Nakano Y, Iwasaki S, Yoko H, Udagawa T, Li S, Saeki Y, Yoshihisa T, Tanaka K, et al. 2020. Ribosomal protein S7 ubiquitination during ER stress in yeast is associated with selective mRNA translation and stress outcome. *Sci Rep* **10**: 19669.

Matsuo Y, Ikeuchi K, Saeki Y, Iwasaki S, Schmidt C, Udagawa T, Sato F, Tsuchiya H, Becker T, Tanaka K, et al. 2017. Ubiquitination of stalled ribosome triggers ribosome-associated quality control. *Nat Commun* **8**: 159.

Matsuo Y, Tesina P, Nakajima S, Mizuno M, Endo A, Buschauer R, Cheng J, Shounai O, Ikeuchi K, Saeki Y, et al. 2020. RQT complex dissociates ribosomes collided on endogenous RQC substrate SDD1. *Nat Struct Mol Biol* **27**: 323–332.

Matsuura-Suzuki E, Shimazu T, Takahashi M, Kotoshiba K, Suzuki T, Kashiwagi K, Sohtome Y, Akakabe M, Sodeoka M, Dohmae N, et al. 2022. METTL18-mediated histidine methylation of RPL3 modulates translation elongation for proteostasis maintenance. *eLife* **11**: e72780.

Mauro VP, Edelman GM. 2002. The ribosome filter hypothesis. *Proc Natl Acad Sci U S A* **99**: 12031–12036.

Meyer C, Garzia A, Morozov P, Molina H, Tuschl T. 2020. The G3BP1-Family-USP10 Deubiquitinase Complex Rescues Ubiquitinated 40S Subunits of Ribosomes Stalled in Translation

from Lysosomal Degradation. *Mol Cell* **77**: 1193-1205.e5.

Millrine D, Peter JJ, Kulathu Y. 2023. A guide to UFMylation, an emerging posttranslational modification. *FEBS J* febs.16730.

Mishima Y, Fukao A, Kishimoto T, Sakamoto H, Fujiwara T, Inoue K. 2012. Translational inhibition by deadenylation-independent mechanisms is central to microRNA-mediated silencing in zebrafish. *Proc Natl Acad Sci* **109**: 1104–1109.

Mishima Y, Han P, Ishibashi K, Kimura S, Iwasaki S. 2022. Ribosome slowdown triggers codon-mediated mRNA decay independently of ribosome quality control. *EMBO J* **41**: 1–17.

Mishima Y, Tomari Y. 2016. Codon Usage and 3' UTR Length Determine Maternal mRNA Stability in Zebrafish. *Mol Cell* **61**: 874–885.

Monem PC, Arribere JA. 2023. A ubiquitin language communicates ribosomal distress. *Semin Cell Dev Biol* S1084-9521: 00072-1.

Moriya Y, Kawano S, Okuda S, Watanabe Y, Matsumoto M, Takami T, Kobayashi D, Yamanouchi Y, Araki N, Yoshizawa AC, et al. 2019. The jPOST environment: an integrated proteomics data repository and database. *Nucleic Acids Res* **47**: D1218–D1224.

Muona M, Ishimura R, Laari A, Ichimura Y, Linnankivi T, Keski-Filppula R, Herva R, Rantala H, Paetau A, Pöyhönen M, et al. 2016. Biallelic Variants in UBA5 Link Dysfunctional UFM1 Ubiquitin-like Modifier Pathway to Severe Infantile-Onset Encephalopathy. *Am J Hum Genet* **99**: 683–694.

Nakahata S, Kotani T, Mita K, Kawasaki T, Katsu Y, Nagahama Y, Yamashita M. 2003. Involvement of Xenopus Pumilio in the translational regulation that is specific to cyclin B1 mRNA during oocyte maturation. *Mech Dev* **120**: 865–880.

Narita M, Denk T, Matsuo Y, Sugiyama T, Kikuguchi C, Ito S, Sato N, Suzuki T, Hashimoto S, Machová I, et al. 2022. A distinct mammalian disome collision interface harbors K63-linked polyubiquitination of uS10 to trigger hRQT-mediated subunit dissociation. *Nat Commun* **13**: 6411.

Nguyen AT, Prado MA, Schmidt PJ, Sendamarai AK, Wilson-Grady JT, Min M, Campagna DR, Tian G, Shi Y, Dederer V, et al. 2017. UBE2O remodels the proteome during terminal erythroid

differentiation. *Science* **357**: eaan0218.

Norris K, Hopes T, Aspden JL. 2021. Ribosome heterogeneity and specialization in development. *Wiley Interdiscip Rev RNA* **12**: 1–23.

Okuda S, Watanabe Y, Moriya Y, Kawano S, Yamamoto T, Matsumoto M, Takami T, Kobayashi D, Araki N, Yoshizawa AC, et al. 2017. jPOSTrepo: an international standard data repository for proteomes. *Nucleic Acids Res* **45**: D1107–D1111.

Oltion K, Carelli JD, Yang T, See SK, Wang H-Y, Kampmann M, Taunton J. 2023. An E3 ligase network engages GCN1 to promote the degradation of translation factors on stalled ribosomes. *Cell* **186**: 346-362.e17.

Panasenko OO, Collart MA. 2012. Presence of Not5 and ubiquitinated Rps7A in polysome fractions depends upon the Not4 E3 ligase. *Mol Microbiol* **83**: 640–653.

Parks MM, Kurylo CM, Dass RA, Bojmar L, Lyden D, Vincent CT, Blanchard SC. 2018. Variant ribosomal RNA alleles are conserved and exhibit tissue-specific expression. *Sci Adv* **4**: eaao0665.

Peng J, Schwartz D, Elias JE, Thoreen CC, Cheng D, Marsischky G, Roelofs J, Finley D, Gygi SP. 2003. A proteomics approach to understanding protein ubiquitination. *Nat Biotechnol* **21**: 921–926.

Peshkin L, Wühr M, Pearl E, Haas W, Freeman RM, Gerhart JC, Klein AM, Horb M, Gygi SP, Kirschner MW. 2015. On the Relationship of Protein and mRNA Dynamics in Vertebrate Embryonic Development. *Dev Cell* **35**: 383–394.

Pochopien AA, Beckert B, Kasvandik S, Berninghausen O, Beckmann R, Tenson T, Wilson DN. 2021. Structure of Gcn1 bound to stalled and colliding 80S ribosomes. *Proc Natl Acad Sci U S A* **118**: e2022756118.

Radford HE, Meijer HA, de Moor CH. 2008. Translational control by cytoplasmic polyadenylation in Xenopus oocytes. *Biochim Biophys Acta - Gene Regul Mech* **1779**: 217–229.

Radhakrishnan A, Chen YH, Martin S, Alhusaini N, Green R, Coller J. 2016. The DEAD-Box Protein Dhh1p Couples mRNA Decay and Translation by Monitoring Codon Optimality. *Cell* **167**: 122-132.e9.

Rappsilber J, Mann M, Ishihama Y. 2007. Protocol for micro-purification, enrichment, pre-fractionation and storage of peptides for proteomics using StageTips. *Nat Protoc* **2**: 1896–1906.

Reschke M, Clohessy JG, Seitzer N, Goldstein DP, Breitkopf SB, Schmolze DB, Ala U, Asara JM, Beck AH, Pandolfi PP. 2013. Characterization and Analysis of the Composition and Dynamics of the Mammalian Riboproteome. *Cell Rep* **4**: 1276–1287.

Richardson CD, Ray GJ, DeWitt MA, Curie GL, Corn JE. 2016. Enhancing homology-directed genome editing by catalytically active and inactive CRISPR-Cas9 using asymmetric donor DNA. *Nat Biotechnol* **34**: 339–344.

Richter JD, Lasko P. 2011. Translational Control in Oocyte Development. *Cold Spring Harb Perspect Biol* **3**: a002758.

Rose CM, Isasa M, Ordureau A, Prado MA, Beausoleil SA, Jedrychowski MP, Finley DJ, Harper JW, Gygi SP. 2016. Highly Multiplexed Quantitative Mass Spectrometry Analysis of Ubiquitylomes. *Cell Syst* **3**: 395-403.e4.

Rothschild D, Susanto TT, Spence JP, Genuth NR, Sinnott-Armstrong N, Pritchard JK, Barna M. 2023. A comprehensive rRNA variation atlas in health and disease. http://biorxiv.org/lookup/doi/10.1101/2023.01.30.526360 (Accessed August 26, 2023).

Roundtree IA, Evans ME, Pan T, He C. 2017. Dynamic RNA Modifications in Gene Expression Regulation. *Cell* **169**: 1187–1200.

Russo G, Curcio F, Bulli G, Aran L, Della-morte D, Testa G, Cacciatore F, Bonaduce D, Abete P. 2018. Oxidative stress, aging, and diseases. *Clin Interv Aging* **13**: 757–772.

Salsman J, Dellaire G. 2017. Precision genome editing in the CRISPR era. *Biochem Cell Biol* **95**: 187–201.

Sanz E, Yang L, Su T, Morris DR, McKnight GS, Amieux PS. 2009. Cell-type-specific isolation of ribosome-associated mRNA from complex tissues. *Proc Natl Acad Sci U S A* **106**: 13939–13944.

Scavone F, Gumbin SC, Da Rosa PA, Kopito RR. 2023. RPL26/uL24 UFMylation is essential for

ribosome-associated quality control at the endoplasmic reticulum. *Proc Natl Acad Sci* **120**: e2220340120.

Schmitt K, Kraft AA, Valerius O. 2021. A multi-perspective proximity view on the dynamic head region of the ribosomal 40s subunit. *Int J Mol Sci* **22**: 11653.

Schosserer M, Minois N, Angerer TB, Amring M, Dellago H, Harreither E, Calle-Perez A, Pircher A, Gerstl MP, Pfeifenberger S, et al. 2015. Methylation of ribosomal RNA by NSUN5 is a conserved mechanism modulating organismal lifespan. *Nat Commun* **6**: 6158.

Schuller AP, Wu CCC, Dever TE, Buskirk AR, Green R. 2017. eIF5A Functions Globally in Translation Elongation and Termination. *Mol Cell* **66**: 194-205.e5.

Selbach M, Schwanhäusser B, Thierfelder N, Fang Z, Khanin R, Rajewsky N. 2008. Widespread changes in protein synthesis induced by microRNAs. *Nature* **455**: 58–63.

Seydoux G. 1996. Mechanisms of translational control in early development. *Curr Opin Genet Dev* **6**: 555–561.

Shao S, Hegde RS. 2014. Reconstitution of a Minimal Ribosome-Associated Ubiquitination Pathway with Purified Factors. *Mol Cell* **55**: 880–890.

Sharma S, Lafontaine DLJ. 2015. 'View From A Bridge': A New Perspective on Eukaryotic rRNA Base Modification. *Trends Biochem Sci* **40**: 560–575.

Sheets MD, Fox CA, Dowdle ME, Blaser SI, Park S. 2018. Controlling the Messenger: Regulated Translation of Maternal mRNAs in Xenopus laevis Development. *Adv Exp Med Biol* **953**: 49-82.

Shi Z, Fujii K, Kovary KM, Genuth NR, Röst HL, Teruel MN, Barna M. 2017. Heterogeneous Ribosomes Preferentially Translate Distinct Subpools of mRNAs Genome-wide. *Mol Cell* **67**: 71-83.e7.

Shiraishi C, Matsumoto A, Ichihara K, Yamamoto T, Yokoyama T, Mizoo T, Hatano A, Matsumoto M, Tanaka Y, Matsuura-Suzuki E, et al. 2023. RPL3L-containing ribosomes determine translation elongation dynamics required for cardiac function. *Nat Commun* **14**: 1–17.

Silva GM, Finley D, Vogel C. 2015. K63 polyubiquitination is a new modulator of the oxidative stress response. *Nat Struct Mol Biol* **22**: 116–123.

Simms CL, Yan LL, Zaher HS, Simms CL, Yan LL, Zaher HS. 2017. Ribosome Collision Is Critical for Quality Control during No-Go Decay Article Ribosome Collision Is Critical for Quality Control during No-Go Decay. *Mol Cell* **68**: 361-373.e5.

Simsek D, Barna M. 2017. An emerging role for the ribosome as a nexus for post-translational modifications. *Curr Opin Cell Biol* **45**: 92–101.

Simsek D, Tiu GC, Flynn RA, Byeon GW, Leppek K, Xu AF, Chang HY, Barna M. 2017. The Mammalian Ribo-interactome Reveals Ribosome Functional Diversity and Heterogeneity. *Cell* **169**: 1051-1065.e18.

Sitron CS, Park JH, Brandman O. 2017. Asc1, Hel2, and Slh1 couple translation arrest to nascent chain degradation. *RNA* **23**: 798–810.

Snaurova R, Vdovin A, Durech M, Nezval J, Zihala D, Jelinek T, Hajek R, Simicek M. 2022. Deubiquitinase OTUD1 Resolves Stalled Translation on polyA and Rare Codon Rich mRNAs. *Mol Cell Biol* **42**: e0026522.

Sonenberg N, Hinnebusch AG. 2009. Regulation of Translation Initiation in Eukaryotes: Mechanisms and Biological Targets. *Cell* **136**: 731–745.

Song L, Luo Z-Q. 2019. Post-translational regulation of ubiquitin signaling. *J Cell Biol* **218**: 1776–1786.

Spence J, Gali RR, Dittmar G, Sherman F, Karin M, Finley D. 2000. Cell cycle-regulated modification of the ribosome by a variant multiubiquitin chain. *Cell* **102**: 67–76.

Sugiyama T, Li S, Kato M, Ikeuchi K, Ichimura A, Matsuo Y, Inada T. 2019. Sequential Ubiquitination of Ribosomal Protein uS3 Triggers the Degradation of Non-functional 18S rRNA. *Cell Rep* **26**: 3400-3415.e7.

Sundaramoorthy E, Leonard M, Mak R, Liao J, Fulzele A, Bennett EJ. 2017. ZNF598 and RACK1 Regulate Mammalian Ribosome-Associated Quality Control Function by Mediating Regulatory 40S

Ribosomal Ubiquitylation. *Mol Cell* **65**: 751-760.e4.

Tadros W, Lipshitz HD. 2009. The maternal-to-zygotic transition: a play in two acts. *Development* **136**: 3033–3042.

Takehara Y, Yashiroda H, Matsuo Y, Zhao X, Kamigaki A, Matsuzaki T, Kosako H, Inada T, Murata S. 2021. The ubiquitination-deubiquitination cycle on the ribosomal protein eS7A is crucial for efficient translation. *iScience* **24**: 102145.

Tanguturi P, Kim KS, Ramakrishna S. 2020. The role of deubiquitinating enzymes in cancer drug resistance. *Cancer Chemother Pharmacol* **85**: 627–639.

Tatsumi K, Yamamoto-Mukai H, Shimizu R, Waguri S, Sou Y-S, Sakamoto A, Taya C, Shitara H, Hara T, Chung CH, et al. 2011. The Ufm1-activating enzyme Uba5 is indispensable for erythroid differentiation in mice. *Nat Commun* **2**: 181.

Teixeira FK, Lehmann R. 2019. Translational Control during Developmental Transitions. *Cold Spring Harb Perspect Biol* **11**: a032987.

Tramutola A, Triani F, Di Domenico F, Barone E, Cai J, Klein JB, Perluigi M, Butterfield DA. 2018. Poly-ubiquitin profile in Alzheimer disease brain. *Neurobiol Dis* **118**: 129–141.

Truitt ML, Ruggero D. 2016. New frontiers in translational control of the cancer genome. *Nat Rev Cancer* **16**: 288–304.

Tryon RC, Pisat N, Johnson SL, Dougherty JD. 2013. Development of translating ribosome affinity purification for zebrafish. *genesis* **51**: 187–192.

Vejnar CE, Messih MA, Takacs CM, Yartseva V, Oikonomou P, Christiano R, Stoeckius M, Lau S, Lee MT, Beaudoin JD, et al. 2019. Genome wide analysis of 3′ UTR sequence elements and proteins regulating mRNA stability during maternal-to-zygotic transition in zebrafish. *Genome Res* **29**: 1100–1114.

Vejnar CE, Moreno-Mateos MA, Cifuentes D, Bazzini AA, Giraldez AJ. 2016. Optimization strategies for the CRISPR-Cas9 genome-editing system. *Cold Spring Harb Protoc* **2016**: 829–832.

Vind AC, Snieckute G, Blasius M, Tiedje C, Krogh N, Bekker-Jensen DB, Andersen KL, Nordgaard C, Tollenaere MAX, Lund AH, et al. 2020. ZAKα Recognizes Stalled Ribosomes through Partially Redundant Sensor Domains. *Mol Cell* **78**: 700–713.

Walczak CP, Leto DE, Zhang L, Riepe C, Muller RY, DaRosa PA, Ingolia NT, Elias JE, Kopito RR. 2019. Ribosomal protein RPL26 is the principal target of UFMylation. *Proc Natl Acad Sci U S A* **116**: 1299–1308.

Walden H, Muqit MMK. 2017. Ubiquitin and Parkinson's disease through the looking glass of genetics. *Biochem J* **474**: 1439–1451.

Wan L, Juszkiewicz S, Blears D, Bajpe PK, Han Z, Faull P, Mitter R, Stewart A, Snijders AP, Hegde RS, et al. 2021. Translation stress and collided ribosomes are co-activators of cGAS. *Mol Cell* **81**: 2808-2822.e10.

Wang L, Xu Y, Rogers H, Saidi L, Noguchi CT, Li H, Yewdell JW, Guydosh NR, Ye Y. 2020. UFMylation of RPL26 links translocation-associated quality control to endoplasmic reticulum protein homeostasis. *Cell Res* **30**: 5–20.

Wang L, Xu Y, Yun S, Yuan Q, Satpute-Krishnan P, Ye Y. 2023. SAYSD1 senses UFMylated ribosome to safeguard co-translational protein translocation at the endoplasmic reticulum. *Cell Rep* **42**: 112028.

Wang Y, Arribas-layton M, Chen Y, Lykke-andersen J, Sen GL. 2015. DDX6 Orchestrates Mammalian Progenitor Function through the mRNA Degradation and Translation Pathways. *Mol Cell* **60**: 118–130.

Warner JR, Mcintosh KB. 2009. How Common Are Extraribosomal Functions of Ribosomal Proteins? *Mol Cell* **34**: 3–11.

Winata CL, Łapiński M, Pryszcz L, Vaz C, Ismail MHB, Nama S, Hajan HS, Lee SGP, Korzh V, Sampath P, et al. 2018. Cytoplasmic polyadenylation-mediated translational control of maternal mRNAs directs maternal-to-zygotic transition. *Dev Camb* **145**: 1–12.

Wormington WM, Brown DD. 1983. Onset of 5 S RNA gene regulation during Xenopus embryogenesis. *Dev Biol* **99**: 248–257.

Wu CC-C, Peterson A, Zinshteyn B, Regot S, Green R. 2020. Ribosome Collisions Trigger General Stress Responses to Regulate Cell Fate. *Cell* **182**: 1–13.

Xu X, Xiong X, Sun Y. 2016. The role of ribosomal proteins in the regulation of cell proliferation, tumorigenesis, and genomic integrity. *Sci China Life Sci* **59**: 656–672.

Xue S, Barna M. 2012. Specialized ribosomes: A new frontier in gene regulation and organismal biology. *Nat Rev Mol Cell Biol* **13**: 355–369.

Xue S, Tian S, Fujii K, Kladwang W, Das R, Barna M. 2015. RNA regulons in Hox 5′ UTRs confer ribosome specificity to gene regulation. *Nature* **517**: 33–38.

Yan LL, Simms CL, McLoughlin F, Vierstra RD, Zaher HS. 2019. Oxidation and alkylation stresses activate ribosome-quality control. *Nat Commun* **10**: 1–15.

Yan LL, Zaher HS. 2021. Ribosome quality control antagonizes the activation of the integrated stress response on colliding ribosomes. *Mol Cell* **81**: 614-628.e4.

Yang R, Wang H, Kang B, Chen B, Shi Y, Yang S, Sun L, Liu Y, Xiao W, Zhang T, et al. 2019. CDK5RAP3, a UFL1 substrate adaptor, is critical for liver development. *Development* **146**: dev.169235.

Yusupova G, Yusupov M. 2014. High-Resolution Structure of the Eukaryotic 80S Ribosome. *Annu Rev Biochem* **83**: 467–486.

Zhang BQ, Chen ZQ, Dong YQ, You D, Zhou Y, Ye BC. 2022. Selective recruitment of stress-responsive mRNAs to ribosomes for translation by acetylated protein S1 during nutrient stress in Escherichia coli. *Commun Biol* **5**: 892.

Zhang M, Zhu X, Zhang Y, Cai Y, Chen J, Sivaprakasam S, Gurav A, Pi W, Makala L, Wu J, et al. 2015. RCAD/Ufl1, a Ufm1 E3 ligase, is essential for hematopoietic stem cell function and murine hematopoiesis. *Cell Death Differ* **22**: 1922–1934.

Acknowledgements

I would like to express my gratitude for Dr. Yuichiro Mishima for providing me with the opportunity to study and Dr. Hiroyuki Takeda for supporting the preparation of this manuscript and giving me insightful comments. I owe my completion of my Ph.D. course to their substantial supports, encouragement, and patients.

I would like to express my deepest gratitude for Dr. Koshi Imami and Dr. Yasushi ishihama for providing me with the data of mass spectrometry analysis. They also continuously motivated me and told me the proteomics field. Without their contributions to sciences, I would never know such a fascinating proteomics world.

I would like to thank Dr. Shinobu Chiba and Dr. Hiraku Takada for technical support and helpful discussion.

I would like to express my gratitude for Dr. Nobuhiro Nakamura, Dr. Chihiro Hama, Dr. Akira Kurosaka, and Dr. Naosuke Nakamura for insightful comments.

I would like to thank Dr. Yuki Sanpei for supporting and encouraging me when I faced difficulties.

I would like to offer my special thanks to Kimi Wakabayashi for fish maintenance and technical support.

Finally, I am grateful to lab alumni, Chihiro Hayashida, Tomoki Takayanagi, Noboru Okamoto, Keigo Nishimoto, Hayate Iida, Toru Irie, Kensho Saeki, Shinichi Tachihara, and Yuki Negoro for their continuous supports.